EVALUATING THE RETROFITTING METHODS FOR A BATTERED PILE DOLPHIN STRUCTURE

A THESIS SUBMITTED TO
THE GRADUATE SCHOOL OF NATURAL AND APPLIED SCIENCES
OF
MIDDLE EAST TECHNICAL UNIVERSITY

BY

AYŞEGÜL ACAR

IN PARTIAL FULFILLMENT OF THE REQUIREMENTS
FOR
THE DEGREE OF MASTER OF SCIENCE
IN
CIVIL ENGINEERING

APRIL 2024

Approval of the thesis:

EVALUATING THE RETROFITTING METHODS FOR A BATTERED PILE DOLPHIN STRUCTURE

submitted by **AYŞEGÜL ACAR** in partial fulfillment of the requirements for the degree of **Master of Science** i**n Civil Engineering, Middle East Technical University** by,

Prof. Dr. Naci Emre Altun
Dean, **Graduate School of Natural and Applied Sciences** _____

Prof. Dr. Erdem Canbay
Head of the Department, **Civil Engineering** _____

Prof. Dr. Uğurhan Akyüz
Supervisor, **Civil Engineering, METU** _____

Examining Committee Members:

Prof. Dr. Ahmet Yakut
Civil Engineering, METU _____

Prof. Dr. Uğurhan Akyüz
Civil Engineering, METU _____

Prof. Dr. Murat Altuğ Erberik
Civil Engineering, METU _____

Prof. Dr. Veysel Şadan Özgür Kırca
Civil Engineering, ITU _____

Prof. Dr. Gökhan Özdemir
Civil Engineering, Eskişehir Technical Uni. _____

Date: 24.04.2024

I hereby declare that all information in this document has been obtained and presented in accordance with academic rules and ethical conduct. I also declare that, as required by these rules and conduct, I have fully cited and referenced all material and results that are not original to this work.

Name Last name : Ayşegül, Acar

Signature :

ABSTRACT

EVALUATING THE RETROFITTING METHODS FOR A BATTERED PILE DOLPHIN STRUCTURE

Acar, Ayşegül
Master of Science, Civil Engineering
Supervisor : Prof. Dr. Uğurhan Akyüz

January 2024, 113

Battered pile systems have been widely used in national and international ports. However, past earthquakes have caused the performance of these systems to be questioned, and the use of battered pile systems in new projects is prohibited in many current specifications. There are various retrofitting methods for ports where battered pile systems are used. This thesis study compares the retrofitting of existing battered pile structures using the traditional method and the relatively newer and less common approach involving lead rubber bearings.

A dolphin structure located in Aliağa, Izmir was chosen as a case study. The conventional retrofitting approach involves adding additional piles to the structure. For the lead rubber bearing system, a new cap beam has been designed beneath the existing battered piles, with plans to sever the connection to the pile cap and replace it with lead rubber bearings.

Keywords: Seismic Performance, Dolphin, Lead Rubber Bearing, Retrofit, Batter Piles

ÖZ

EĞİK KAZIKLI DOLFEN YAPISI İÇİN GÜÇLENDİRME YÖNTEMLERİNİN DEĞERLENDİRİLMESİ

Acar, Ayşegül
Yüksek Lisans, İnşaat Mühendisliği
Tez Yöneticisi : Prof. Dr. Uğurhan Akyüz

Ocak 2024, 113

Eğik kazıklı sistemler ulusal ve uluslararası limanlarda yaygın olarak kullanılmaktadır. Ancak geçmişte yaşanan depremler bu sistemlerin performansının sorgulanmasına neden olmuş ve mevcut birçok şartnamede yıpranmış kazıklı sistemlerin yeni projelerde kullanılması yasaklanmıştır. Bu sistemin halihazırda kullanıldığı limanlar için ise çeşitli güçlendirme yöntemleri bulunmaktadır. Bu tez çalışmasında, mevcut eğik kazıklı yapının güçlendirilmesi, geleneksel yöntemle ve nispeten daha yeni ve daha az yaygın olan kurşun kauçuk mesnetlerle güçlendirme yöntemiyle karşılaştırılmıştır.

Örnek çalışma olarak İzmir Aliağa'da bulunan bir dolfen yapısı seçilmiştir. Geleneksel yöntem ile güçlendirmede yapıya daha fazla kazık eklenerek yapının güçlendirilmesi planlanmaktadır. Kurşun kauçuk izolatör sisteminde ise mevcut eğik kazıkların altında yeni başlık kirişi tasarlanması ve kazık başlık bağlantısının kesilerek yerine kurşun kauçuk izolatörler konulması planlanmıştır.

Anahtar Kelimeler: Sismik Performans, Dolfen, Kurşun Kauçuk İzolatör, Güçlendirme, Eğik Kazıklar

To my family...

ACKNOWLEDGMENTS

I would like to express my gratitude to Prof. Dr. Uğurhan Akyüz for his invaluable guidance and support during the preparation of this dissertation. I would also like to thank for sharing his valuable knowledge. Additionally, I extend my appreciation to my thesis committee members, Prof. Dr. Ahmet Yakut, Prof. Dr. Murat Altuğ Erberik, Prof. Dr. Özgür Kırca, and Prof. Dr. Gökhan Özdemir, for their helpful involvement in the thesis defense committee.

I would like to express my special thanks to my esteemed employer, Özgür Akarsu, whose significant role in my professional education and career development, through patient teaching and mentoring, has been immensely appreciated. I am also grateful to Nazlıcan Yılmaz and all my colleagues at Nis Engineering for their support.

Special appreciation is due to my dear friends Artun Baki and Demirhan Sever, who unwaveringly stood by me during the challenging process of completing my thesis study. Likewise, I extend my thanks to my beloved friends Zeynep Akay, Sena Şatır and Bensu Atlamaz for their endless support and belief.

Lastly, I express my deepest appreciation to my parents, Meral and Selami Acar, and my brothers, Osman and Turhan Acar, for their love and support throughout my life.

TABLE OF CONTENTS

LIST OF TABLES

TABLES

LIST OF FIGURES

FIGURES

LIST OF ABBREVIATIONS

ABBREVIATIONS

AFAD	Disaster and Emergency Management Presidency
API	American Petroleum Institute
FPS	Friction Pendulum System
HDRB	High Damping Rubber Bearing
KYLDY-2020	Guidelines for Coastal and Port Structures Under the Effect of Earthquakes
LDNRB	Low Damping Natural Rubber Bearing
LRB	Lead Rubber Bearing
MOTEMS	Marine Oil Terminal Engineering and Maintenance Standards
PEER	Pacific Earthquake Engineering Research Center
POLA	Port of Los Angeles
PIANC	The World Association for Waterborne Transport Infrastructure
TBEC-2018	Turkish Building Earthquake Code

LIST OF SYMBOLS

SYMBOLS

A_G	Gross area of pile
A_L	Area of lead plug
A_P	Gross end area of pile
A_R	Total rubber area
A_s	Side surface area of pile
B_L	Diameter of lead plug
c	Undrained shear strength
d_i	Inner diameter of steel pipe pile
d_o	Outer diameter of steel pipe pile
D	Diameter of steel pipe pile
D_D	Design displacement
D_y	Yield displacement
E	Earthquake load
E_0	Modulus of elasticity of rubber
E_c	Compression modulus of isolator unit
E_h	Horizontal earthquake load
E_s	Modulus of elasticity of structural steel
E_v	Vertical earthquake load
E_V	Modulus of rigidity

f	Unit skin friction capacity
f_{cc}	Characteristic strength of concrete
f_{cd}	Design strength of concrete
f_{ce}	Expected strength of concrete
f_{yc}	Characteristic yield strength of steel
f_{yd}	Design yield strength of steel
f_{ye}	Expected yield strength of steel
F_{cr}	Critical buckling stress
F_e	Elastic buckling stress
F_y	Yield force
F_Q	Characteristic strength of isolator unit
G	Dead load
h	Depth
i	Radius of inertia
G_v	Shear modulus of rubber
K	Bulk modulus of rubber
K_1	Elastic stiffness
K_2	Post yield stiffness
K_{eff}	Effective stiffness
K_v	Vertical stiffness
L_c	Buckling length
M_c	Bending moment capacity

M_n	Nominal bending moment strength
M_r	Design bending moment
N_q	Bearing capacity factor
P_0'	Effective overburden pressure at the point in question
P_c	Axial compression capacity
P_{cr}	Buckling load
P_n	Nominal axial compression strength
P_r	Design axial compression force
P_{str}	Axial load capacity
Q	Live load
Q_f	Skin friction resistance
Q_p	Total end bearing
Q_s	Environmental resistance
S	Shape factor
S_{ae}	Spectral acceleration
t	Thickness of one layer of rubber
T_{eff}	Effective period
T_r	Rubber thickness
W	Wind force
W_e	Elastic inertia moment
W_s	Weight of the structure
α	Dimensionless factor

β	Shaft friction factor (=Ktanδ)
β_{eff}	Effective damping
γ	Shear strain
h	Damping scale factor
υ	Rotation
τ_{pb}	Yield stress of lead
Ψ	c/ P_0' for the point in question

CHAPTER 1

INTRODUCTION

Maritime trade holds a crucial role in the global economy, with 10.648 million tons of products transported through international maritime transport in 2020 (UNCTAD, 2021). Given that Turkey is a peninsula country surrounded by sea on three sides, it is strategically positioned for maritime transportation. As depicted in Figure 1-1, maritime transport constituted 86.58% of the total weight in 2022.

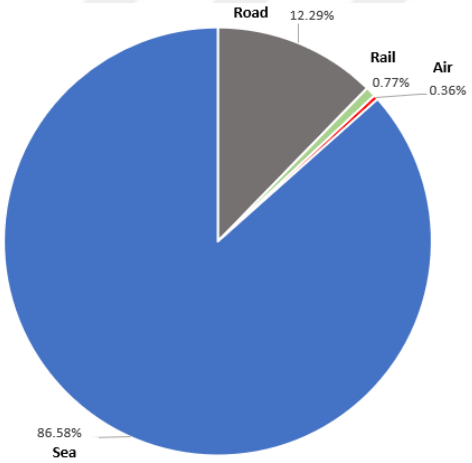

Figure 1-1. Distribution of Foreign Trade by Transport Types on Weight Basis (UTIKAD, 2022)

Ports occupy a crucial role in maritime transportation. During project design, consideration is given to geotechnical conditions, seismic factors, ship type and size, and the structural requirements of the port. The construction of a port can varies depending on its location and intended use. Offshore platforms, piers, breakwaters, seawalls, and floating structures are commonly used structures in marine facilities. Marine structures can be constructed on fill, bored piles, steel piles, etc., in accordance with technical specifications.

1.1 Problem Statement

Many national and international organizations have published standards for the design of marine structures. Examples of standards and codes include Earthquake Resistant Design of Port and Harbor Structures in Turkey (The Ministry of Transport, Maritime Affairs and Communications of the Turkish Republic, 2020); Seismic Design Guidelines for Port Structures (PIANC, 2001); Port of Los Angeles seismic code (POLA, 2004); Marine Oil Terminal Engineering and Maintenance Standards (MOTEMS, 2005); and American Society of Civil Engineers - Seismic Design of Piers and Wharves (ASCE 61-14, 2014). In Turkey, the primary references published by The Ministry of Transport, Maritime Affairs, and Communications of the Turkish Republic are 'Earthquake Resistant Design of Port and Harbor Structures in Turkey' and 'Coastal Structures Planning and Design Technical Principles'.

In the past, the battered pile system was widely preferred in ports in Turkey. Despite their successful use under static loads in various projects, recent earthquakes have revealed the poor performance of these piles, with observed damages (Ravazi el al., 2007). For example, during the Loma Prieta Earthquake in 1989, the batter piles at the Port of Oakland's 7th Street Terminal experienced tensile forces exceeding their capacity, resulting in the failure of deck connections (PIANC, 2001). Such damages caused by previous earthquakes has prompted engineers to question the performance of battered pile systems, particularly under seismic forces.

In addition to the poor performance of battered pile systems during earthquakes, there are also practical disadvantages, such as the challenge of manufacturing piles at the specified slope and angle in the project.

The construction of battered pile systems has been discouraged in Turkey for new projects due to their weakness in seismic excitations (The Ministry of Transport, Maritime Affairs, and Communications of the Turkish Republic, 2020). However, considering the economic impracticality of demolishing and rebuilding existing structures, retrofitting existing ports with battered piles can be considered after

assessing their structural safety. The retrofitting process may involve conventional methods, such as adding new cap beams and piles to the system. As an alternative method, seismic isolation for battered pile systems was introduced for the first time in the design guide, Design: Piers and Wharves, published by United Facilities Criteria (UFC) in 2005.

Seismic isolators are used in high seismic regions, and their use is becoming more widespread day by day. The use of seismic isolators, typically employed in bridges and buildings, is observed in port structures abroad. However, this method is not preferred in Turkey due to its limited popularity and uncertainties regarding its construction.

1.2 Literature Review

Seismic isolation is defined as control systems that absorb the energy generated during an earthquake, preventing damage to the structure. This method aims to improve the behavior of structures subjected to destructive seismic forces, thus protecting both structural and non-structural elements. The purpose of using seismic isolation is to reduce the earthquake's demand on the building rather than increase the building's ability to withstand earthquakes.

Seismic isolation is basically a system placed between the superstructure and the substructure. The isolation plane creates a separating surface between the ground and the superstructure, preventing vibrations caused by earthquakes or any external dynamic load from reaching the carrier system. Thus, the behavior of the structure remains in the elastic region, and most of the deformations occur at the seismic isolation level. Also, the seismic isolator has sufficient flexibility and displacement capacity in the horizontal direction and sufficient rigidity in the vertical direction. Thus, it can withstand both vertical and horizontal loads.

The fundamental principle of seismic base isolation is to diminish the seismic response of a structure by extending its natural vibration period. Seismic isolators

inherently represent flexible systems, and this achieved flexibility is the primary factor in elongating the natural vibration period of the structure. Therefore, this increase in the natural vibration period leads to a significant decrease in the acceleration values that will affect the structure and an increase in the horizontal movement ability of the structure, as shown in Figure 1-2. Moreover, it is also a factor contributing to a decrease in the values of base shear forces.

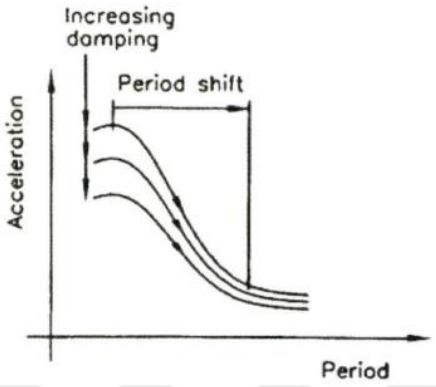

Figure 1-2 Period elongation and its effect on acceleration (Skinner, et al., 1993)

1.2.1 Brief History

Seismic isolation systems, designed to protect structures from the damaging effects of earthquakes, have been studied since the mid-20th century. One of the earliest instances of seismic isolation is the rotating element bearing system developed by engineer David Stevenson for a lighthouse in Japan in 1868 (Naeim & Kelly,1999).

Between 1876 and 1895, mining engineer John Milne carried out seismic isolation studies using iron balls and plates. While the study demonstrated good performance under mild seismic effects, it faced challenges under wind loads. To overcome this, Milne reduced the diameter of the balls, successfully solving the issue. He published this study in the journal of the British Association for the Advancement of Science (Makris, 2019). Later, J.A. Calantarients, a medical doctor, suggested separating buildings from their foundations in a letter to the Director of the Seismological

Service of Chile in 1909 and conducted studies on this proposal (Naeim & Kelly, 1999).

The first known modern seismic isolation design is the Tokyo Imperial Hotel, designed by Frank Lloyd Wright. Upon discovering a soft mud layer beneath a stiff layer during geotechnical studies, Wright aimed to move the structure with the stiff soil by driving piles. The building remained undamaged during the Tokyo earthquake that occurred in 1923, just two years after its construction (Makris, 2019).

Rubber material, which is frequently used for seismic isolation today, was first used in a 3-story school building in Macedonia in 1969. Since rubber is a flexible material, it was crushed due to the weight of the structure, and the desired result was not achieved. Thus, it prioritized the use of seismic isolation methods using steel plates together with rubber. The first seismic isolated structure made using rubber laminated with steel layers is a 3-story reinforced concrete school in Marseille, France (Makris, 2019).

Lead-core rubber bearings came into our lives in the late 1970s. The first building designed and built using lead-core insulation units was the "William Clayton" building in New Zealand, which was completed in 1981 (Naeim & Kelly, 1999).

1.2.2 Types of Seismic Isolation Systems

Various isolation systems are used to separate the superstructure and substructure. The most basic types of isolators used are rubber systems and friction systems. Low damping natural rubber bearings, high damping natural rubber bearings, and lead rubber bearings are examples of rubber systems. The friction pendulum system is an example of a friction system.

1.2.2.1 Low Damping Natural Rubber Bearings (LDNRB)

Low damping natural rubber bearings have the simplest structure among isolators. They are manufactured by placing rubber layers and steel layers between the top and bottom plates. While rubber layers resist lateral force, steel layers resist vertical force and attempt to prevent the rubber layer from swelling. The effective damping is usually around 2–3%. A notable disadvantage is that they cannot be used alone; an additional damping system is definitely needed.

1.2.2.2 High Damping Rubber Bearings (HDRB)

The use of high-damping rubber bearings began with the development of low-damping natural rubber bearings. By incorporating additional materials, effective damping can be increased to 10–20%. Some disadvantages of high-damping rubber bearings are higher costs compared to some solutions and significant performance variability depending on the production process.

1.2.2.3 Lead Rubber Bearings (LRB)

The distinguishing feature of lead rubber bearings is the incorporation of a lead core in the middle of rubber and steel plates. These bearings are often favored for their minimum maintenance requirements, extended service life, and proven performance. However, factors like environmental conditions, including temperature, can influence their performance, and the price and displacement capacity should be carefully considered. A significant disadvantage of lead rubber bearings is that the strength of the lead core cannot be evaluated after the isolator system has been used.

1.2.2.4 Friction Pendulum Bearings (FPS)

The friction pendulum system is formed by a sliding joint and a curvilinear steel surface. Its purpose is to diminish the horizontal force in a structure by utilizing the damping generated through the friction between these two elements that constitute the isolator during an earthquake. The friction pendulum system shares advantages with rubber systems mentioned above.

1.3 The Aim and Research Objectives

The aim of this study is to compare the retrofitting of the battered pile dolphin structure using conventional methods and seismic isolators, focusing on both engineering and economic considerations. The research will investigate the performance of the selected case study under seismic and static forces following retrofitting with these two distinct methods.

The objectives of this research are as follows:

- To assess the seismic performance of the structure retrofitted with different methods.
- To elucidate the advantages and disadvantages encountered during the application of each retrofitting plan.
- To conduct an economic comparison between the two retrofitting plans.

1.4 The Outline of the Thesis

In the first chapter, a concise overview of maritime trade and ports is provided. Subsequently, literature review, along with the purpose and objectives of this study, are explained.

In the second chapter, the design, modeling and regulations of lead rubber bearings and port structures are explained.

The third section encompasses the case study selected for this research. It covers the location and description of the structure, geotechnical studies, earthquake studies and retrofitting plans.

In section 4, the analysis and the results are presented. The structure was analyzed under three conditions for both methods: DD-2a earthquake, DD-1 earthquake, and static conditions. This section concludes with a comparison of the two retrofit plans.

The final section consolidates the study with the conclusion and recommendations.

CHAPTER 2

DESIGN CONSIDERATIONS AND REGULATIONS

This section includes information on the design and analysis of lead rubber bearings and marine structures.

2.1 Lead Rubber Bearings

Lead rubber bearings were first used in New Zealand in 1975, and they have since become a common choice in countries with high seismic activity (Naeim & Kelly, 1999). They are manufactured by adding rubber and steel plate layers and a lead core between the bottom and top plates (Figure 2-1). Lead is selected as the material for the plug for several reasons, including its low yielding stress (10 MPa), consistent mechanical properties, and favorable fatigue properties.

The central lead plug maintains high initial stiffness, ensuring structural stability during static loadings and minor earthquake events. Under these loadings, structures exhibit behavior as if the base is fixed. In the event of an earthquake, the lead plug yields and dissipates energy through hysteresis damping, facilitated by the plastic deformation of the lead.

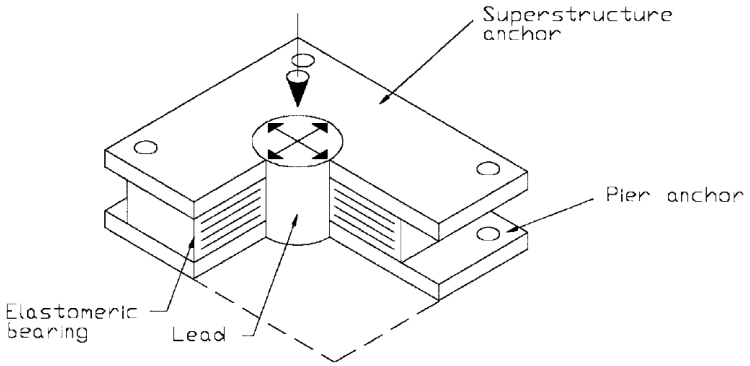

Figure 2-1 Lead rubber bearing (Naeim & Kelly, 1999)

2.1.1 Modeling

There are 3 important parameters for the design of lead rubber bearings. These parameters are elastic stiffness (K_1), post yield stiffness (K_2) and characteristic strength (Q).

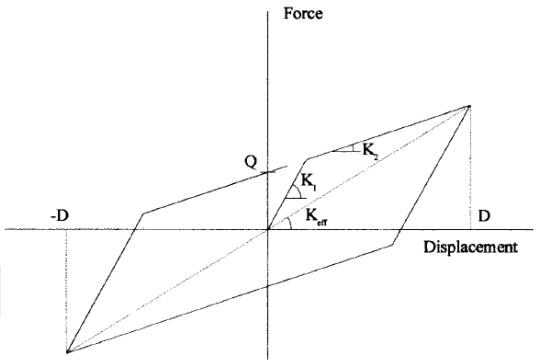

Figure 2-2 Hysteresis loop of lead rubber bearings (Naeim and Kelly, 1999)

In the first stage, the weight of the structure that the isolator will carry and target period of the system is determined. Afterwards, the effective stiffness is obtained using Equation 2-1.

$$T_{eff} = 2\pi\sqrt{\frac{W_s}{K_{eff}g}} \qquad \text{Equation 2-1}$$

The post-yield stiffness is calculated using the formula provided below. D represents design displacement. At this stage, the target displacement is used, but the process continues iteratively until the design displacement is achieved.

$$K_{eff} = K_2 + \frac{F_Q}{D_D} \qquad \text{Equation 2-2}$$

Calculating the elastic stiffness can be challenging; therefore, to obtain the elastic stiffness, it is determined by multiplying the post-yield stiffness by an empirical coefficient (Naeim & Kelly, 1999).

$$K_1 = 10K_2 \qquad \text{Equation 2-3}$$

Yield displacement and effective damping ratio are determined using the following equations.

$$D_y = \frac{F_y}{K_1} \quad \text{Equation 2-4}$$

$$\beta_{eff} = \frac{4}{2\pi}\frac{F_Q(D_D - D_y)}{K_{eff}D_D^2} \quad \text{Equation 2-5}$$

The damping scale factor is determined by the equation below, which depends on the effective damping.

$$\eta = \sqrt{\frac{10}{5 + \beta_{eff}}} \quad \text{Equation 2-6}$$

The design displacement, the final value in the hysteresis loop illustrated in Figure 2-1, is calculated based on acceleration, effective period, and the damping scale factor. Iterative calculations continue until the selected target displacement in the initial stage aligns with the value derived from Equation 2-7.

$$D_D = 1.3\left(\frac{g}{4\pi^2}\right)T^2\eta S_{ae} \quad \text{Equation 2-7}$$

To determine the size of the isolator following equations are used.

$$F_Q = nA_p\tau_{pb} \quad \text{Equation 2-8}$$

$$K_2 = n\frac{G_v A_r}{T_r} \quad \text{Equation 2-9}$$

$$\frac{B}{80} \le t \le \frac{B}{40} \quad \text{Equation 2-10}$$

For the calculation of vertical stiffness of isolator following formulas are used.

$$E_c = E_0(1 + 2kS^2) \quad \text{Equation 2-11}$$

$$S = \frac{B^2 - B_L^2}{4Bt} \quad \text{Equation 2-12}$$

$$E_V = \frac{1}{\frac{1}{E_c} + \frac{1}{K}} \quad \text{Equation 2-13}$$

$$K_v = \frac{E_V A_r}{T_r} \qquad \text{Equation 2-14}$$

2.1.2 Code Provisions (TBEC-2018)

National and international specifications have been published for seismic isolators. TBEC-2018, which came into force in 2019, was used in this thesis study. The following load combinations given in TBEC-2018 were used in the calculations.

$$1.4G + 1.6Q \qquad \text{Equation 2-15}$$

$$1.2G + Q \pm E \qquad \text{Equation 2-16}$$

$$0.9G \pm E \qquad \text{Equation 2-17}$$

Here, G represents the dead load, Q represents the live load, and E represents the earthquake load. TBEC-2018 stipulates the examination of isolators under DD-1 and DD-2 earthquake levels. However, in accordance with the guidelines outlined in the Earthquake Resistant Design of Port and Harbor Structures in Turkey (KLYDY-2020), the analysis of dolphin structures is carried out using DD-2a and DD-1 earthquake levels. Given that the study focuses on the design of isolators for a dolphin structure, the earthquake levels considered are DD-1 and DD-2a.

After the preliminary design of the isolators as per Section 2.1.1., analyses are conducted. These analyses assess the strain limits and vertical stability of the isolators under earthquake load, dead load, and live load conditions. The strain that occurs in the static case is characterized by three components.

- Shear strain caused by compression:

$$\gamma_{c,st} = \frac{6SP_{K1}}{A_r E_c} \qquad \text{Equation 2-18}$$

Where P_{K1} is the vertical load under the load combination given in Equation 2-15, A_r is the surface area of the elastomer layer, S is the shape factor, and E_c is the compression modulus of the isolator. The shear strain resulting from compression must be less than or equal to 3.5.

- Shear strain resulting from horizontal displacement due to environmental effects:

$$\gamma_{s,st} = \frac{\Delta_s}{T_r} \qquad \text{Equation 2-19}$$

The symbol Δ_s represents the horizontal displacement caused by horizontal force, while T_r denotes the total thickness of the elastomer layers.

- Shear strain resulting from the relative rotation between the upper and lower plates of the isolator unit:

$$\gamma_{r,st} = \frac{B^2\theta_s}{2tT_r} \qquad \text{Equation 2-20}$$

θ_s represents the design rotation angle, set to a minimum of 0.005 radians. B refers to the diameter of the elastomer, and t refers to the elastomer layer thickness.

The sum of strains resulting from compression, horizontal displacement, and relative rotation under static loads will be limited to less than 5.

In the case of an earthquake, strains resulting from compression force and horizontal displacement are calculated using equations Equation 2-21 and Equation 2-22. The sum of these two values, along with half of the strain resulting from relative rotation in Equation 2-20, must be limited to less than 6. Additionally, the strain resulting from horizontal displacement must be less than 2.

$$\gamma_{c,E} = \frac{6SP_{K2}}{A_{re}E_c} \qquad \text{Equation 2-21}$$

$$\gamma_{s,E} = \frac{D}{T_r} \qquad \text{Equation 2-22}$$

P_{K2} is the vertical load obtained under the load combination given in Equation 2-16.

Vertical stability in elastomer isolators also requires checking. If there is no horizontal displacement, the buckling load of elastomer isolators for lead rubber bearings will be calculated using Equation 2-23.

$$P_{cr} = 0.218\frac{G_v B^4}{tT_r}\frac{(1-\frac{B_L}{B})(1-\frac{{B_L}^2}{B^2})}{1+{B_L}^2/B^2} \quad \text{Equation 2-23}$$

In cases involving horizontal displacement, the buckling load under the earthquake effect will be calculated using Equation 2-24.

$$P_{cr}{}' = P_{cr}(A_{re}/A) \quad \text{Equation 2-24}$$

The axial load capacity is calculated using Equation 2-25.

$$P_{str} = \frac{3.5A_{re}E_c}{6S} \quad \text{Equation 2-25}$$

The buckling load limits are provided below for two cases, with and without horizontal displacement.

$$min(P_{cr}, P_{str})/P_{K1} \geq 2 \quad \text{Equation 2-26}$$

$$min(P_{cr}{}', P_{str})/P_{K2} \geq 1.1 \quad \text{Equation 2-27}$$

2.2 Marine Structures

Marine structures function as parking areas for marine vehicles such as ships and boats, trade centers where ships unload and load their cargo, places where cranes are located, and where customs offices are usually located. They serve various types of ships, including passenger ships, cargo ships, fishing boats, general cargo ships, tankers, LNG-LPG ships, and more. Marine structures play a crucial role in shielding ships from waves, currents, and wind, and they are designed based on the specific needs of the terminal they serve. The design process takes into account factors such as land and sea traffic, environmental considerations, and geotechnical conditions.

Ports are not confined to a single type of structure; rather, they can encompass a variety of structures. For instance, a container port may incorporate both a breakwater structure and a piled-quay structure. The breakwater serves to shield the quay and ships from waves, while handling and ship docking operations are conducted at the piled quay. Therefore, the selection of structure types in port design takes into account factors such as soil conditions, wave effects, design expertise,

construction methodologies (including material supply, construction equipment, construction time, etc.), and feasibility studies. Regardless of the specific structure type, a common characteristic of all port structures is that they are soil-structure interactive systems.

The following section provides examples of various structural systems used in ports and outlines the damage these systems have incurred in past earthquakes.

2.2.1 Berthing Structures and Failure Types

Berthing structures can be classified into three types according to their position: wharf, pier, and dolphin.

Wharves are structures parallel to the sea. They are categorized structurally based on their interaction with the sea and their stability under external loads. Closed wharves are designed to absorb sea effects on their front surfaces without transmitting them to their rear surfaces. On the other hand, open wharves are created by extending the dock platforms from the seaside to the top point of the filling area. As anticipated, open wharves tend to be more flexible structures compared to closed wharves.

Piers extend from the land into the sea, while dolphins are island-shaped structures independent of the land in the sea.

2.2.1.1 Quay Walls

Quay walls resist the horizontal and vertical loads acting on them with their own dead weight and base friction. Quay walls can be constructed using various methods, including caissons, blocks, and sheet piles. Caisson quay walls are monolithic structures, whereas block quay walls are formed by stacking concrete blocks on top of each other (Figure 2-3). Sheet pile quay walls are created by establishing a sheet pile wall with structures such as steel piles on the seaside and anchoring it to the backfill using tensile elements like tie-rods.

Commonly, system failure in block and caisson structures occurs when the structure undergoes significant displacements due to earthquake loads, experiences foundation settlement or liquefaction, and encounters backfill pressure. In sheet pile quay walls, damage or failure can result from three main factors. Firstly, the movement of the quay towards the sea and the burying of the tension element, leading to the loss of its function due to the liquefaction of the filling material underneath, may deteriorate the carrier system. The second scenario may unfold when the backfill exerts pressure on the sheet piles due to earthquake movement, causing cracks in the sheet pile and resulting in structural failure. Thirdly, failure may occur due to issues with anchoring. These system failures are illustrated in the drawings below.

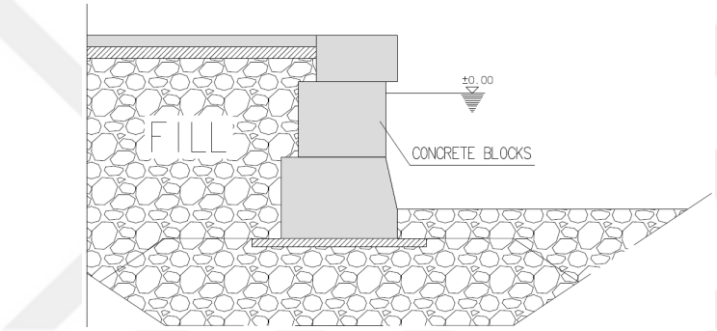

Figure 2-3 Cross-section of a typical block quay wall

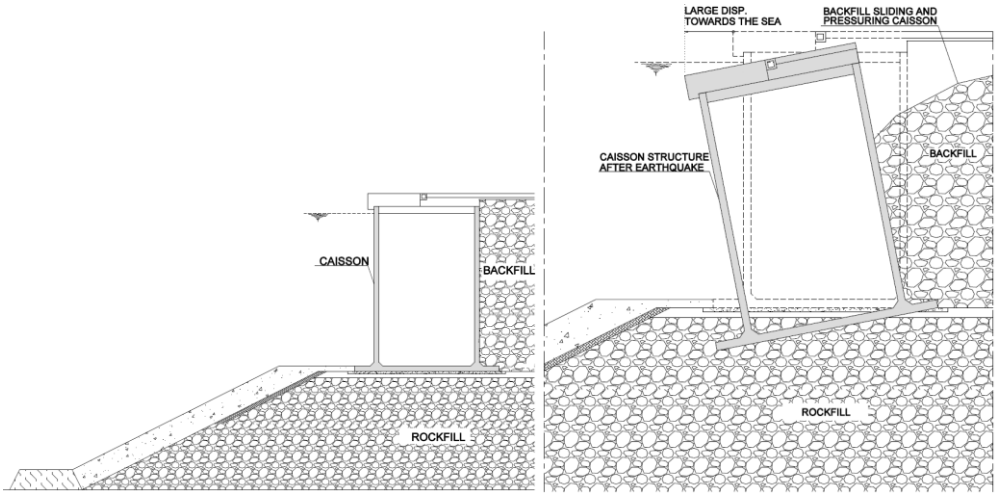

Figure 2-4 Caisson quay wall, (a)Typical cross-section, (b) Damage representative drawing

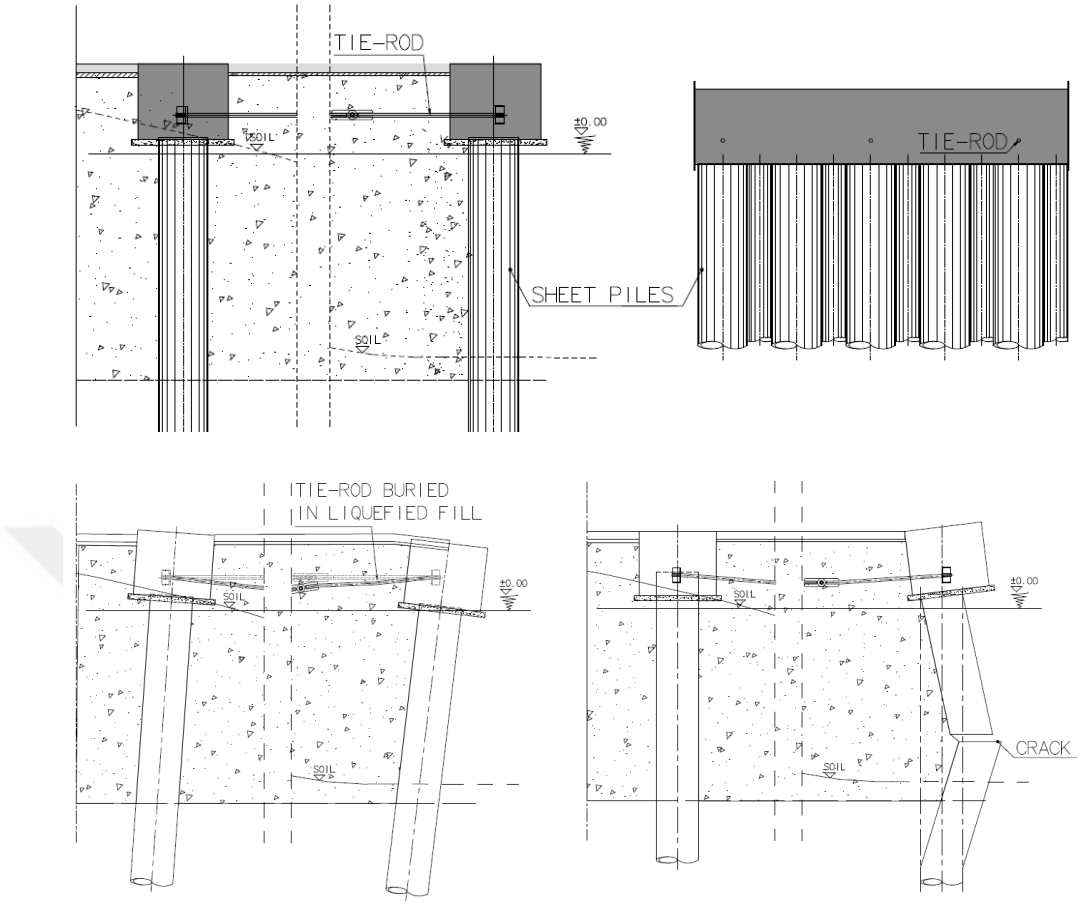

Figure 2-5 Sheet pile quay wall, (a) Typical cross-sections, (b) Damage representative drawings

2.2.1.2 Pile-Supported Wharves

Pile-supported wharves are created by driving piles into a sloped fill and constructing a superstructure atop it. Similar to previous systems, one of the primary causes of failure in these systems is liquefaction during an earthquake. The liquefaction effect induces a high moment in the piles, leading to permanent deformations. Furthermore, past projects have shown that significant moment, especially in piles that remain within the fill, result in the short column effect. In general, permanent deformations in piles are observed in pile-to-cap connections and in areas where the largest moment occurs in the remaining part of the piles within the fill.

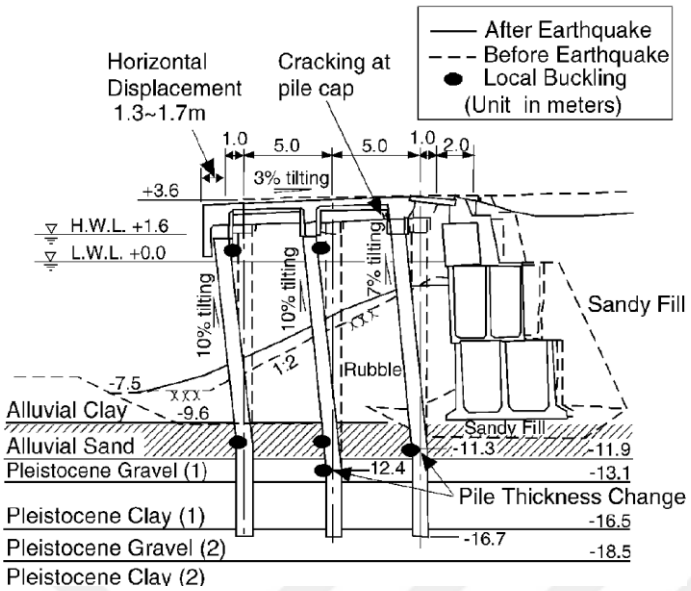

Figure 2-6 Cross-section of a pile supported wharf (PIANC, 2001)

2.2.1.3 Piers and Dolphins

Piers and dolphins are manufactured on piles. Both piers and dolphins may feature either batter or vertical piles. It's worth noting that vertical piles and batter piles exhibit different behaviors under earthquake conditions, leading to system failures for distinct reasons.

In vertical pile systems, piles resist the earthquake effect by bending and shearing, imparting greater elasticity to the structure (PIANC, 2001). However, seismic movements can lead to bending-related damages in the pile-to-cap connection, necessitating repairs and retrofitting post-earthquake. On the contrary, batter piles make the structure considerably more rigid, enhancing its performance under berthing loads, tie-down loads, and crane loads.

In batter pile systems, during an earthquake, batter piles primarily respond by developing significant axial compressive or tensile forces. Bending moments are generally of secondary importance in batter piles (PIANC, 2001). Batter piles begin to move within elastic and inelastic limits due to the earthquake forces. When piles fail in tension, they emerge from the ground, causing both horizontal and vertical

movement. This behavior of the pile is referred to as 'pole vault' due to its similarity in movement (Harn, 2004). The resulting vertical movement in the structure induces large tensile forces and may lead to the failure of other piles.

Given that the earthquake performance of vertical pile systems is deemed more successful that of battered pile systems, they are often preferred in regions prone to intense seismic activity, such as Turkey. Additionally, the use of battered pile systems in new construction is prohibited in KYLDY-2020.

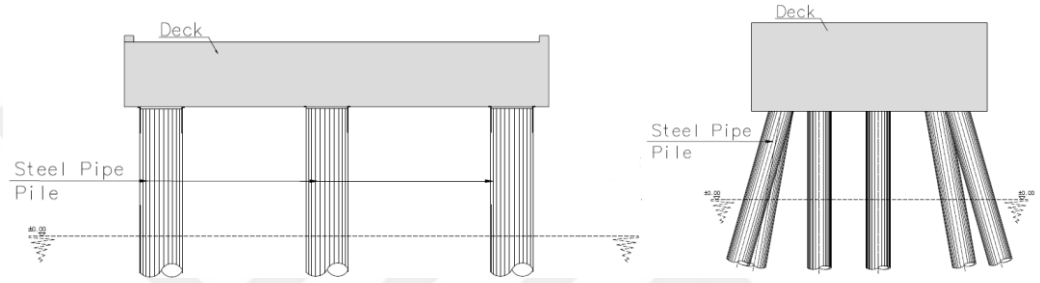

Figure 2-7 Cross-section of a dolphin structure, (a) Vertical piles, (b) Batter piles

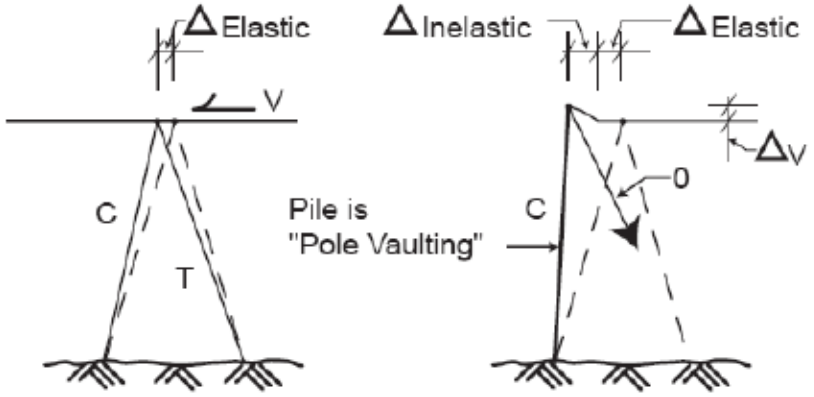

Figure 2-8 The pole-vaulting behavior (Harn, 2004)

2.2.2 Code Provisions (KYLDY-2020)

Up until 2020, the “Earthquake Technical Principles for the Construction of Coastal Port and Harbor Structures, Railways, and Airports” published in 2008 were used for the earthquake-resistant design of newly built and enlarged coastal port, railway,

and airport structures. This regulation also served to evaluate the earthquake performance of existing structures. However, the Ministry of Transport, Maritime Affairs, and Communications of the Turkish Republic has issued a code for the Earthquake Resistant Design of Port and Harbor Structures in Turkey (Official Gazette, October 6, 2020, No. 31266). This code came to enforcement as of Oct. 6, 2021. This updated regulation categorizes coastal and port structures into three main classifications.

- Gravity type and sheet pile quay walls
- Pile supported wharf and piers
- Coastal fortifications and breakwaters

A performance-based evaluation and design approach was used in the design of coastal and port structures (KLYDY, 2020). In this approach, seismic loads are assessed through the evaluation of two distinct cases.

- Analyzing the structure within elastic limits under frequent earthquakes with short recurrence periods.
- Analyzing the structure within inelastic limits and adhering to accepted damage limits during rare earthquakes with long recurrence periods.

According to KYLDY-2020, coastal and harbor structures are categorized into three categories of risk. Structures designated as 'important structures' (RC = 1) are crucial for safety, require immediate use post-earthquake, and often house explosive chemicals. Examples include oil loading and unloading stations. 'Normal structures' (RC=2) encompass those that would lead to significant economic losses after an earthquake, such as container terminals and dry bulk cargo terminals. 'Simple structures' (RC=3) are those easily reconstructed after earthquake damage and do not pose a life safety risk even when extensively damaged, including breakwaters and coastal fortifications.

The performance levels of pile-supported wharves and piers are determined based on these risk categories (refer to Table 2-1).

Table 2-1 Performance levels

Earthquake Ground Motion Level	*Risk Categories of Coastal and Port Structures*		
	RC= 1	*RC= 2*	*RC= 3*
DD-3	-	CO	CD
DD-2a	CO/LD*	-	-
DD1	CD/CP*	CP	-

* The performance levels for existing structures

The performance levels are defined as follows:

Continuous Operation (CO): This performance level corresponds to a condition where either no damage or very limited damage occurs at port structures and/or their components during an earthquake. Under these circumstances, port operations continue without disruption.

Controlled Damage (CD): This performance level corresponds to a condition where damage occurs in port structures and/or their components during an earthquake. In such instances, prolonged interruptions in the related port operations can be anticipated.

Collapse Prevention (CP): This performance level corresponds to a state before collapse in port structures and/or their components during an earthquake. The associated port operations are terminated in this scenario.

Limited Damage (LD): This performance level is indicative of a condition where port structures and/or their components experience limited, non-extensive, and reparable damage during an earthquake. Such circumstances may lead to short-term interruptions, lasting a few weeks or months, in the associated port operations.

Calculations for pile supported wharves and piers are carried out in two stages. In the first stage, it is aimed at preventing the structure from being damaged by an earthquake, and it is checked for frequent earthquakes. In the second stage,

deformation in the structure is allowed and controlled, provided that it remains within the limit values under rare earthquakes. The calculation and evaluation method to be used is decided according to the earthquake ground motion level, seismic design class, and risk category in Table 3.6 of KYLDY-2020.

Table 2-2 Calculation and evaluation methods

Coast. and Port Str. Risk Category	Calc. and Evaluation Stage	Levels of Earthquake Ground Motions	Seismic Design Category		
			SDC = 1	SDC = 2,3	SDC = 4
RC=1	Stage-1	DD-2a	METHOD 1 Linear Elastic Analysis / Force-Based Evaluation	METHOD 1 Linear Elastic Analysis / Force-Based Evaluation	METHOD 1 Linear Elastic Analysis / Force-Based Evaluation
	Stage-2	DD-1	METHOD 2.3 Nonlinear Analysis (THA) / Deformation-Based Evaluation	METHOD 2.1 Linear Elastic Analysis (Mixed Method) / Deformation-Based Evaluation	-
RC=2	Stage-1	DD-3	METHOD 1 Linear Elastic Analysis / Force-Based Evaluation	METHOD 1 Linear Elastic Analysis / Force-Based Evaluation	METHOD 1 Linear Elastic Analysis / Force-Based Evaluation
	Stage-2	DD-1	METHOD 2.2 Nonlinear Analysis (Pushover Method) / Deformation-Based Evaluation	METHOD 2.1 Linear Elastic Analysis / Deformation-Based Evaluation	-
RC=3	Stage-1	DD-3	METHOD 1 Linear Elastic Analysis / Force-Based Evaluation	METHOD 1 Linear Elastic Analysis / Force-Based Evaluation	METHOD 1 Linear Elastic Analysis / Force-Based Evaluation

The earthquake ground motion levels used in the 1st stage and 2nd stage are defined below.

DD-1: Very rare earthquake ground motion with a 2% probability of exceeding the spectral magnitudes in 50 years (recurrence period of 2475 years).

DD-2a: Frequent earthquake ground motion with a 30% probability of exceeding spectral magnitudes in 50 years (recurrence period is 144 years).

DD-3: Very frequent earthquake ground motion with a 50% probability of exceeding the spectral magnitudes in 50 years (recurrence period of 72 years).

To determine the calculation and evaluation method, the short period design spectral acceleration coefficient for the DD-2 earthquake level will be identified, and the seismic design category will be obtained from Table 3.1 in KYLDY-2020.

Table 2-3 Seismic design categories (SDC)

Short Period Design Spectral Acceleration Coefficient at DD-2 Earthquake Ground Motion Level (SDS)	*Seismic Design Categories*
$S_{DS} < 0.33$	SDC = 4
$0.33 \leq S_{DS} < 0.67$	SDC = 3
$0.67 \leq S_{DS} < 1.00$	SDC = 2
$1.00 < S_{DS}$	SDC = 1

Strain limits for deformation-based evaluation are presented in Table 2-4.

Table 2-4 Strain limits

	Performance Level		
Strain Limits	*CD*	*CP*	*LD**
Concrete compressive strain	0.0135	0.018	0.004
Reinforcement steel strain	0.04	0.053	0.015
Steel pile strain	0.02	0.0265	0.0075

*LD: Limited Damage. Used only for existing structures.

2.2.3 Modeling Rules

2.2.3.1 Modeling of Pile Deck and Carrier Systems in the First Stage

The rules regarding the modeling of piled deck and carrier systems are defined in this section to be used in the linear calculation to be made within the scope of the first stage calculation, design, and evaluation.

- The decks at each anode consist of reinforced concrete elements with monolithic connections that transfer moments with each other and with the piles.
- The deck carrier system must have sufficient in-plane stiffness and strength to safely transfer earthquake forces and other horizontal loads from the deck to the piles and between the piles. In cases where this is not sufficient, appropriate transfer elements should be arranged on the deck.
- Piled quay/pier carrier systems will always be modeled in three dimensions, including piles, pile caps, if any, deck beams, and plates. It is essential to consider the finite stiffness of the deck slabs within their own planes. However, in cases where in-plane stiffnesses are shown to be very large compared to pile horizontal stiffnesses, a rigid diaphragm assumption can be made for in-plane displacements at each deck anchor.
- Earthquake effects in two horizontal directions perpendicular to each other will always be taken into account. The damping ratio will be taken as 5%.
- For reinforced concrete piles and deck beams modeled with frame elements, 50% of the gross section stiffness corresponding to bending behavior will be used as effective section stiffness. There will be no reduction in gross stiffness for shear and axial behavior. In cases where deck slabs are modeled with shell elements, all section stiffnesses corresponding to in-plane and out-of-plane deformations will be taken as 50% of the gross section stiffnesses.
- The monolithic connection of steel pipe piles to the pile cap or deck will be provided by reinforced concrete reinforcement extending to the deck from

the concrete filled into the pile along the wetting zone. The steel pipe section will be inserted under the pile cap or deck to the maximum extent possible. In a monolithic connection, a reinforced concrete section with a diameter equal to the inner diameter of the pipe pile will be taken as the basis.,

- In addition to the mass of the pile itself in the case of piles in water and the mass of water inside the section in the case of pipe piles, additional water mass will be taken into account.

2.2.3.2 Modeling of Pile Deck and Carrier Systems in the Second Stage

Modeling rules to be used in the calculations to be made within the scope of second-stage calculation, design, and evaluation are defined in this section.

- The general rules given in 2.2.3.1 regarding the first stage are also valid for the second stage, except for the effective section stiffnesses defined for concrete piles.
- As stated in KYLDY-2020 Section 3.4 as the basic principle of ductile behavior in piled decks and carrier systems, plastic deformations will only be allowed in piles. Deck beams and floor slabs, defined as capacity-protected elements, will be modeled to behave linearly under the influence of earthquakes. In this context, in battered pile systems, necessary precautions will be taken to prevent plastic deformations in the deck beams and slabs due to elastic and plastic axial deformations in the piles.
- Plastic deformations in piles are generally expected to occur at the pile-deck connection within the scope of the inertial interaction. However, due to the kinematic interaction defined, plastic deformations may also occur in battered piles and at depths where the soil layers show sudden changes in stiffness and strength.
- Nonlinear behavior in vertical piles, which are predominantly under the influence of bending moments along with axial force, is generally modeled with the plastic hinge approach. In reinforced concrete, prestressed concrete,

and steel pipe piles, the plastic hinge will be defined at the point where the pile meets the deck. The finite length region below and above the point where the bending moment reaches the effective yield moment defined in KYLDY-2020 ANNEX 7B is called the plastic hinge length, and the spread of plastic deformations throughout this region is assumed to be constant.

- In the second stage, the rules given in 2.2.3.1 are valid for modeling the masses.

CHAPTER 3

CASE STUDY

3.1 Project Information

3.1.1 Location and Description

As part of this thesis, a case study was conducted on an LPG terminal located in the Aliağa district of Izmir. The terminal features 1 loading platform, 4 breasting dolphins, and 4 mooring dolphins. The layout plan of this system is illustrated below, with 'B' representing breasting dolphins, 'M' representing mooring dolphins, and 'LUP' representing the loading-unloading platform.

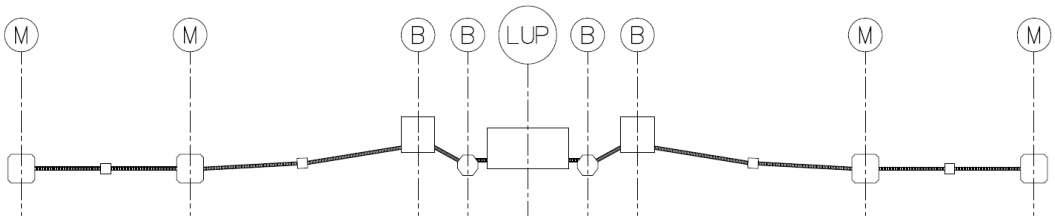

Figure 3-1 Terminal layout plan

The loading platform, measuring 24 meters in length and 12 meters in width, was used for the study. The loading platform is supported by a total of 16 steel piles, each measuring 32 inches in diameter and 14 mm in thickness. Among these, 8 piles are oriented vertically, and the remaining 8 are battered. The wall thickness of the existing piles was determined based on the NDT report prepared in April 2017, while the pile lengths were determined from the PIT report prepared in October 2017, considering the most critical values. The battered piles were driven with a slope of 1/3.5 and rotated 10° in specified directions, as illustrated in Figure 3-2. The superstructure was constructed using precast slabs on the first-phase cap beam and

cast-in-situ slabs on top. To protect the cast-in-situ slab, a 10 cm layer of pavement concrete was applied to the structure (Figure 3-3).

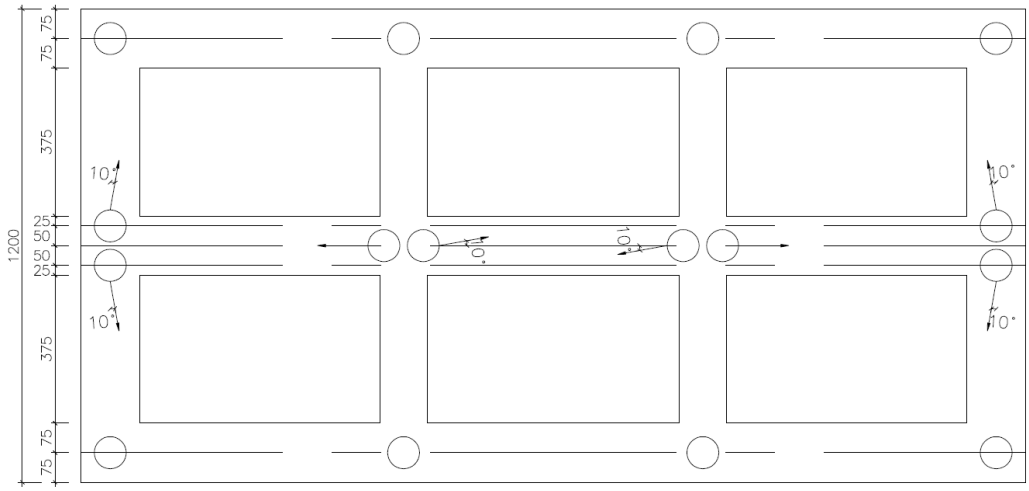

Figure 3-2 Loading platform pile application plan

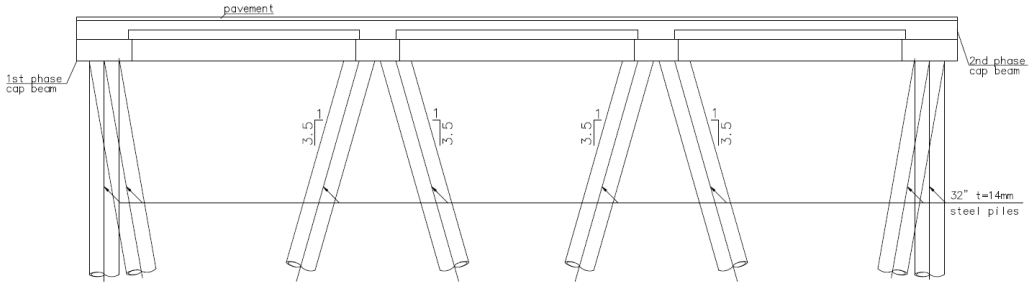

Figure 3-3 Cross-section of the loading platform

3.1.2 Materials

The material properties used in the calculations were taken from the measurements conducted in August 2017 and are presented below.

Superstructure concrete elements (C25);

Elastic modulus, E = 30,000 MPa

Poisson's ratio, $\nu = 0.2$

Characteristic compressive strength, f_{ck}= 25 MPa

Concrete plug (C30);

Elastic modulus, E = 32,000 MPa

Poisson's ratio, ν = 0.2

Characteristic compressive strength, f_{ck}= 30 MPa

Reinforcement Steel (S420);

Elastic modulus, E = 210,000 MPa

Characteristic yield strength, f_{yk}= 420 MPa

Steel pipe piles (St44);

Elastic modulus, E = 210,000 MPa

Poisson's ratio, ν = 0.3

Yield stress, σ_y= 275 MPa

The material properties to be used in new structures are presented below;

Superstructure concrete elements (C35);

Elastic modulus, E = 33,000 MPa

Poisson's ratio, ν = 0.2

Characteristic compressive strength, f_{ck}= 35 MPa

Concrete plug (C40);

Elastic modulus, E = 34,000 MPa

Poisson's ratio, ν = 0.2

Characteristic compressive strength, f_{ck}= 40 MPa

Reinforcement Steel (S420);

Elastic modulus, E = 210,000 MPa

Characteristic yield strength, f_{yk}= 420 MPa

Steel pipe piles (St52);

Elastic modulus, E = 210,000 MPa

Poisson's ratio, ν = 0.3

Yield stress, σ_y= 355 MPa

In force-based design, design strengths for concrete, reinforcing steel and structural steel are defined by dividing the relevant characteristic strengths by the material safety coefficients.

For concrete: $f_{cd} = f_{cc}/1.5$ Equation 3-1

For steel: $f_{yd} = f_{yc}/1.15$ Equation 3-2

In deformation-based design, design strengths for concrete, reinforcing steel and structural steel are defined by multiplying the relevant characteristic strengths by the material following coefficients.

For concrete: $f_{ce} = 1.3f_{cc}$ Equation 3-3

For steel: $f_{ye} = 1.2f_{yc}$ Equation 3-4

3.1.3 Loads

3.1.3.1 Dead Load

Dead loads include the weight of the structure itself and the constant loads on it. The weight of the structure is calculated by the SAP2000 program, which is a structural calculation program.

Unit weight of reinforced concrete: γ_c = 25.0 kN/m³

Unit weight of steel elements: γ_{st} = 78.5 kN/m³

3.1.3.2 Live Load

A uniformly distributed live load of 10 kN/m² was taken into account on the loading platform.

3.1.3.3 Temperature Load

Temperature changes of ± 20°C were taken into account in the analyses.

3.1.3.4 Wind Load

The maximum wind speed in the project area was determined to be 30.84 m/s. The wind force on the structures was calculated according to TS 498.

$$W = C_p \times v^2/1600 \qquad \text{Equation 3-5}$$

3.1.3.5 Wave Load

As a result of wave studies conducted in the area where the structure is located, the wave height in front of the structure was determined to be 2.25 meters and its period was 5.2 seconds. Wave loads were calculated and applied to the structure according to the Airy linear wave theory defined in the SAP2000 program.

3.1.3.6 Seismic Loads

Seismic loads were determined according to KLYDY-2020, and the earthquake spectrums to be used in the analyses are given in Chapter 3.3.

In the analyses, the seismic loads were combined with the combinations given below, as indicated in Section 6.2 of the KLYDY.

$$E_h = \pm {E_d}^{(X)} \pm 0.3{E_d}^{(Y)} \qquad \text{Equation 3-6}$$

$$E_h = \pm 0.3{E_d}^{(X)} \pm {E_d}^{(Y)} \quad \text{Equation 3-7}$$

E_d^X and E_d^Y symbolize the earthquake effects calculated separately under the influence of earthquakes in the X and Y earthquake directions perpendicular to each other in any section, and E_h symbolizes the horizontal earthquake load based on the design in which directional coupling has been applied.

$$G + Q \pm E_h \pm 0.3E_v \quad \text{Equation 3-8}$$

$$0.9G \pm E_h \pm 0.3E_v \quad \text{Equation 3-9}$$

G represents the dead load, Q represents the live load, and E_v represents the vertical earthquake load.

3.2 Geotechnical Studies

3.2.1 Soil Properties

The ground and foundation survey was conducted in the relevant field, based on drilling carried out in November 2017. Boreholes 4 and 5 were utilized to establish the idealized soil profile. The soil profile observed in the first 30 meters, as a result of studies within the scope of the geotechnical survey, classifies the soil as ZC according to Table 8.1 of KYLDY-2020.

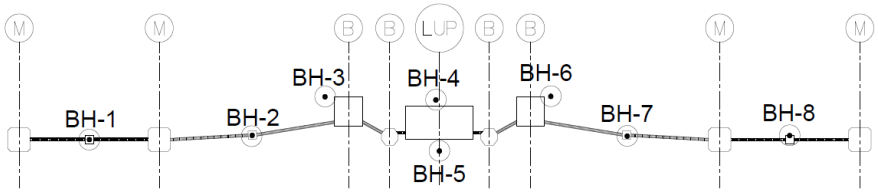

Figure 3-4 Borehole locations

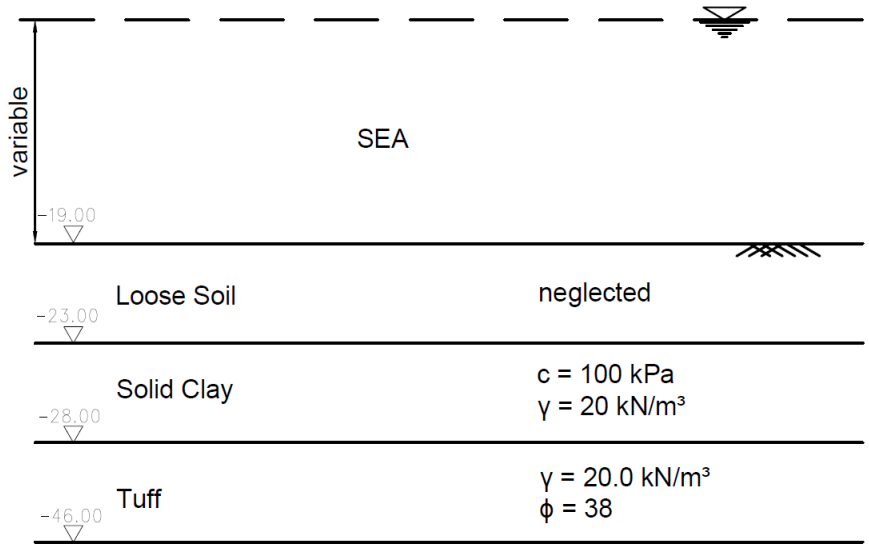

Figure 3-5 Idealized soil profile

3.2.2 Pile-Soil Interaction

In accordance with KYLDY-2020 Section 9.4, the pile-soil interaction (KZE-B) method will be used in seismic calculations. This method breaks down deck-pile-soil interaction into two components: kinematic interaction and inertia interaction.

For the horizontal interaction between the structure and the soil, p-y curves along the pile are defined as a pair of pure pressure springs at each node. For the vertical interaction, t-z curves were specified at the pile tip to represent friction along the pile, while q-w curves were defined to capture the tip resistance. The p-y curves, along with the resulting t-z/q-w curves, will be created for static and seismic conditions based on the pile diameters used within the project.

p-y curves

In the analysis of offshore project piles, soils are characterized by nonlinear springs that vary with depth and soil type. In p-y curves, p represents soil pressure per unit length of pile, and y represents pile deflection. While the most accurate results for p-y curves are obtained through testing, empirical formulas have been developed for various soil types over time.

For this project, p-y curves were obtained using the API soft clay and massive rock p-y models in the program called 'lpile'. These curves were then defined as one-joint links at each node in the SAP 2000.

t-z and q-w curves

To model the pile-soil interaction, t–z springs are used for axial behavior (representing environmental friction), and q-w springs are used for axial pile tip behavior. These interactions will be defined as a composite spring in the SAP2000 model, as illustrated in Figure 3-6. The non-linear tip link was obtained from a program called 'apile'.

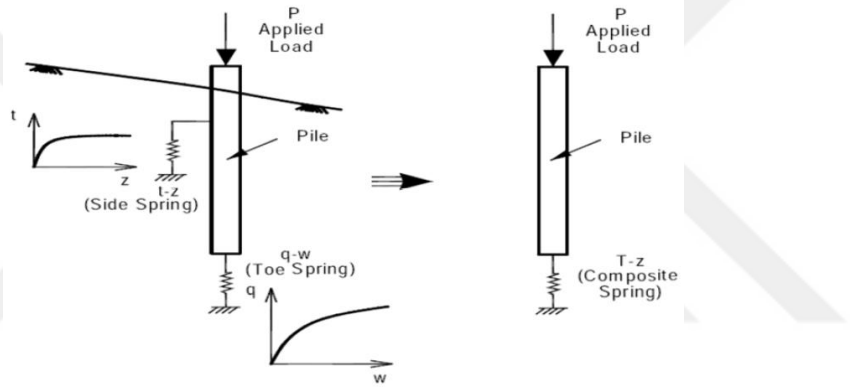

Figure 3-6 Vertical soil-structure interaction demonstration (POLB,2012)

The p-y curves for each depth and diameter, along with the pile end link, can be found in Appendix A.

3.3 Earthquake Studies

The purpose of the kinematic interaction calculation is to assess the internal forces and deformations in the piles resulting from the propagation of earthquake waves in the ground. In the kinematic interaction calculation using the KZE-B method, free-field analyses will be conducted by simulating and scaling the earthquake record across seven time domains. This simulation is based on the DD-1 spectrum curve

defined in the bedrock of the field. The maximum values of total displacements obtained for the record will be calculated over time. Subsequently, these maximum values will be averaged over seven earthquakes to establish the total earthquake displacement profile along the piles.

The total earthquake displacement profile will then be applied as ground displacement to the system from the relevant pile node points. Simultaneously, the spectrum curve determined at the ground surface will serve as the basis for determining the inertia loads in the second stage.

DD-1, DD-2, and DD-2a level elastic design spectrums were obtained from the Interactive Seismic Hazard Map (AFAD, Ministry of Interior Turkey) and given below.

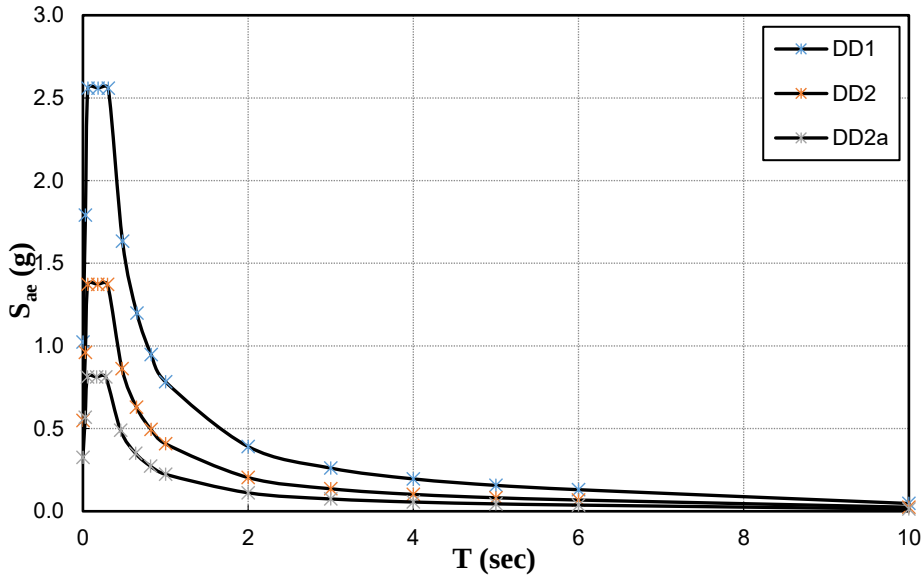

Figure 3-7 Elastic design acceleration spectra

3.3.1 Ground Motions

This section outlines the data related to ground motions caused by earthquakes, which serves as the foundation for conducting analyses under the influence of seismic effects.

For DD-1 level seismic analysis, ground motion records that are compatible with the design spectrum are needed for the nonlinear analysis. Three sources can be used to obtain ground motions: artificial records, synthetic records, and real recordings. Real accelerograms were used in this study. The location of the site within the scope of the project and its distance to active fault lines are shown in Figure 3-8.

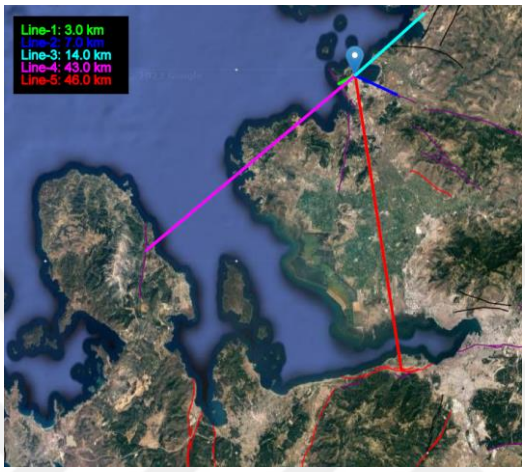

Figure 3-8 Location of the site and active fault map that will pose an earthquake hazard (http://yerbilimleri.mta.gov.tr)

The selection of ground motions will be determined by considering earthquake magnitudes that align with the earthquake ground motion level based on the design, fault distances, source mechanisms, and local soil conditions. Earthquakes significant enough to impact the region are anticipated to originate from five active fault lines in close proximity to the site (see Figure 3-8). The names and lengths of these faults are summarized in Table 3-1.

Table 3-1 Active fault lengths that pose an earthquake hazard in the site

Fault Name	*Approx. Fault Length (km)*
Yenifoça Fault	3.0
Zeytindağ Fault	7.0
Güzelhisar Fault	14.0
Mordoğan Fault	43.0
İzmir Fault	46.0

The faults listed in Table 3-1 are within an area of approximately 50 km. Ground motions with instrumental or historical information related to these faults are gathered from various sources, including AFAD, the Earthquake Research Department, Kandilli Observatory and Earthquake Research Institute, the International Seismology Center, and the US Geological Survey. Earthquakes with magnitudes greater than 5.0 that occurred between 1900 and 2023 are depicted in Figure 3-9, and their respective details, such as formation dates, locations, depths, and moment magnitudes, are summarized in Table 3-2.

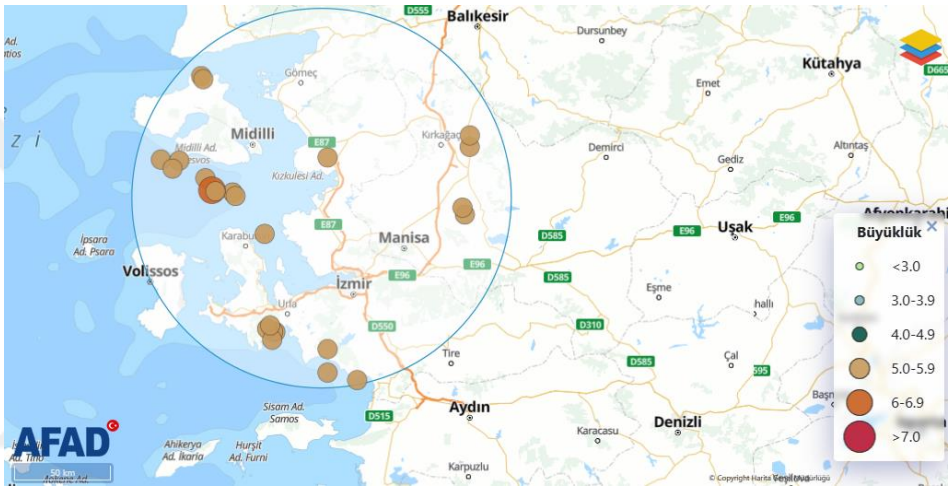

Figure 3-9 Instrumental seismicity since 1900 (Greater than magnitude 5.0)

Table 3-2 Earthquake occurrence dates, locations, depths, moment magnitudes

Date (UTC)	*Latitude*	*Longitude*	*Depth*	*Type*	*Magn.*	*Location*
12-06-2017	38.8486	26.313	15.96	Mw	6.2	Aegean Sea
20-10-2005	38.1535	26.6708	15.4	Md	5.9	Aegean Sea
17-10-2005	38.2202	26.6586	18.6	Md	5.8	Urla
10-04-2003	38.19	26.69	18.7	Md	5.6	Aegean Sea

3.3.1.1 Selection and Scaling of Ground Motions

As seen in Figure 3-9, there are no past earthquake records compatible with the earthquake ground motion level based on the design in the region where the structure is located. Thus, Peer NGA Data Bank was used in the selection of earthquake ground motions and a total of seven records were selected. In determining these ground motions, factors such as earthquake magnitudes (Mw), source mechanisms, local ground conditions, and fault distances compatible with the earthquake ground motion level based on the design were carefully considered. The search criteria were: Strike-Slip and Reverse Fault, R_{JB}= 0-90 km, R_{RUP}= 0-90 km and Mw=7-8. The characteristics of the selected earthquakes are provided in Table 3-3 and in the Figure 3-10 DD-1 level elastic design spectrum is compared with the selected ground motions.

The original acceleration records are given in Appendix B. Below is a summary of the considerations taken into account for the selected ground motions.

- Seven sets of spectrum-compatible ground motion sets were generated.
- In order to be suitable for the DD-1 earthquake level, earthquakes of magnitudes 7-8 were preferred.
- The duration of the strong ground motion part was not shorter than 5 times the first natural vibration period of the structure, or 15 seconds.
- Where there was no permanent displacement in the selected records, the absence of permanent displacement was confirmed in the scaled records.

Table 3-3 Selected earthquake records that are compatible with the design spectrum for the earthquake level DD-1

RSN	*Earthquake*	*Year*	*Magnitude*	*Mechanism*	*Rjb (km)*	*Rrup (km)*
1148	Kocaeli, Turkey	1999	7.51	Strike Slip	10.56	13.49

Table 3-3 (continued)

RSN	*Earthquake*	*Year*	*Magnitude*	*Mechanism*	*Rjb (km)*	*Rrup (km)*
1182	Chi-Chi, Taiwan	1999	7.62	Reverse Oblique	9.76	9.76
1184	Chi-Chi, Taiwan	1999	7.62	Reverse Oblique	19.93	19.96
1611	Düzce, Turkey	1999	7.14	Strike Slip	0.21	0.21
1612	Düzce, Turkey	1999	7.14	Strike Slip	4.17	4.17
1614	Düzce, Turkey	1999	7.14	Strike Slip	11.46	11.46
2113	Denali, Alaska	2002	7.9	Strike Slip	53.02	54.78

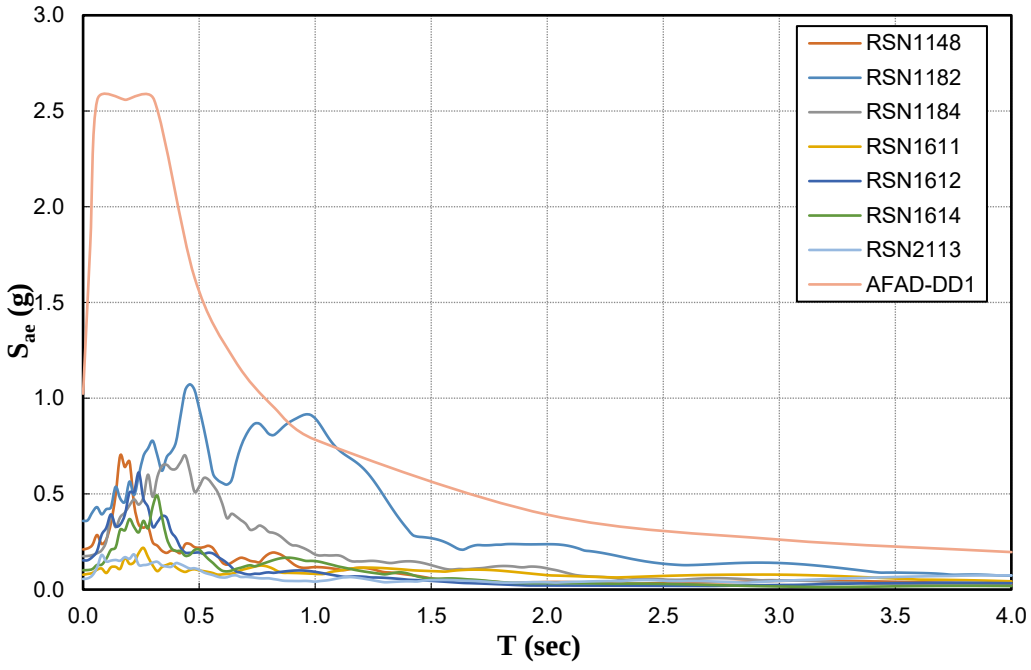

Figure 3-10 The comparison of the spectra of selected and unscaled 7 ground motion records with the elastic design spectrum for the earthquake level DD-1

The earthquake records can be scaled using a simple scaling method or transformed to achieve spectral matching. However, it has been stated that earthquake ground motions should be converted to ensure spectral compatibility with the design spectrum of selected earthquake records, enabling their use in site-specific ground response analyses or other calculations in the time domain.

The rules to be applied during the conversion phase are as follows:

- The averages of the transformed earthquake ground motion spectra should not be smaller than the design spectrum ordinates for all periods.
- The amplitudes of the selected records between the 0.2Tp and 1.5Tp periods of the spectra should not be smaller than the amplitudes of the design spectrum in the same period range. For earthquake scaling, the period interval was determined by taking into account the structure's period and the short-period region.
- The scaling coefficients of the selected earthquakes were chosen between 0.25-4.0 (Fahjan, 2008).

In this context, the spectra obtained from earthquake ground motions were converted in accordance with the "Earthquake Resistant Design of Port and Harbor Structures in Turkey" for the DD-1 earthquake level. The acceleration records used as earthquake motion in the analysis and the acceleration-time and displacement-time graphs created by iteratively adding wavelets to the original acceleration record within a certain period in the time domain and in a limited time are given in the appendices. Spectral acceleration spectra and averages for the DD-1 earthquake level are given below.

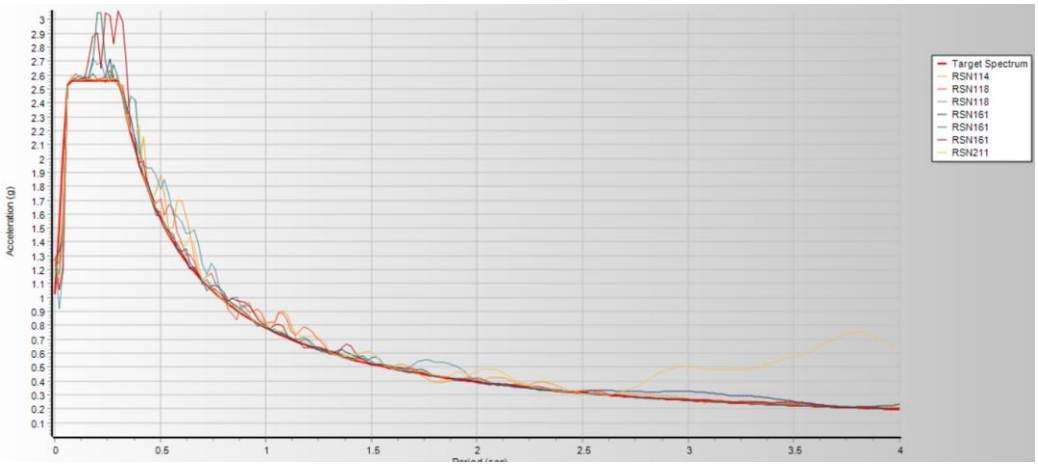

Figure 3-11 Spectral acceleration spectra and averages of selected earthquake ground motions (scaled for DD-1 earthquake level) for DD-1 earthquake level

3.3.2 Free-Field Analysis

The free-field analyses of the dolphin structure were completed using the Deep Soil software to determine the spectrum curve and kinematic displacement values. These analyses were conducted based on the idealized soil profile and bedrock soil class of the field. The displacement-depth graph and the average spectrum-period graph obtained from the free-field analyses are presented below.

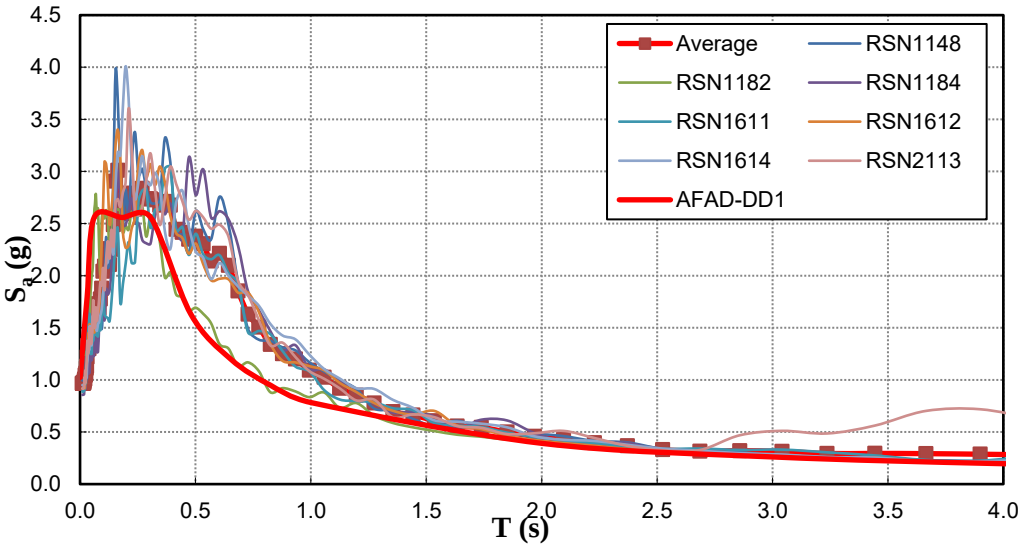

Figure 3-12 The average spectrum-period graph

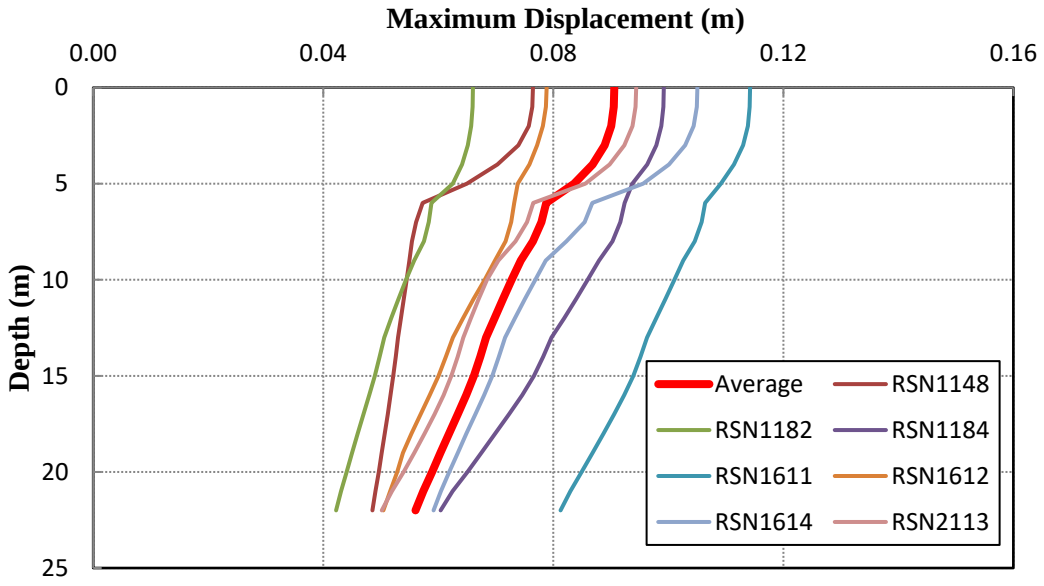

Figure 3-13 The maximum displacement-depth graph

3.4 Retrofitting Plans

This thesis proposes two retrofitting plans: the first involves additional pile driving, a conventional method, while the second introduces lead rubber bearings to the system.

3.4.1 Conventional Retrofitting Plan

The proposed retrofitting plan is illustrated in the figure below. As depicted, 4 new piles have been added to the system. Following the preliminary analysis, 4 of the piles were chosen as 52" 22 mm. Minimum wall thickness control for the new piles is provided in Appendix C. Similar to the existing piles, a driving slope of 1/3.5 was selected for the new piles.

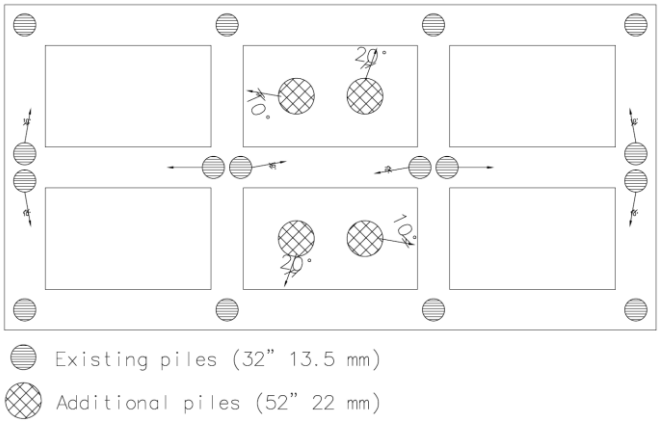

Figure 3-14 Conventional retrofitting plan

3.4.2 Lead Rubber Bearing Retrofitting Plan

To enhance the seismic performance of the existing battered piles, new cap beams will be constructed beneath the current cap beams, and the connection of the piles to the superstructure will be facilitated through the incorporation of lead rubber bearings. This approach is intended to enhance the lateral load performance of the piles and reduce shear forces by extending the structural period. Plan and cross-section of the proposed system is illustrated in Figure 3-15.

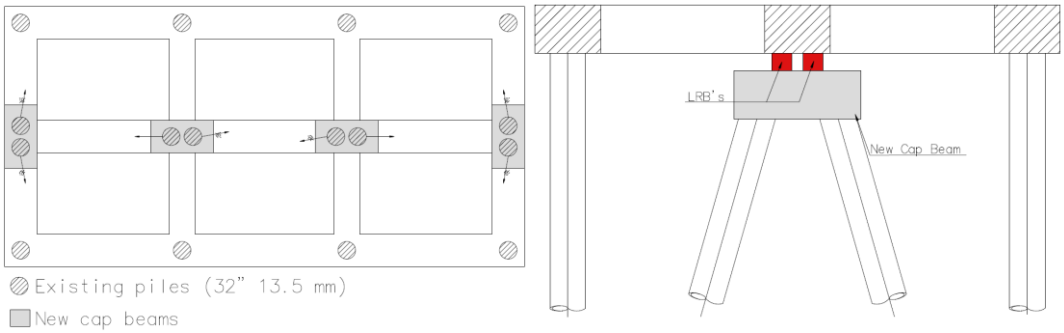

Figure 3-15 Plan and cross-section of the proposed lead rubber bearing retrofitting system

CHAPTER 4

ANALYSIS AND RESULTS

4.1 Retrofitting a Dolphin Structure Using Additional Steel Piles

4.1.1 First Stage Analysis (DD-2a Level Earthquake)

In structures categorized under coastal port risk category 1, it is desirable to calculate and ensure a continuous operation performance level during the first-stage analysis. However, for existing structures, Chapter 11 of KYLDY-2020 states that limited damage performance level control with a non-linear calculation method in the first-stage analysis can also be used.

Since the structure was observed to operate within elastic limits under the DD2-a earthquake, the analysis of the structural system will be based on linear behavior (Method 1) and force-based evaluation and design, as shown in Table 2-2. In this case, the evaluation criterion is based on whether the "internal force demands (effects)" obtained from the calculation are equal to or less than the "internal force capacities (strengths)".

The DD-2a earthquake spectrum given in Figure 3-7 was used in the calculations at this stage. In the linear calculation, both horizontal and vertical earthquake effects will be directly applied without any reduction, and they will be combined with dead load and live load as specified in Equation 3-4 and Equation 3-5.

The dolphin structure was modeled in three dimensions in accordance with the specifications defined earlier (see Figure 4-1). Fifty percent of the section stiffness corresponding to the effective section stiffness for bending behavior was utilized in the pile cap connection, cap beams, and slab. As the piles are situated in water, an

additional water mass was defined at each point using KYLDY-2020 Equation 6.4. The three-dimensional model view is presented below.

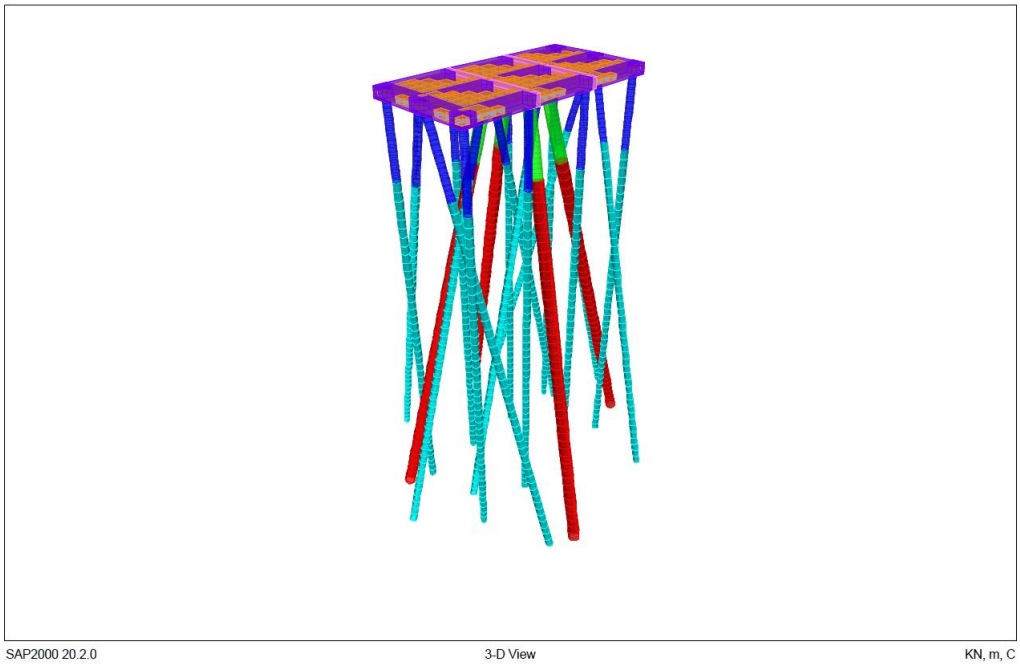

Figure 4-1 Conventional retrofit model view

In modal calculation methods, the number of modes considered must adhere to the rule that the total earthquake loads' modal effective masses, calculated in the same directions for each mode under the influence of earthquake ground motions in horizontal and vertical directions, should not be less than 95% of the total mass of the structure (KYLDY-2020). The modal properties of the dolphin in X and Y directions are provided in the table below. As evident from the table, the total mass participation ratio exceeds 95%, in accordance with KYLDY-2020.

Table 4-1 Modal properties of the dolphin

Mode Number	*Period*	*mx*	*my*
1	1.23584	0.25015	0.61503
2	1.10672	8.024E-05	1.402E-06
3	1.02279	0.61624	0.2526

Table 4-1 (continued)

Mode Number	*Period*	*mx*	*my*
.	.	.	.
.	.	.	.
60	0.01313	0.00020	0.04265
Total	-	0.97071	0.97158

For the first stage of analysis, the strength of steel pipe piles and cap-to-beam connections against internal force demands was checked. Subsequently, the bearing capacity of the steel pipe piles against axial forces was examined.

4.1.1.1 Design Check of Steel Pipe Piles Against Axial Force and Bending Moment Internal Force Demands

The Steel Structures Regulation, published by the Ministry of Environment, Urbanization, and Climate Change in 2016, was used for steel pipe pile control. First, the nominal axial compressive strength must be calculated. The nominal axial compressive strength, P_n, of elements with non-slender cross-section (according to Regulation of Steel Structures Table 5.1A) under the axial pressure force will be calculated with Equation 4-1.

$$P_n = F_{cr} \times A_g \qquad \text{Equation 4-1}$$

Here, the critical buckling stress, F_{cr}, will be obtained by Equation 4-2 or Equation 4-3.

$$for\ \frac{L_c}{i} \leq 4.71\sqrt{\frac{E}{F_y}}\ or\ \frac{F_y}{F_e} \leq 2.25$$

$$F_{cr} = \left[0.658^{\frac{F_y}{F_e}}\right] F_y \qquad \text{Equation 4-2}$$

$$for\ \frac{L_c}{i} > 4.71\sqrt{\frac{E_s}{F_y}}or\ \ \frac{F_y}{F_e} > 2.25$$

$$F_{cr} = 0.877F_e \qquad \text{Equation 4-3}$$

Elastic buckling stress, F_e, for bending buckling, torsional buckling, and/or bending torsion buckling limit states around any of the cross-sectional principal axes of the element under the influence of axial compression force will be calculated with Equation 4-4.

$$F_e = \frac{\pi^2 E_s}{(\frac{L_c}{i})^2} \qquad \text{Equation 4-4}$$

To calculate the nominal bending moment strength, the cross-section must be classified as compact, non-compact, or slender according to Table 5.1B (The Steel Structures Regulation, 2016). All steel pipe cross-sections used in the project meet the non-compact cross-section condition. Thus, nominal bending moment strength will be calculated using Equation 4-5. The elastic inertia moment, W_e, for circular tube sections can be calculated from Equation 4-6.

$$M_n = \left(\frac{0.021E_s}{\left(\frac{D}{t}\right)} + F_y\right)W_e \qquad \text{Equation 4-5}$$

$$W_e = \frac{\pi(d_o^4 - d_i^4)}{32d_o} \qquad \text{Equation 4-6}$$

The interaction of bending moment and axial compression force in elements with double or single symmetry axes under the effect of bending around their geometric axes should be limited by Equation 4-7 and Equation 4-8.

$$\frac{P_r}{P_c} \geq 0.2 \rightarrow \frac{P_r}{P_c} + \frac{8}{9}(\frac{M_{rx}}{M_{cx}} + \frac{M_{ry}}{M_{cy}}) \leq 1.0 \qquad \text{Equation 4-7}$$

$$\frac{P_r}{P_c} < 0.2 \rightarrow \frac{P_r}{2P_c} + (\frac{M_{rx}}{M_{cx}} + \frac{M_{ry}}{M_{cy}}) \leq 1.0 \qquad \text{Equation 4-8}$$

Here, P_r is the design axial compression force obtained from the load combinations for the column, P_c is the axial compressive strength for the column, and M_{cx} and M_{cy}

are the bending moment strengths of the column in the strong and weak axes, respectively. The reduction factor for strength will be taken as 0.9, as stated in the Steel Structures Regulation (2016).

$$P_c = 0.9 \times P_n \qquad \text{Equation 4-9}$$

$$M_c = 0.9 \times M_n \qquad \text{Equation 4-10}$$

As stated in the conventional strengthening plan, 32" × 13.5 mm and 52" × 22 mm steel piles are used in the project. Steel section controls according to the above equations are given in this section, respectively.

32” 13.5 mm Steel Pipe Pile

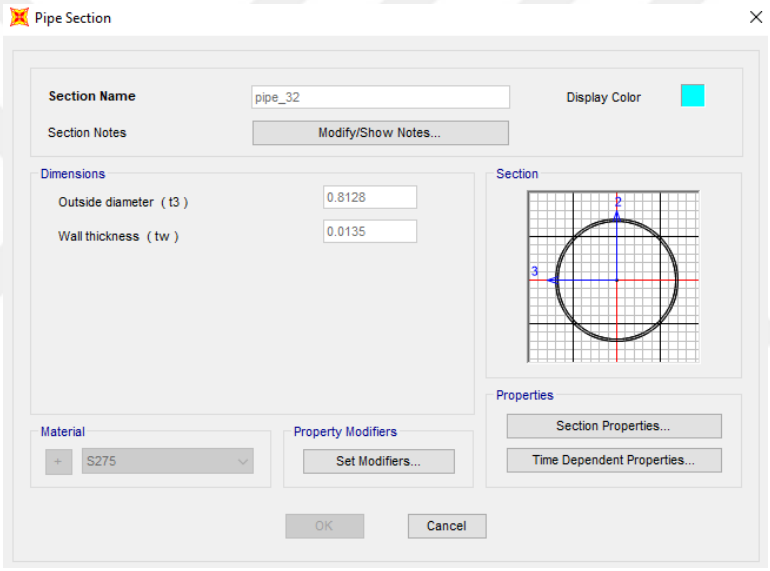

Figure 4-2 Steel pipe pile cross-section (32” 13.5 mm)

The nominal axial compressive strength and nominal bending moment strength of the 32” × 13.5 mm pile section are obtained as 4721.10 kN and 1951.72 kNm, respectively. A force-based design check for the section, considering design axial forces and moment values obtained from SAP2000, is presented in the table below.

Table 4-2 Force-based design check – 32” 13.5 mm steel pipe pile

Frame	P_r (kN)	M_{rx} (kN-m)	M_{ry} (kN-m)	P_r/P_c	Total Ratio		Limit	Check
1868	-2391.7	-224.4	-345.9	0.56	0.7715	<	1.0	OK

Table 4-2 (continued)

Frame	P_r (kN)	M_{rx} (kN-m)	M_{ry} (kN-m)	P_r/P_c	Total Ratio		Limit	Check
1869	-2369.4	-224.4	-345.9	0.56	0.7663	<	1.0	OK
1047	-2396.7	-215.2	-330.8	0.56	0.7638	<	1.0	OK
1048	-2379.8	-215.2	-330.8	0.56	0.7598	<	1.0	OK
1868	-2390.4	-212.6	-323.0	0.56	0.7583	<	1.0	OK

52” 22 mm Steel Pipe Pile

The nominal axial compressive strength and nominal bending moment strength of the 52” × 22 mm pile section are obtained as 19242.00 kN and 10075.82 kNm, respectively.

As can be seen from the results in the table, steel capacity remained high compared to the analysis results. However, in accordance with the formulas related to the calculation of the minimum wall thickness, the pile wall thickness is taken as 22 mm.

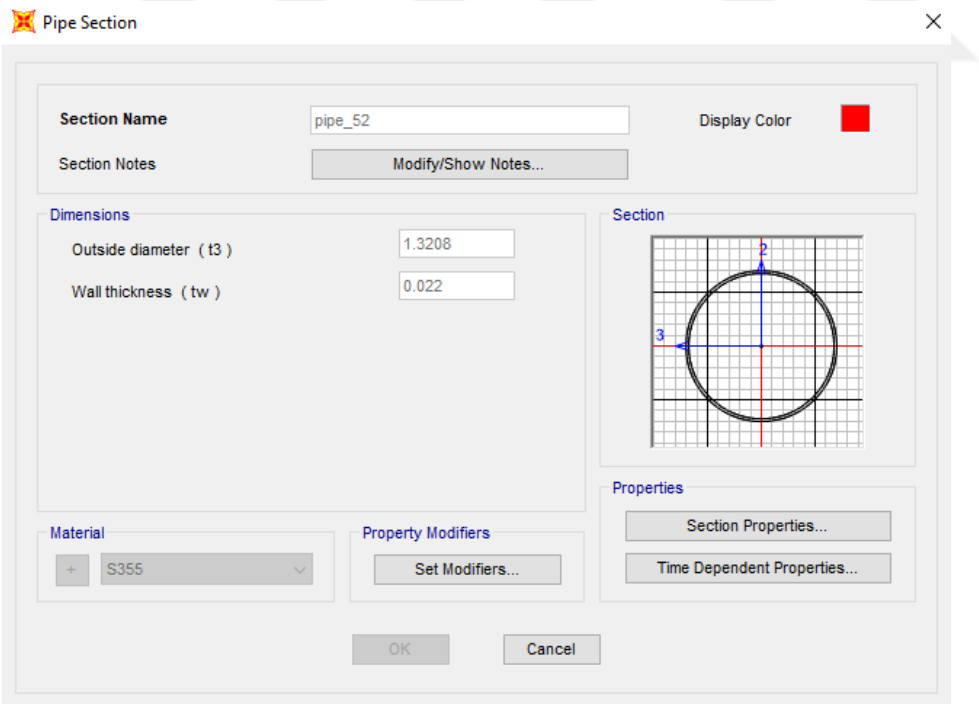

Figure 4-3 Steel pipe pile cross-section (52” 22 mm)

Table 4-3 Force-based design check – 52” 22 mm steel pipe pile

Frame	P_r (kN)	M_{rx} (kN-m)	M_{ry} (kN-m)	P_r/P_c	Total Ratio		Limit	Check
2051	-3963.8	-875.013	-1348.79	0.223	0.39	<	1	OK
1898	-3961.6	-875.17	-1348.22	0.229	0.39	<	1	OK
2083	-3940.2	-875.013	-1348.79	0.228	0.39	<	1	OK
1899	-3937.9	-875.17	-1348.22	0.227	0.38	<	1	OK
2338	-3752.0	-1085.77	-1316.66	0.217	0.39	<	1	OK

4.1.1.2 Design Check of Reinforced Concrete Pile Plug Against Axial Force and Bending Moment Internal Force Demands

To assess the reinforced concrete pile plug, the initial step involves creating an interaction diagram for each section. Subsequently, axial and moment forces are extracted from the model at the pile-to-cap connection. If the obtained values fall within the interaction diagram, it signifies that the design objective has been achieved and the structure remains within elastic limits in the event of the DD-2a earthquake. As seen below, all values in the two sections remain within the graph.

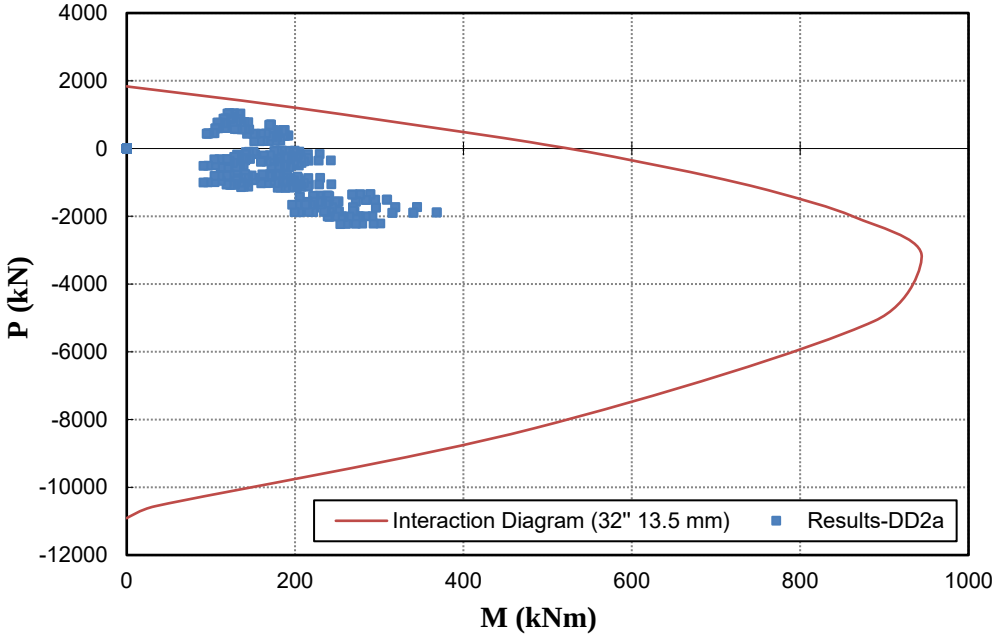

Figure 4-4 Force-based design check – 32” 13.5 mm reinf. concrete pile plug

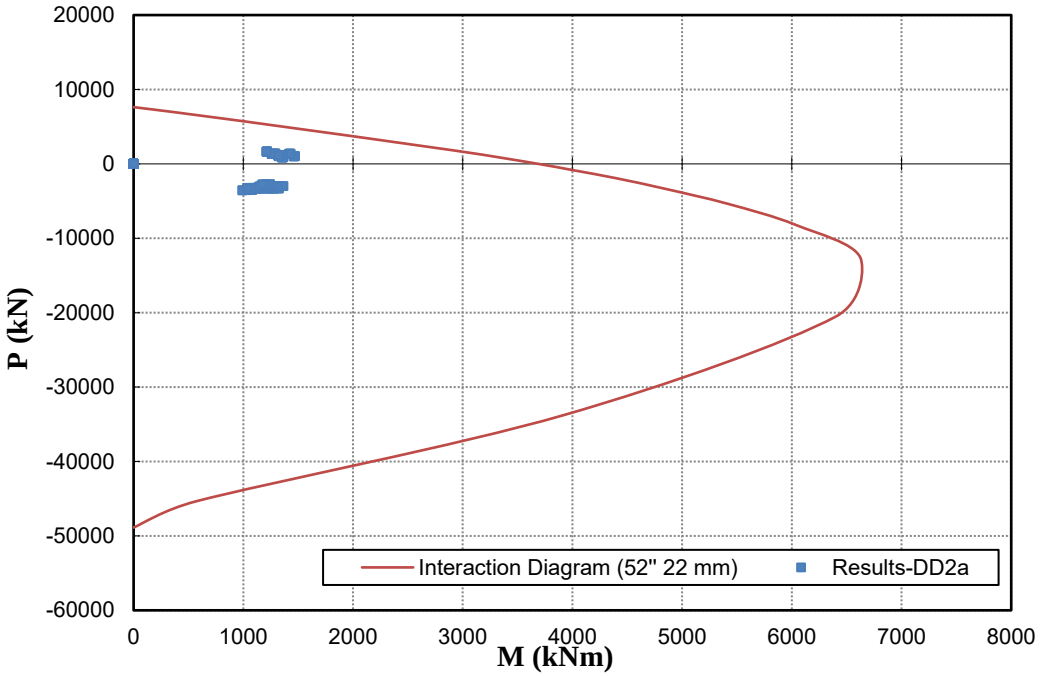

Figure 4-5 Force-based design check – 52” 22 mm reinf. concrete pile plug

4.1.2 Second Stage Analysis (DD-1 Level Earthquake)

Given that the structure selected for the thesis holds coastal port risk category 1, the initial proposed design objective in the second-stage analysis is damage control. However, for existing structures, the 11th chapter of KYLDY-2020 details that collapse prevention can also serve as a design goal in the second-stage analysis. In the calculations prepared, both collapse prevention and controlled damage limits are presented.

As indicated in Table 2-2, the analysis of the structure under the DD1 earthquake will be based on nonlinear behavior (Method 2.2), and the assessment will be conducted based on deformation criteria.

The nonlinear calculation employed the pushover analysis method, initiating the analysis by exerting force on the structure in five directions from the gravity point.

Performance points in these directions were determined using the ATC-40 method, as shown below and presented in Table 4-4.

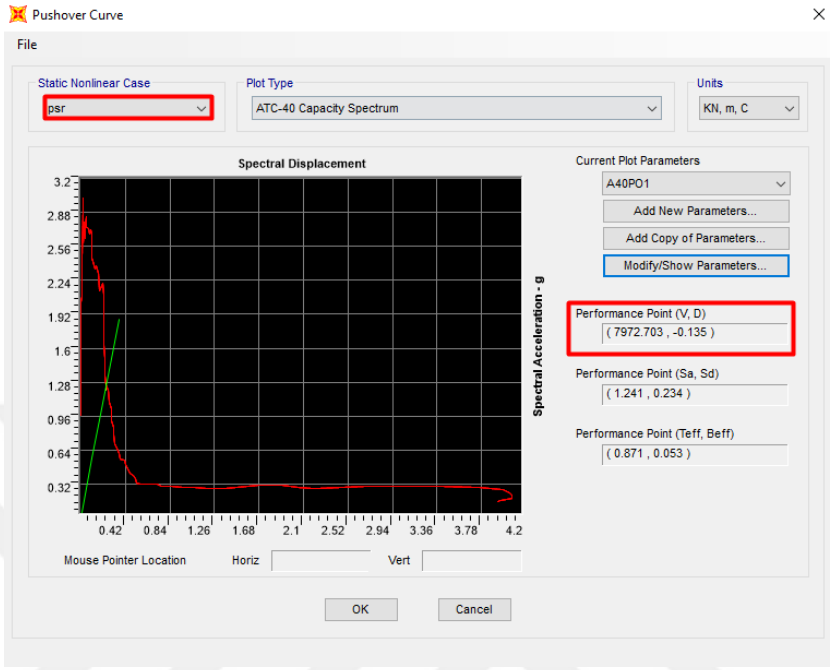

Figure 4-6 Pushover curve (+x direction)

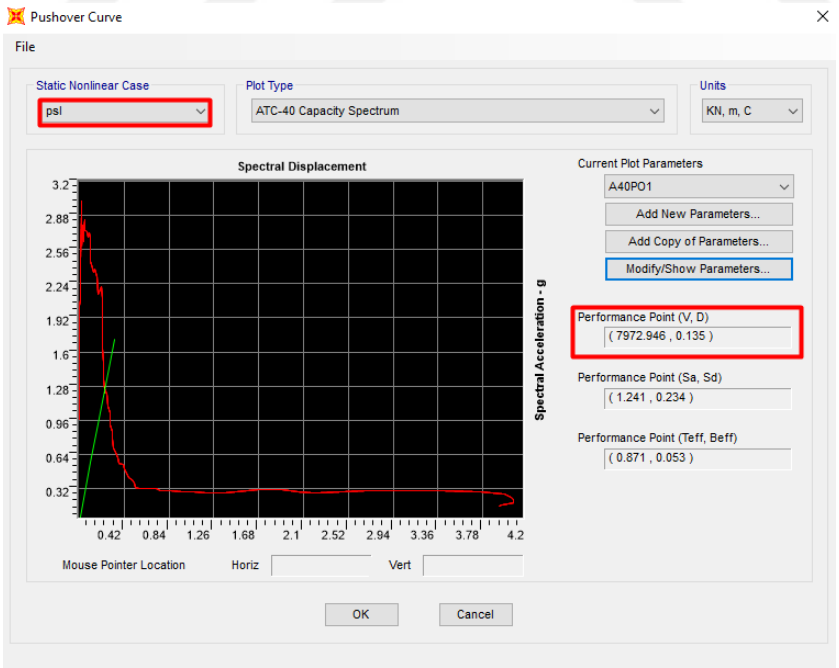

Figure 4-7 Pushover curve (-x direction)

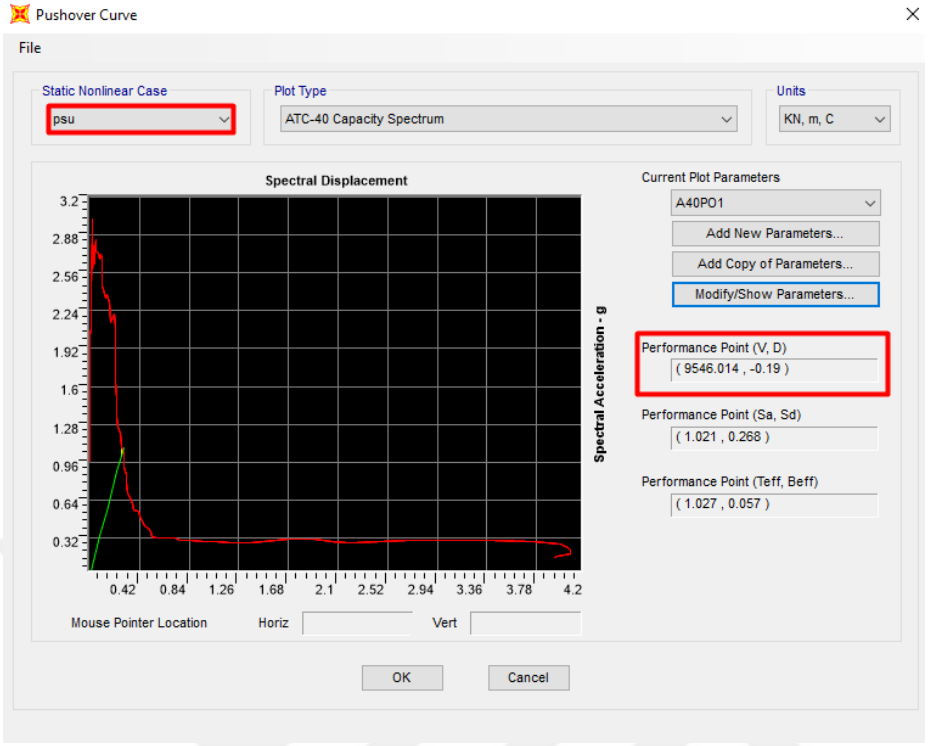

Figure 4-8 Pushover curve (+y direction)

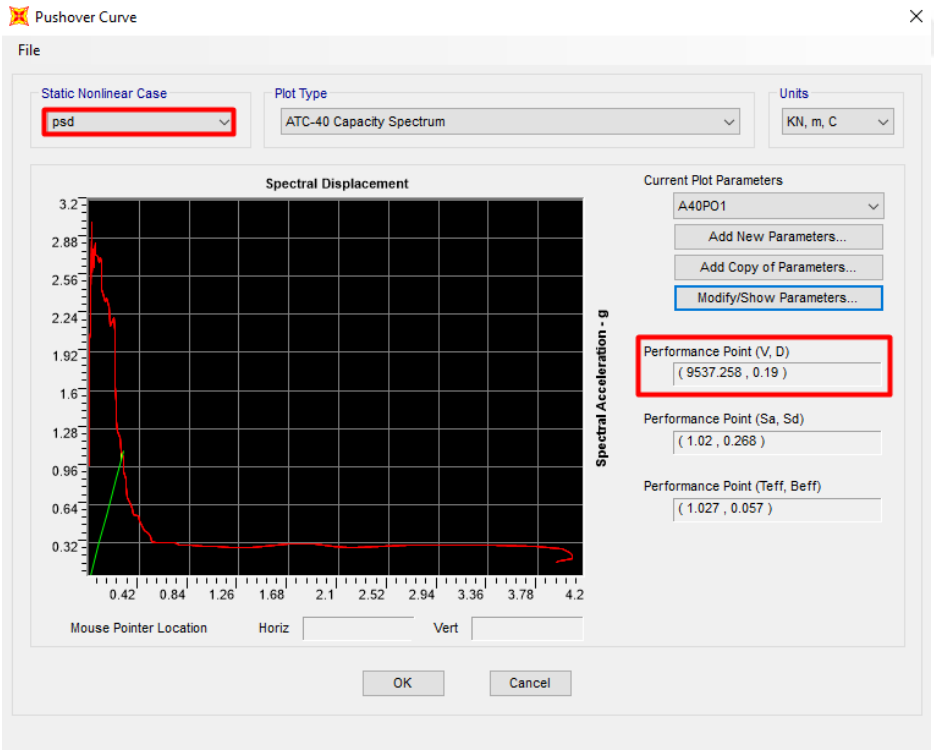

Figure 4-9 Pushover curve (-y direction)

Table 4-4 Performance points

Direction	*Shear (kN)*	*Displacement (m)*
+x	7972.703	0.135
-x	7972.946	0.135
+y	9546.014	0.190
-y	9537.258	0.190

Subsequently, the shear forces at this performance point were applied to the structure from the gravity point (see Appendix D). The assessment involved checking the pile-to-cap connection, steel pile stress, and axial pile capacity using the combinations specified in Section 3.1.3.6.

Kinematic and inertial interaction effects, considering displacements and internal forces in the piles and deck, shall be combined based on the less favorable outcome of the following two situations:

(a) The sum of 100% of the effects from kinematic interaction and 50% of the effects from inertial interaction;

(b) The sum of 100% of the effects from inertial interaction and 50% of the effects from kinematic interaction.

4.1.2.1 Demand/Capacity Curves of Steel Pipe Piles Due to Plastic Rotation

For steel piles, a cross-section will be formed, accounting for corrosion and material properties. Subsequently, an axial force-curvature diagram will be derived based on the strain limit. The verification process involved checking whether the forces obtained from the model for both 32" and 52" piles fell within the obtained diagram, as described below.

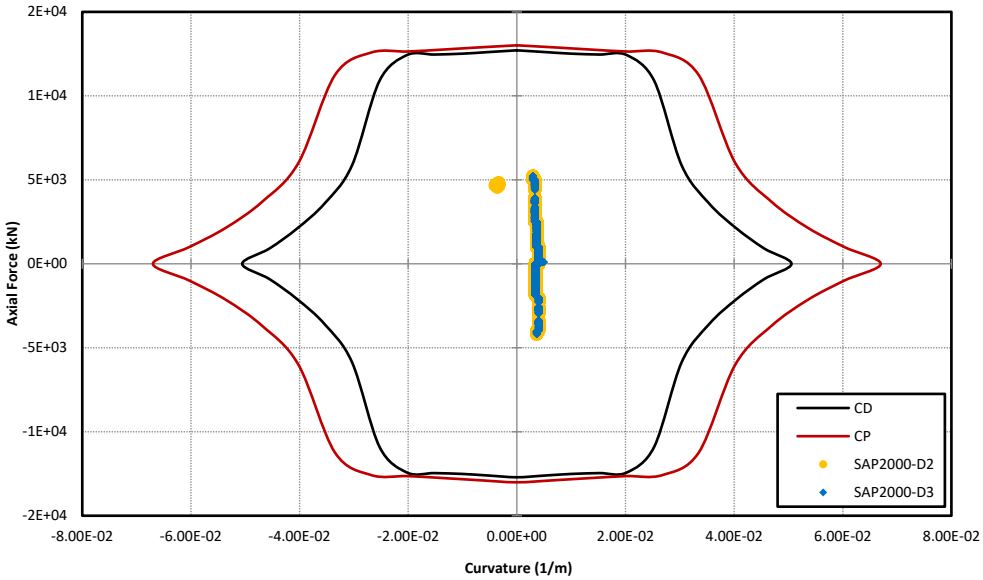

Figure 4-10 Curvature-axial force graph (32” 13.5 mm)

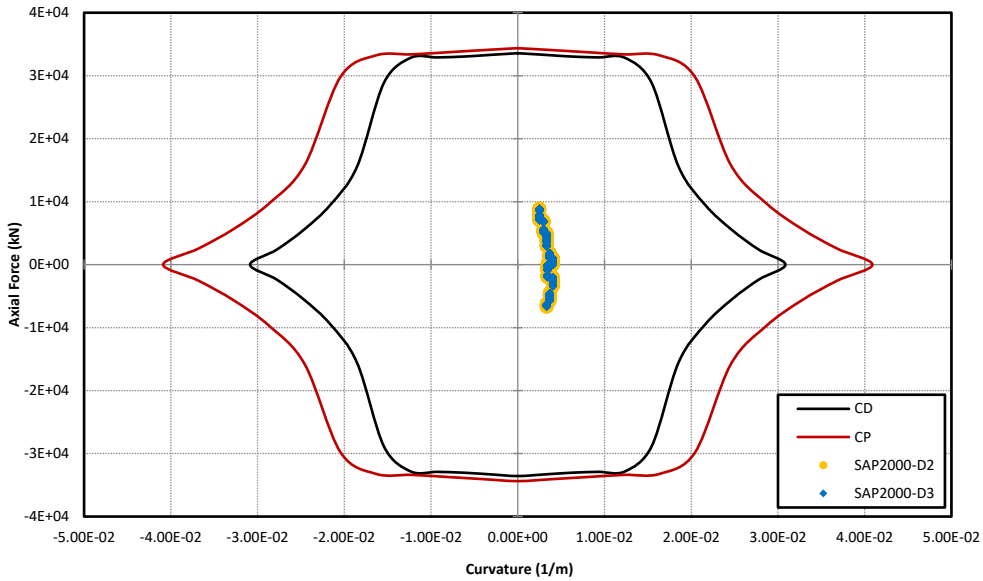

Figure 4-11 Curvature-axial force graph (52” 22 mm)

4.1.2.2 Demand/Capacity Curves of Reinforced Concrete Pile Plug Due to Plastic Rotation

One of the most vulnerable areas for system failures is reinforced concrete plugs. Consequently, the examination of pile-to-cap connections becomes crucial. Similar to steel piles, the reinforced concrete section is defined through a program. Subsequently, axial load and curvature graphs are generated according to the design targets of collapse prevention and controlled damage.

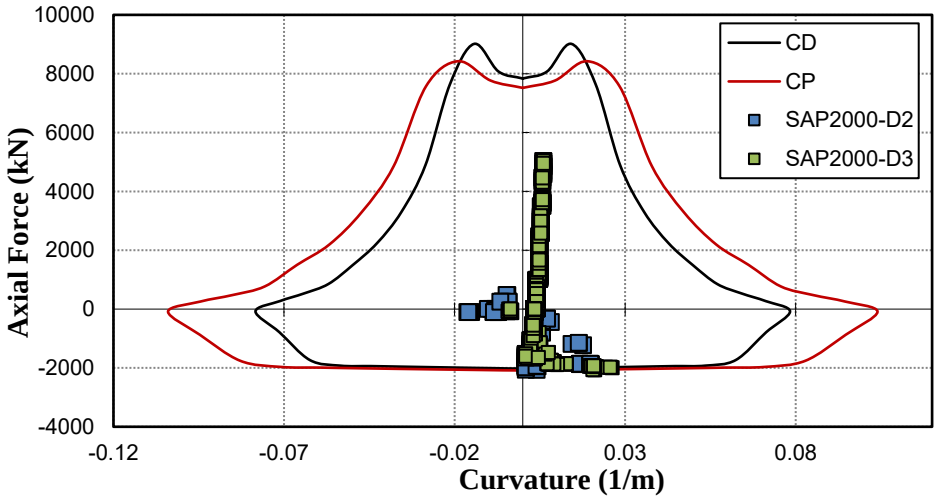

Figure 4-12 Curvature-axial force graph (32” 13.5 mm)

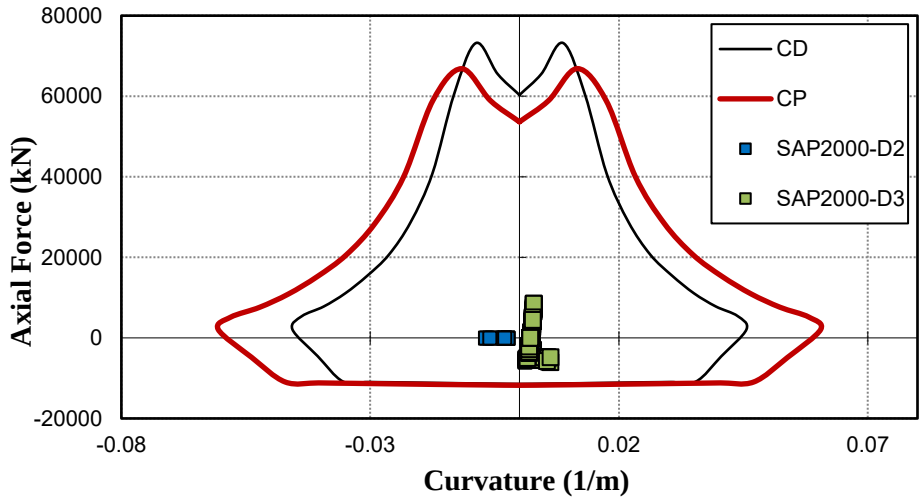

Figure 4-13 Curvature-axial force graph (52” 22 mm)

4.1.3 Static Analysis

The structure has been evaluated under combinations of Ultimate Limit State (ULS) and Serviceability Limit State (SLS) for the loads specified in Coastal Structures Planning and Design Technical Principles (2016). The results for reinforced concrete pile plug and steel pipe piles are outlined below.

4.1.3.1 Design Check of Steel Pipe Piles Against Axial Force and Bending Moment Internal Force Demands

As shown in the conventional retrofit plan, there are 32" 13.5 mm and 52" 22 mm steel piles in the project. The steel design check for these piles is given in this section, respectively.

32” 13.5 mm Steel Pipe Pile

Table 4-5 Force-based design check – 32” 13.5 mm steel pipe pile

Frame	P_r (kN)	M_{rx} (kN-m)	M_{ry} (kN-m)	P_r/P_c	Total Ratio		Limit	Check
1868	-1459.9	-18.3	-61.9	0.344	0.3762	<	1.00	OK
1869	-1459.9	-18.3	-61.9	0.344	0.3762	<	1.00	OK
1047	-1458.4	-18.3	-61.9	0.343	0.3758	<	1.00	OK
1048	-1458.4	-18.3	-61.9	0.343	0.3758	<	1.00	OK
1868	-1465.7	-18.4	-58.3	0.345	0.3758	<	1.00	OK

52” 22 mm Steel Pipe Pile

Table 4-6 Force-based design check – 52” 22 mm steel pipe pile

Frame	P_r (kN)	M_{rx} (kN-m)	M_{ry} (kN-m)	P_r/P_c	Total Ratio		Limit	Check
2289	-2384.4	-66.814	-375.13	0.138	0.1040	<	1.00	OK
2289	-2384.4	-66.814	-375.13	0.138	0.1040	<	1.00	OK
2288	-2381.4	-66.814	-375.13	0.138	0.1039	<	1.00	OK
2288	-2381.4	-66.814	-375.13	0.138	0.1039	<	1.00	OK
2340	-2358.1	-54.534	-382.01	0.136	0.1038	<	1.00	OK

4.1.3.2 Design Check of Reinforced Concrete Pile Plug Against Axial Force-Bending Moment Internal Force Demands

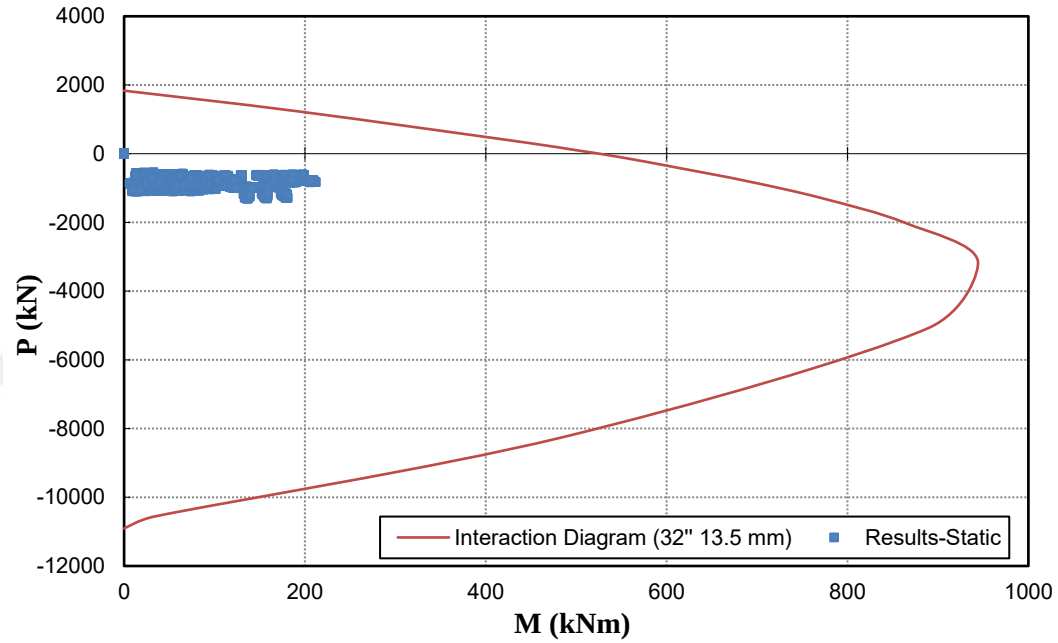

Figure 4-14 Force-based design check – 32” 13.5 mm reinf. concrete pile plug

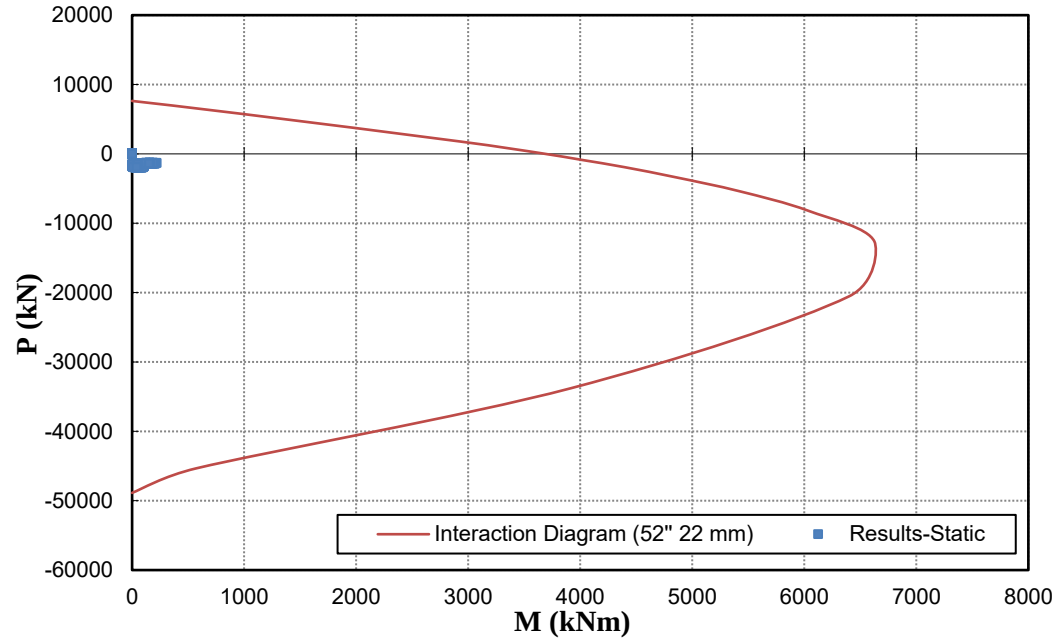

Figure 4-15 Force-based design check – 52” 22 mm reinf. concrete pile plug

4.1.4 Steel Pile Axial Capacity Calculations

The new steel piles intended for design were chosen with a diameter and wall thickness of 52" × 22 mm and a determined pile length of 45 m. The computed pile carrying capacity values exceeded the superstructure loads obtained from the analysis results, ensuring the necessary safety. In the strength calculation for the vertical load-bearing capacity of pile foundations, soil properties from geotechnical investigations and loading tests were utilized. Environmental resistance (Q_s) for static and seismic conditions was considered based on the resistance coefficients for pile foundations provided in Table 10.3 of KLYDY-2020.

The pile carrying capacity under compression conditions was verified by dividing environmental friction (compression) by the strength coefficient of 1.5 and tip resistance by the strength coefficient of 2.0. Similarly, the pile carrying capacity under tension conditions was confirmed by dividing environmental friction (tension) by the strength coefficient of 1.6.

Axial pile capacity calculation followed the guidelines of API RP 2A (2014), where axial pile capacity under compression and tension is determined using the following equations:

$$Q_c = Q_f + Q_p = fA_s + qA_p \quad \text{(Equation 4.5)}$$

$$Q_t = Q_f = fA_s \quad \text{(Equation 4.6)}$$

Where Q_f is the skin friction resistance and Q_p is the total end bearing. Based on the idealized soil profile presented in Figure 3-5, the skin friction in clay and tuff was computed for the existing piles using the formulas designed for cohesive and non-cohesive soils, respectively.

Clay:

$$p'_o = h(\gamma_{clay} - \gamma_{water}) = 57\ kN$$

$$\Psi = \frac{c}{p'_o} = \frac{100}{57} = 1.75 > 1$$

$$\alpha = 0.5\Psi^{-0.25} = 0.43$$

$$f = \alpha c = 43.445\ kPa$$

$$Q_{f,o} = fA_{s,o}h = 43.44 \times 2.553x5 = 555\ kN$$

$$Q_{f,i} = fA_{s,i}h = 43.44 \times 2.469x5 = 536\ kN$$

Tuff:

$$p'_o = h(\gamma_{clay} - \gamma_{water}) = 172\ kN$$

$$f = Kp'_o tan\delta = 0.8 \times 172 \times 0.7 = 96.35\ kPa$$

$$Q_{f,o} = fA_{s,o}h = 96.35 \times 2.553x18 = 4428\ kN$$

$$Q_{f,i} = fA_{s,i}h = 96.35 \times 2.469x18 = 4282\ kN$$

As the pile tip remains in tuff, the formula for tip resistance in cohesionless soils is applied. The tip resistance is then multiplied by the tip area to determine the capacity. If the tip capacity exceeds the sum of the inner shaft frictions calculated earlier, indicating no plugging, the tip resistance is considered solely from the pile shaft area. However, if the internal shaft friction exceeds the tip capacity, resistance is computed from the pile tip area, indicating plugging.

$$Q_p = p'_o N_q A_p = 262 \times 50 \times 0.519 = 6797.2\ kN$$

$$\sum Q_{f,i} = 536 + 4282 = 4818\ kN$$

$$\sum Q_{f,i} < Q_p \rightarrow There\ will\ be\ no\ plugging.$$

$$Q_{f,i} = fA_{s,i}h = 96.35 \times 2.469x18 = 4282\ kN$$

$$Q_{p,s} = 0.034 \times 13100 = 444.08\ kN$$

Thus, the capacities of the shaft area for each layer and the pile tip were calculated. As described earlier, the axial capacities obtained by dividing the strength

coefficients for compression and tension situations are summarized for all piles in the table below.

Table 4-7 Axial capacities for steel piles

Pile	*Compression*	*Tension*
32” 13.5 mm	6755.66	6325.27
52” 22 mm	10398.52	9218.43

SAP2000 outputs showing the axial loads occurring under DD-1 earthquake, DD-2a earthquake and static conditions are given below. The results from the SAP2000 models reveal that the most critical axial load occurred during the DD-1 earthquake. It is evident that all piles can safely support the resulting axial loads.

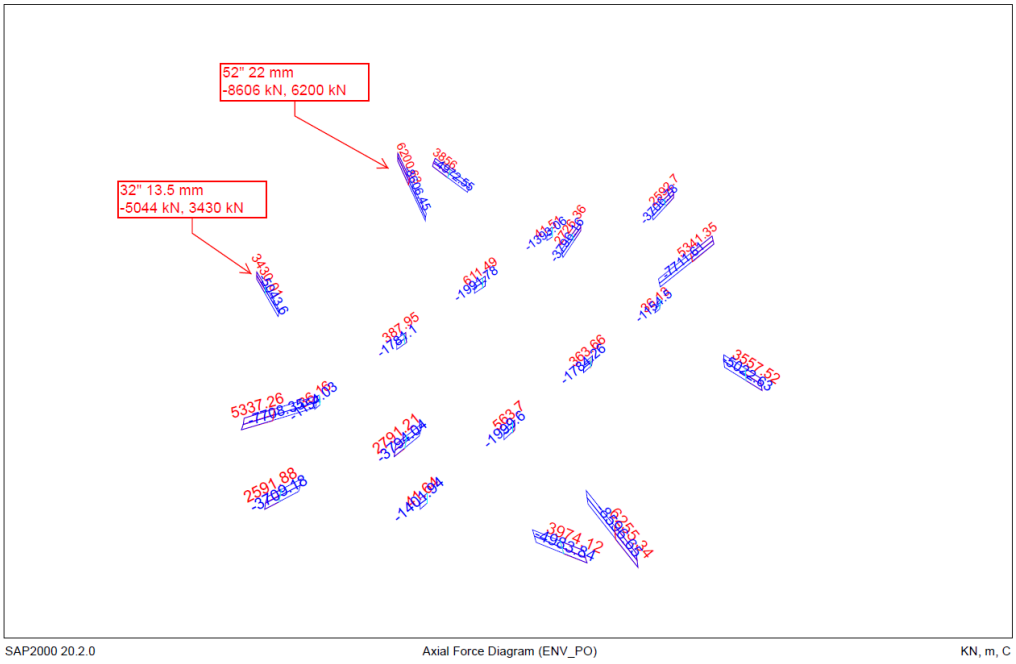

Figure 4-16 Axial force diagram (DD-1)

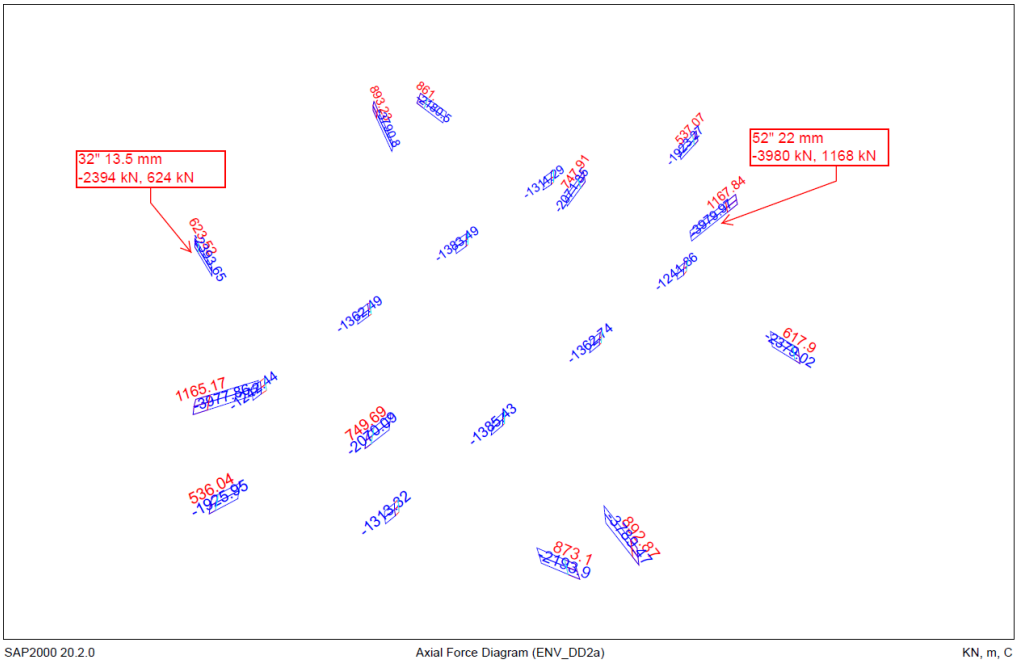

Figure 4-17 Axial force diagram (DD-2a)

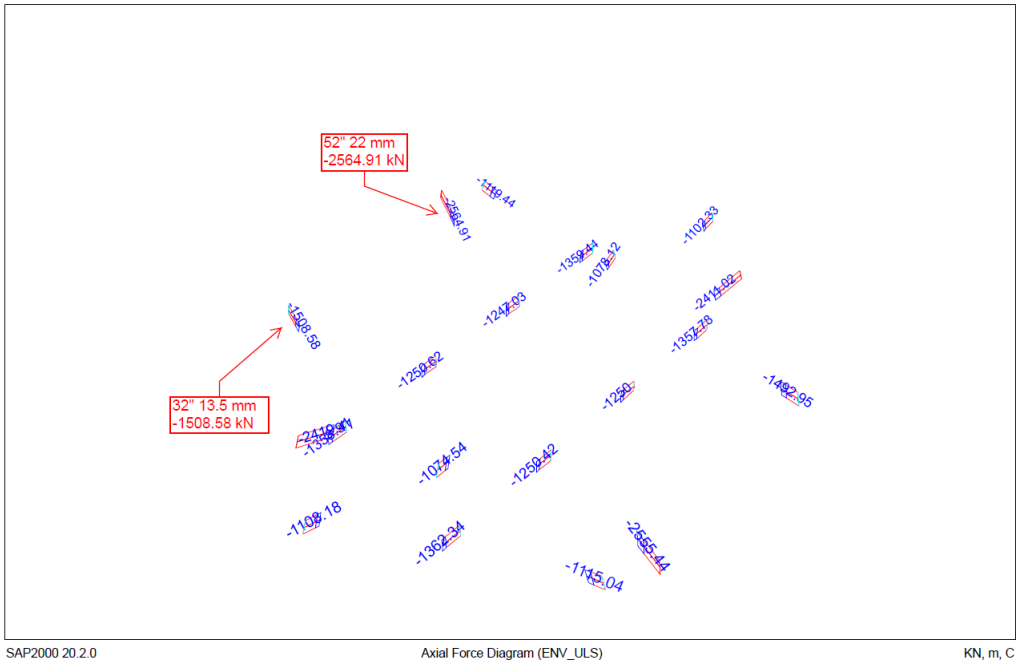

Figure 4-18 Axial force diagram (static)

4.2 Lead Rubber Bearing Retrofit

Before proceeding to the modeling and analysis stage, it is essential to design the lead rubber bearing. The step-by-step design calculation is outlined below.

Table 4-8 Input data

Data	
Seismic Weight	21000 kN
Number of bearings	8 pcs
Yield stress of the lead	10 MPa
Shear modulus of the elastomer	1 MPa
Rubber hardness coefficient	0.75
Target period	1.90 s
Design displacement	366 mm
F_Q/W	0.08

- The target period is determined as 1.90 seconds. The effective stiffness will be calculated using Equation 2-1.

$$1.90 = 2\pi\sqrt{\frac{2625}{K_{eff} \times 9.81}} \rightarrow K_{eff} = 2.926\ kN/mm$$

- The post-yield and elastic stiffnesses are obtained using Equation 2-2 and Equation 2-3.

$$2.926 = K_2 + 210/366 \rightarrow K_2 = 2.354\ kN/mm$$

$$K_1 = 10 \times 2.354 \rightarrow K_1 = 23.54\ kN/mm$$

- The yield displacement is calculated as below. In the preliminary design, the characteristic strength was assumed to be equal to the yield strength.

$$D_y = \frac{210}{23.54} = 8.92\ mm$$

- Effective damping ratio and damping scale factor are determined with following calculations.

$$\beta_{eff} = \frac{4}{2\pi}\frac{210 \times (366 - 8.92)}{2.926 \times 366^2} = 0.12$$

$$\eta = \sqrt{\frac{10}{5 + 12.1}} = 0.764$$

- The design displacement is calculated using Equation 2-7. Iterative calculations continue until the selected target displacement in the initial stage aligns with the value derived from Equation 2-7.

$$S_{ae}{}^{DD-1}(T) = 0.412$$

$$D = 1.3 \times \frac{9.81}{4\pi^2} \times 1.90^2 \times 0.764 \times 0.412 = 366.915\ mm$$

- The size of the isolator calculated using Equation 2-8 to Equation 2-10.

$$210 = A_p \times 10 \rightarrow A_p = 21000\ mm^2$$

$$B_L = \sqrt{\frac{4 \times 21000}{\pi}} = 163.52\ mm$$

$$2.354 = 1 \times \frac{A_r}{220} \rightarrow A_r = 517862.34\ mm^2$$

$$517862.34 = \frac{\pi}{4} \times (B^2 - 163.52^2) \rightarrow B = 839.1\ mm$$

$$\frac{839.1}{80} \leq t \leq \frac{839.1}{40} \rightarrow t = 15\ mm$$

Table 4-9 Properties of the selected lead rubber bearing (LRB-S 850)

Property	Value
K_v (kN/mm)	1901.00
K_{eff} (kN/mm)	1.93
F_y (kN)	300
K_2 (kN/mm)	1.875
β_e	27%

The properties of the isolator selected according to the preliminary design from the manufacturer's catalogue and processed into the SAP2000 model, are given in Table 4-9. The rubber isolator tool in SAP2000 was used to define the lead rubber bearing (Figure 4-19).

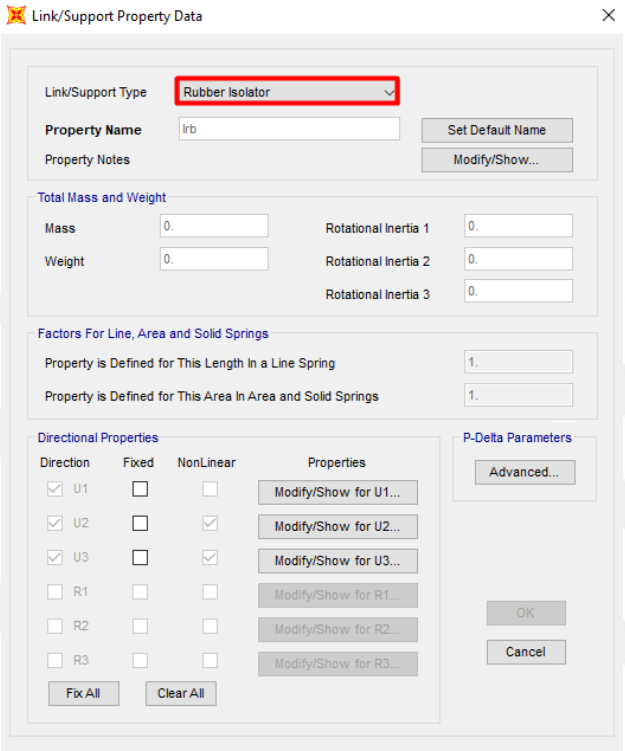

Figure 4-19 Rubber isolator tool

4.2.1 First Stage Analysis (DD-2a Level Earthquake)

It is observed that the retrofitted structure does operate within elastic limits under the DD2-a earthquake. Thus, the analysis of the structure carrier system will be based on linear behavior (Method 1) and the force-based evaluation and design approach will be applied for the design. The three-dimensional model view is given below.

Modal properties of the dolphin in X and Y directions are given in Table 4-10. As can be seen in the table, the total mass participation ratio is more than 95% in accordance with KYLDY-2020.

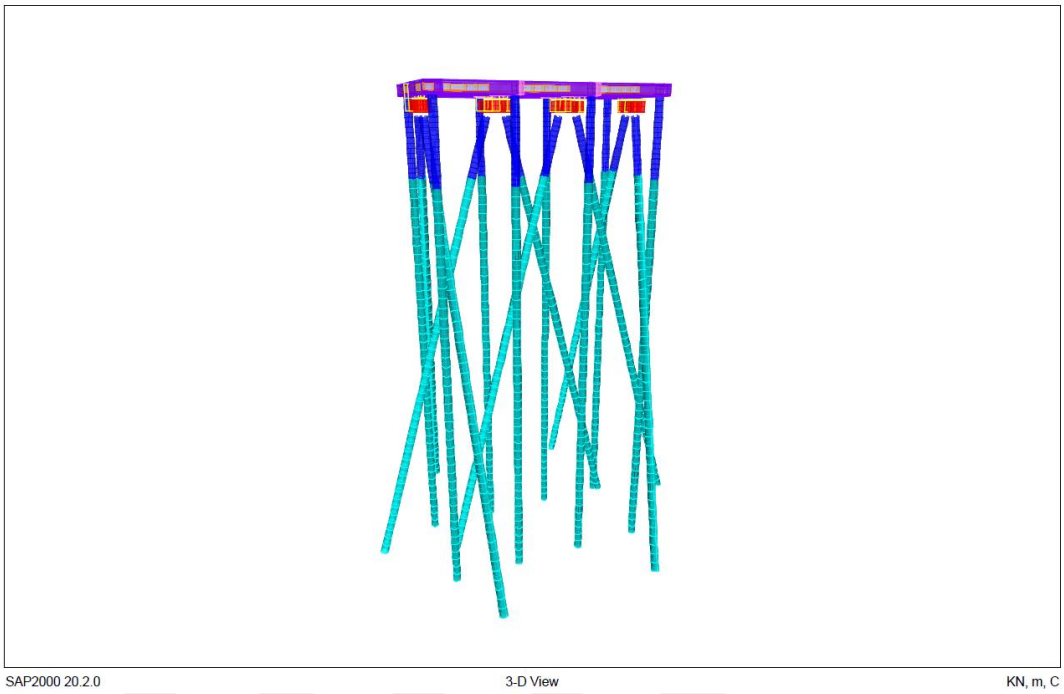

Figure 4-20 Lead rubber bearing retrofit model view

Table 4-10 Modal properties of the dolphin

Mode Number	*Period*	*mx*	*my*
1	1.759	4.01E-01	4.70E-01
2	1.624	4.70E-01	4.02E-01
.	.	.	.
.	.	.	.
60	0.014	0.02201	0.00084
Total	-	0.97182	0.97116

Pile-to-cap connection and steel pipe pile control of existing piles are given below. As can be seen, steel piles show successful performance under the DD-2a earthquake.

Table 4-11 Force-based design check – 32” 13.5 mm steel pipe pile

Frame	P_r (kN)	M_{rx} (kN-m)	M_{ry} (kN-m)	P_r/P_c	Total Ratio		Limit	Check
1304	-3220.10	-135.80	-416.30	0.754	0.976	<	1.00	OK
1150	-3219.80	-136.30	-416.30	0.754	0.976	<	1.00	OK
1305	-3200.60	-135.80	-416.30	0.749	0.971	<	1.00	OK
1458	-3142.90	-154.20	-435.90	0.736	0.970	<	1.00	OK
1151	-3200.30	-136.30	-416.30	0.749	0.971	<	1.00	OK

Reinforced concrete plugs were checked under two conditions: using measured material properties and using reduced material properties. As can be seen in Figure 4-21, with reduced strengths, the elastic limit is exceeded. However, since it is clear that the structure operates under elastic limits, the second method, the deformation-based method, has not been used.

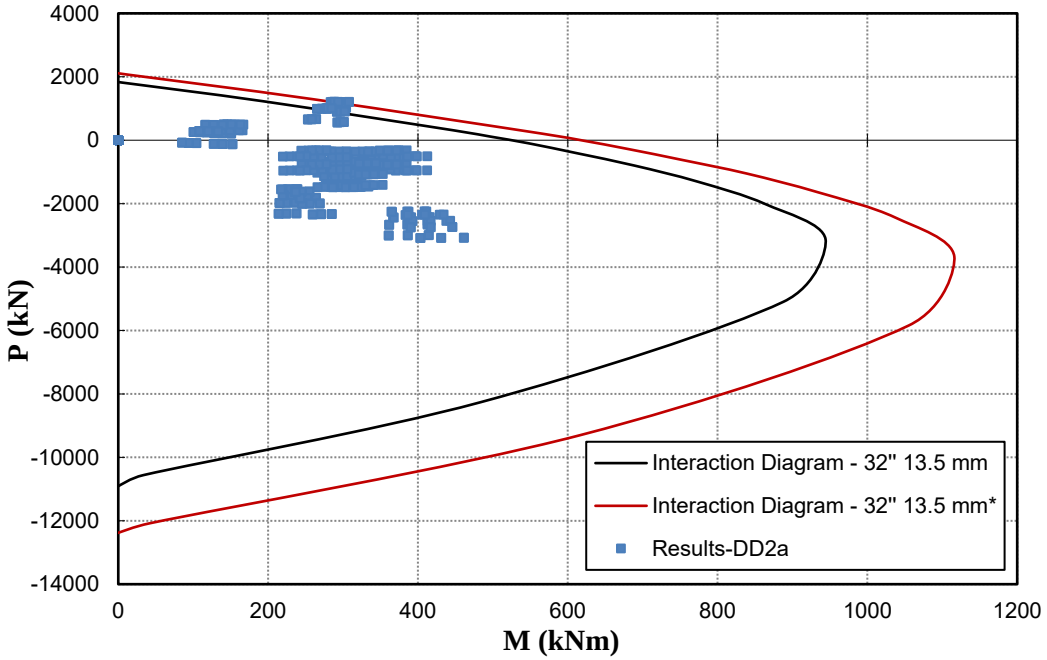

Figure 4-21 Force-based design check – 32” 13.5 mm reinf. concrete pile plug

4.2.2 Second Stage Analysis (DD-1 Level Earthquake)

As in conventional retrofit, the push-over method was used as DD-1 analysis in this model. ATC-40 graphs and performance points are given in the figures below.

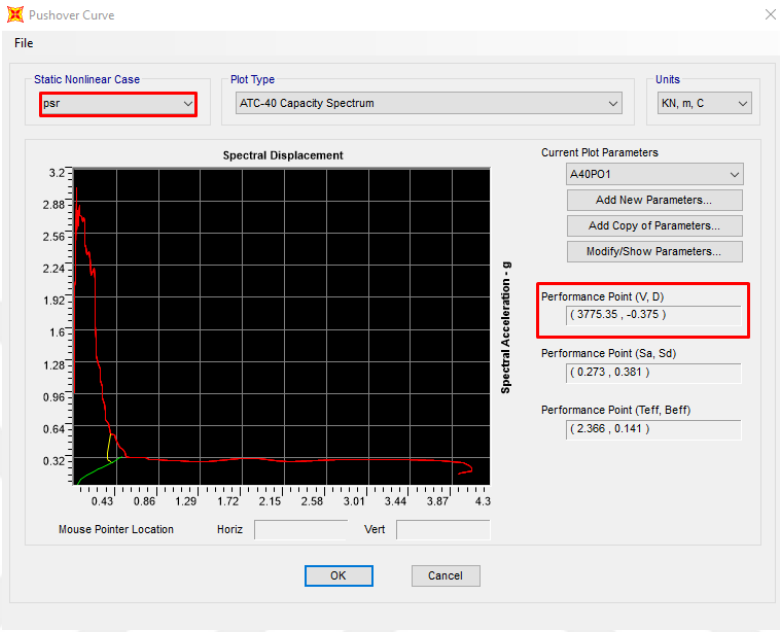

Figure 4-22 Pushover curve (+x direction)

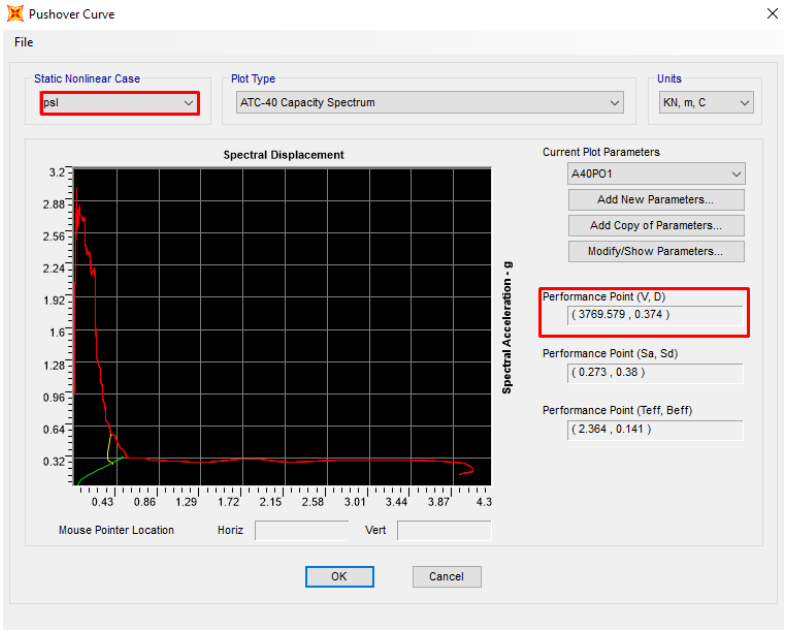

Figure 4-23 Pushover curve (-x direction)

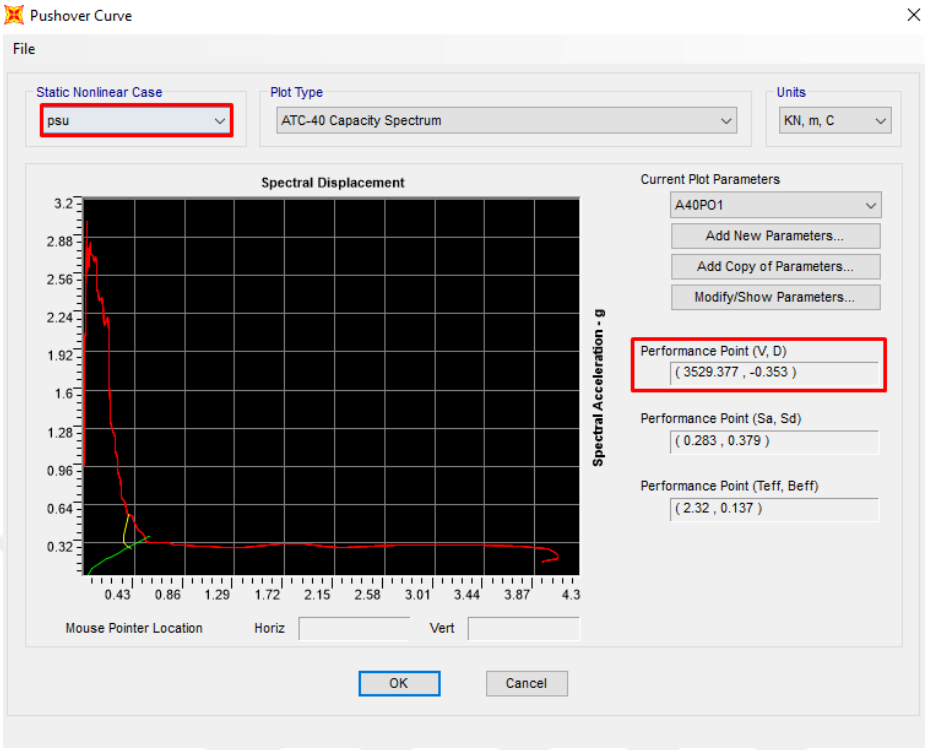

Figure 4-24 Pushover curve (+y direction)

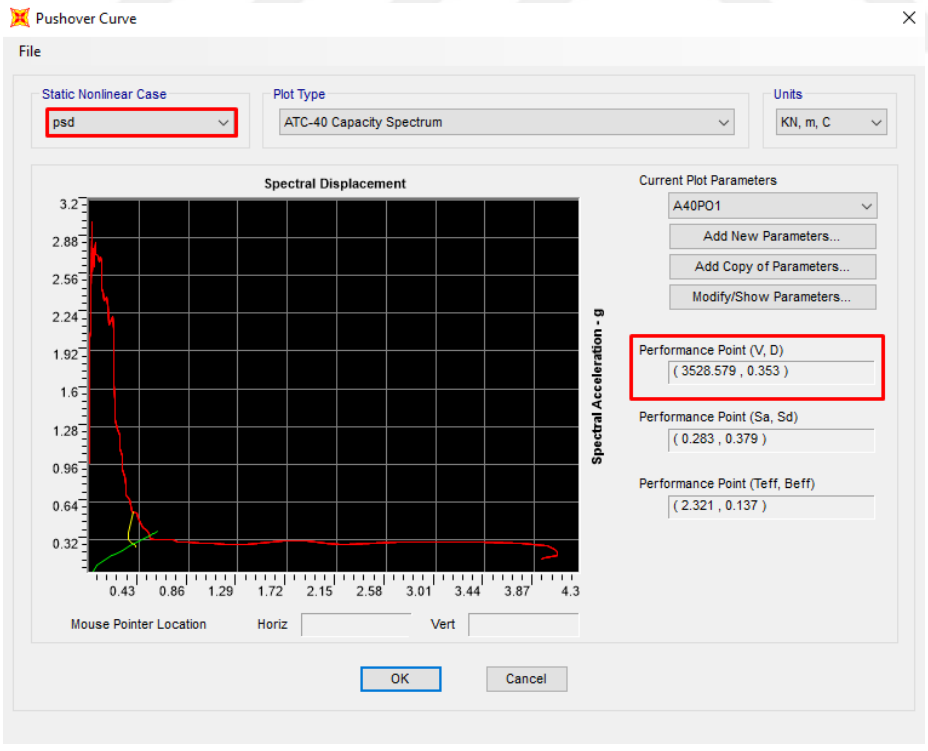

Figure 4-25 Pushover curve (-y direction)

Table 4-12 Performance points

Direction	*Shear (kN)*	*Displacement (m)*
+x	3775.35	0.375
-x	3769.579	0.374
+y	3529.377	0.353
-y	3528.579	0.353

The section controls are given below. It is evident that the piles demonstrate successful performance during the DD-1 earthquake event.

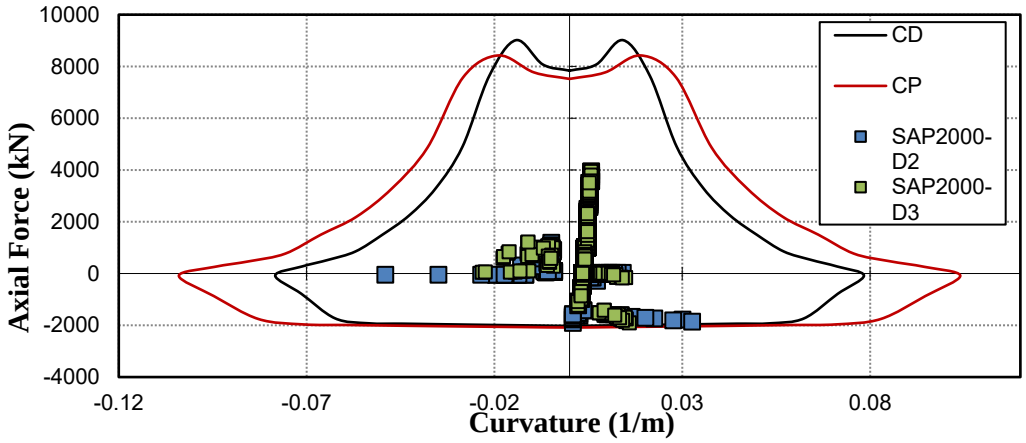

Figure 4-26 Curvature-axial force graph (32” 13.5 mm)

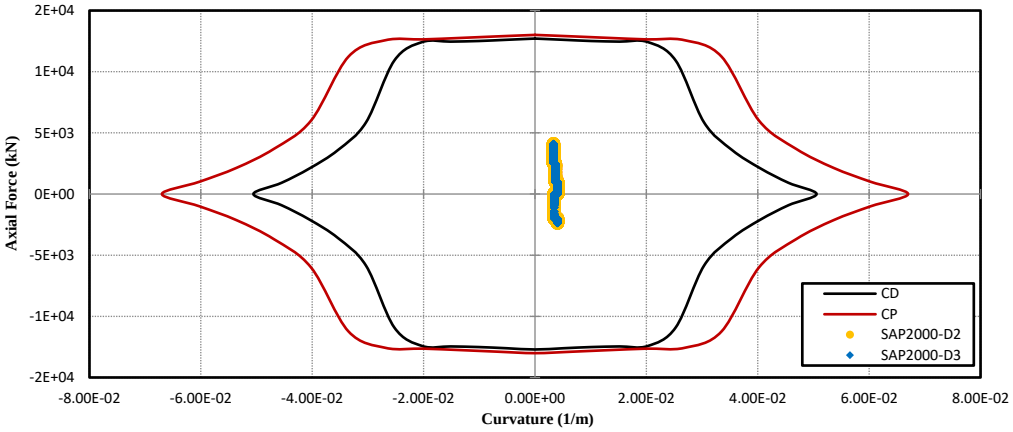

Figure 4-27 Curvature-axial force graph (32” 13.5 mm)

The unit deformation and vertical stability of the isolators used in the system must be controlled and must remain within the limits specified by the regulation. The shear strain control under the DD-1 earthquake based on Section 2.1.2 is given below.

- Shear strain caused by compression:

$$\gamma_{c,st} = \frac{6 \times 14 \times 1621}{567450.17 \times 1180} = 0.20$$

$$\gamma_{c,E} = \frac{6 \times 14 \times 4511}{278584.97 \times 1180} = 1.39$$

- Shear strain resulting from the relative rotation:

$$\gamma_{r,st} = \frac{850^2 \times 0.0176}{2 \times 15 \times 220} = 1.90$$

- Shear strain caused by horizontal displacement:

$$\gamma_{s,E} = \frac{413}{220} = 1.8773$$

Calculations regarding vertical stability are below.

- Critical buckling load in case of no horizontal displacement:

$$P_{cr} = 0.218 \times \frac{1 \times 850^4}{15 \times 220} \times \frac{(1 - \frac{175}{850})(1 - \frac{175^2}{850^2})}{1 + 175^2/850^2} = 25157.28\ kN$$

- Critical buckling load in case of horizontal displacement:

$$P_{cr}' = 25157.28 \times (230748.79/567450.17) = 10229.99\ kN$$

- Axial load capacity due to strain:

$$P_{str} = \frac{3.5 \times 230748.79 \times 1180}{6 \times 14} = 11345.15\ kN$$

- Axial load capacity under vertical loads only:

$$P_{str} = \frac{3.5 \times 567450.17 \times 1180}{6 \times 14} = 27889.63\ kN$$

The compliance of these calculated values with the regulation has been checked in the table below.

Table 4-13 Lead rubber bearings - results

	Result	*Limit*	*Check*
$\gamma_{c,st}$	0.2034	≤ 3.5	OK
$\gamma_{c,st}+\gamma_{s,st}+\gamma_{r,st}$	2.1300	≤ 5	OK
$\gamma_{c,E}+\gamma_{s,E}+0.5\gamma_{r,st}$	4.2323	≤ 6	OK
$\gamma_{S,E}$	1.8773	≤ 2	OK
$\min(P_{cr},P_{str})/P_{K1}$	6.9389	≥ 2	OK
$\min(P'_{cr},P_{str})/P_{K2}$	1.8333	≥ 1.1	OK

4.2.3 Static Analysis

Steel pipe pile design control under static loads are given below. As can be seen from the results, all limits are met in the static case. It is seen that a good amount of capacity is used in steel piles.

Table 4-14 Force-based design check – 32” 13.5 mm steel pipe pile

Frame	**P_r (kN)**	**M_{rx} (kN-m)**	**M_{ry} (kN-m)**	**P_r/P_c**	**Total Ratio**		**Limit**	**Check**
535	-2394.4	-94.7	9.6	0.564	0.612	<	1.00	OK
536	-2394.4	-94.7	9.6	0.564	0.612	<	1.00	OK
484	-2399.2	-87.7	-30.3	0.565	0.612	<	1.00	OK
485	-2399.2	-87.7	-30.3	0.565	0.612	<	1.00	OK
535	-2392.7	-89.6	8.9	0.563	0.609	<	1.00	OK

The results from the analysis model in the interaction diagram are as follows. Given that the selected platform lacks berthing and mooring forces, which are crucial in static situations, earthquake analyses emerge as more critical than static conditions.

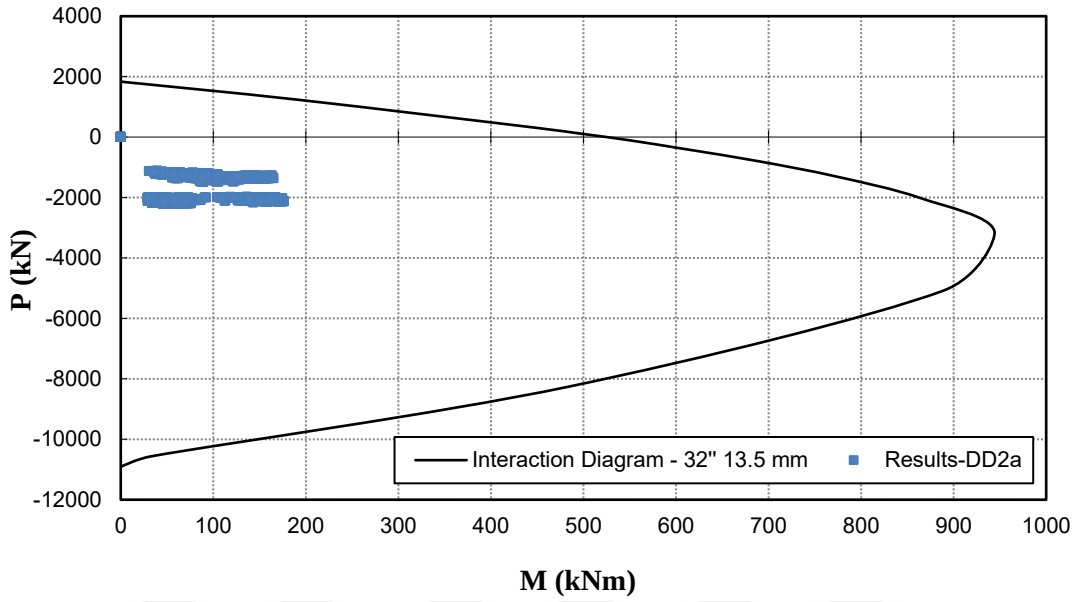

Figure 4-28 Force-based design check – 32” 13.5 mm reinf. concrete pile plug

The axial load capacity of the existing piles is calculated as 6755.66 kN in compression and 6325.25 kN in tension, as given in Table 4-7. As can be seen below, axial load capacity is sufficient.

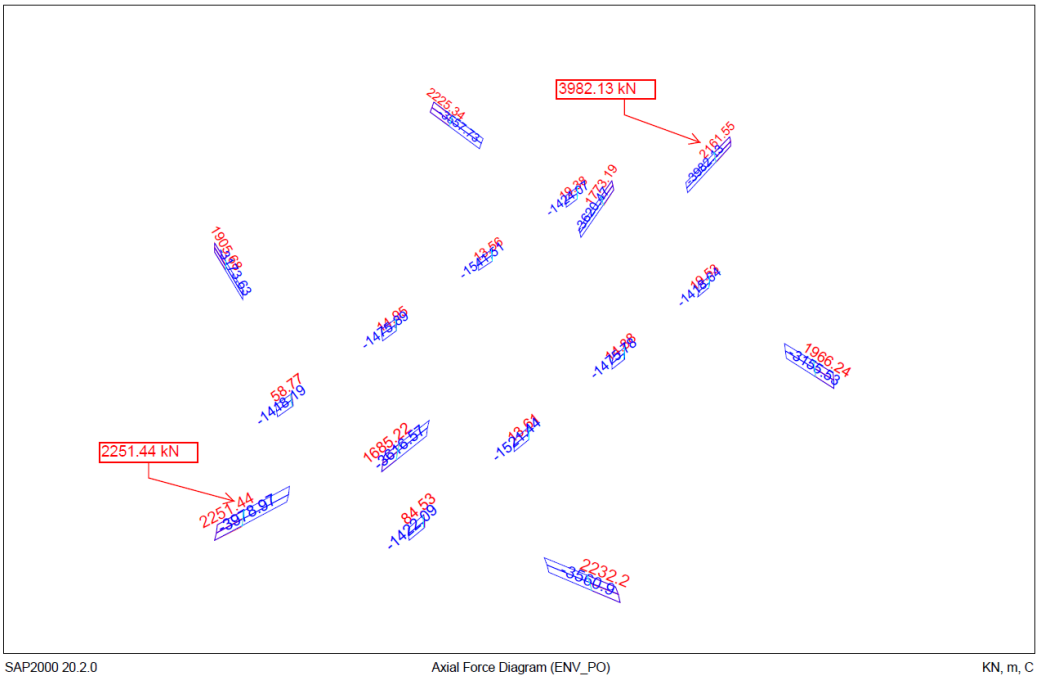

Figure 4-29 Axial force diagram (DD-1)

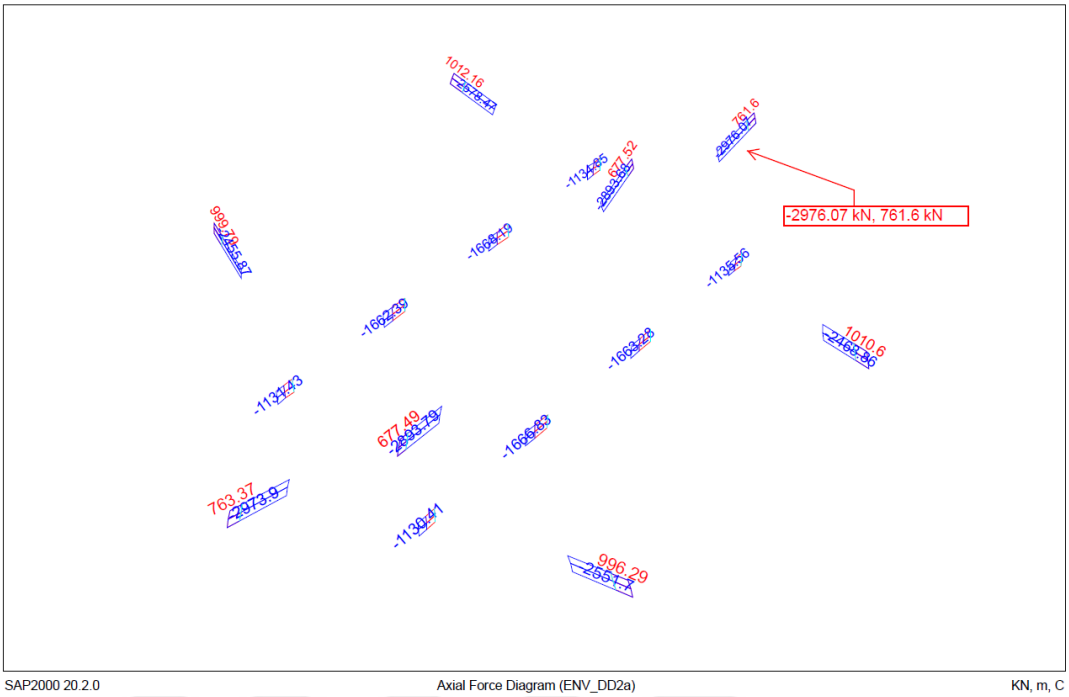

Figure 4-30 Axial force diagram (DD-2a)

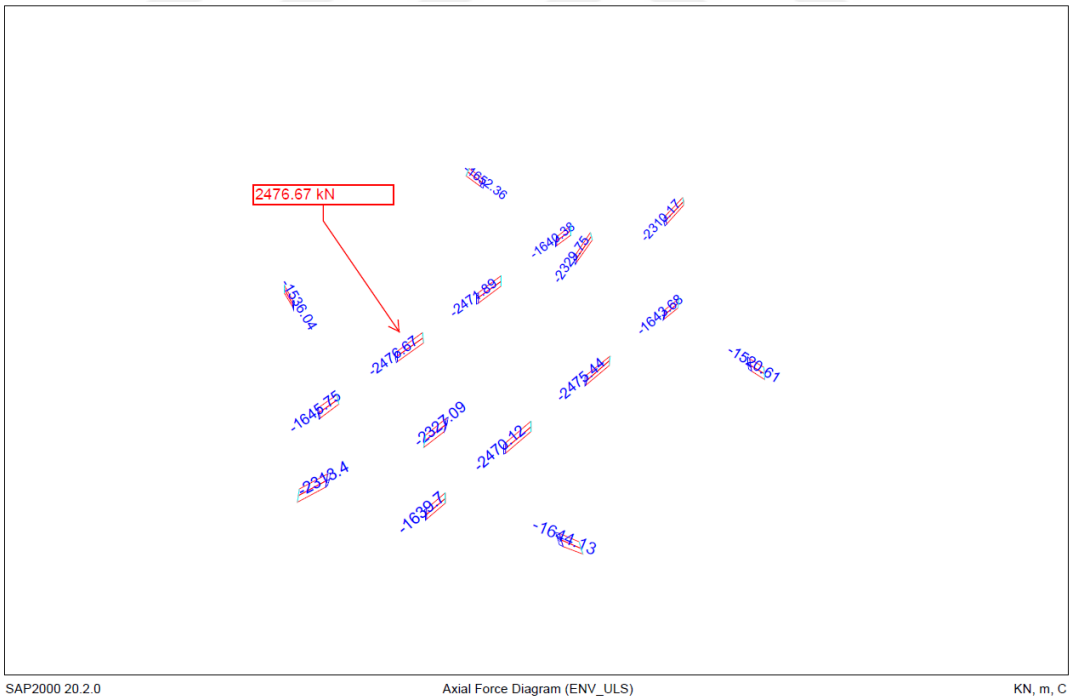

Figure 4-31 Axial force diagram (static)

4.3 Comparison of Retrofit Plans

The period of the existing structure without any retrofitting was determined to be 0.9 seconds. In conventional and lead rubber bearing retrofit models, the periods were obtained as 1.236 s and 1.759 s, respectively. The corresponding acceleration values in the earthquake spectra for these periods are illustrated in Figure 4-32. It is evident that the acceleration value is lower when a longer period is achieved in the retrofit with seismic isolators. The shear forces obtained from the ATC-40 graph in the DD-1 earthquake analysis align with this observation. Specifically, the shear forces in the conventional retrofit are nearly two times higher than those in the lead rubber bearing retrofit.

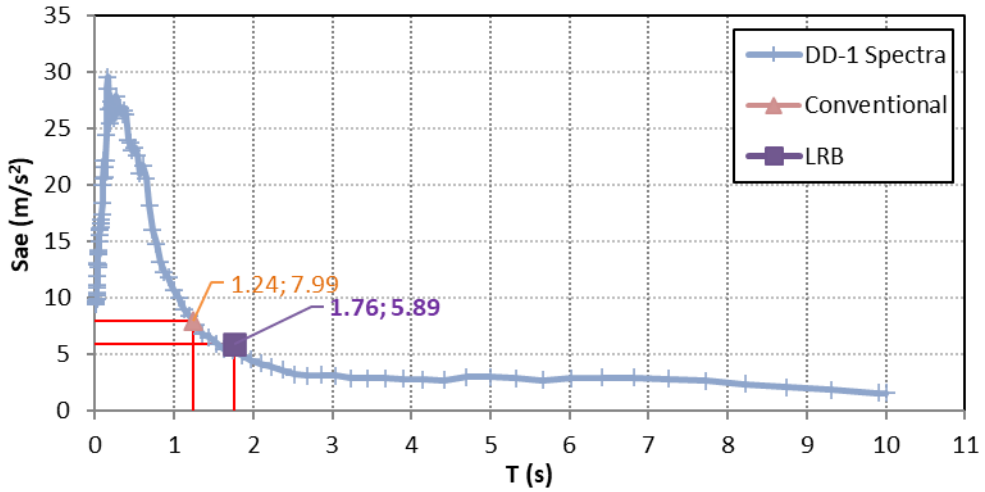

Figure 4-32 DD-1 Earthquake level period-acceleration comparison

Table 4-15 Comparison of performance points

	Direction	*Conventional*	*LRB*	*Change*
Shear force	*+x*	*7972.703*	*3775.35*	-52.65%
Shear force	*-x*	*7972.946*	*3769.579*	-52.72%
Shear force	*+y*	*9546.014*	*3529.377*	-63.03%
Shear force	*-y*	*9537.258*	*3528.579*	-63.00%

As evident from the comprehensive calculations and results, the implementation of lead rubber bearings for strengthening exhibits greater efficacy in seismic performance. Nevertheless, cost analysis in civil engineering plays a crucial role in method selection. Below are the illustrated methodologies and cost calculations conducted for the two methods.

Method-1 (Conventional Retrofitting)

In this method, the first thing to do during the construction phase is to remove the superstructure, as piles will need to be driven over the platform. After the mobilizations are completed, the upper parts of the areas where additional piles will be driven for reinforcement preparations will be cut at a depth of 10-15cm with a joint cutting machine, according to the project. Then, this area will be broken with crushers and the debris from the crushing will be transported out of the port.

In this method, the initial step during the construction phase involves removing the superstructure, as piles will need to be driven over the platform. Once mobilization is complete, the upper portions of the areas designated for additional pile driving, as part of reinforcement preparations, will be cut to a depth of 10-15 cm using a grooving machine, in accordance with the project. Subsequently, this area will be fragmented using crushers, and the debris resulting from the crushing process will be transported away from the platform.

Figure 4-33 Cutting the designated area to a depth of 10-15 cm using a grooving machine and clearing away the debris

The cutting will be done with a concrete cutting machine with diamond socket wire. The cut pieces will be transported to a suitable place and stacked.

Figure 4-34 Cutting and transporting concrete

The prepared steel pipe piles will be positioned and driven into place using a Delmag 46 diesel hammer.

Figure 4-35 Positioning and driving steel pipe piles

Along with pile driving, reinforced concrete manufacturing will begin in accordance with the project. Φ40mm hanger shafts, NPU 300 steel profiles, wood of various sizes, and 22 mm thick film-coated plywood will be used to create the base mold. Once the base formwork is completed, the prepared pile reinforcement will be suspended from the pile head. Upon ensuring the designated space between the pile edge and the reinforcement, concrete will be poured into the pile.

Figure 4-36 Making the base mold, pouring the pile concrete and planting sprouts with epoxy

Then, sprout planting and roughening will be done to integrate the old concrete with the new reinforced concrete section. After the sprouts have settled, rebar will be installed, and the superstructure construction will be finalized by pouring concrete.

Figure 4-37 Rebar installation and concrete pouring

Method-2 (Lead Rubber Bearing Retrofit)

In this method, as no operations will be conducted on the platform, several procedures outlined in the first method will not be implemented. Instead, all operations will be conducted beneath the deck. The initial step will involve preparing reinforcement for constructing new sub-cap beams and piles by setting up formwork underneath the existing cap beams.

Once the reinforcement is positioned, concrete will be poured. Subsequently, shoring will be installed to support the deck in the area where the lead rubber bearings are to be placed, as the piles will require cutting. After securing the deck, the piles will be cut accordingly. Then, the lead rubber bearings will be installed, and the strengthening process will be completed.

Based on the methodologies outlined above, the work items can be divided into three for the first method and four for the second method. The work items and their approximate costs are provided comparatively in the table below.

Table 4-16 Cost summary

Item	**Method-1**	**Method-2**
Deck Demolition	57,660	-
Batter Pile Cutoff	-	640,000
New Pipe Piles	9,500,750	-
Shoring	-	880,000
New Superstructure	681,590	223,515
LRB Installation	-	640,000
Total	**10,240,000.00 TL**	**2,383,515.00 TL**

CHAPTER 5

CONCLUSION AND RECOMMENDATIONS

5.1 Conclusion

The poor performance of battered pile systems in earthquake motion has been the subject of many studies. This study focused on retrofitting the LPG loading platform with battered piles in the Aliağa district of Izmir province, addressing the poor performance of battered pile systems during earthquake motion. Two plans have been proposed to retrofit the structure. In the first retrofit plan, four new piles were added to the system. In the second plan, lead rubber bearings were placed under the existing battered piles. Then, these two systems were compared in various aspects. The observed results are summarized below.

- In the conventional retrofit plan, pile-to-cap connections, steel piles, and axial capacities were checked. After the analysis of the existing piles and additional piles in accordance with KYLDY-2020, it was concluded that they provide all limit values. Thus, the applicability of the proposed plan has been proven.
- In the lead rubber bearing retrofit plan, the carrier system and isolators were checked in accordance with KYLDY-2020 and TBEC-2018 regulations, respectively. All analyses and calculations have shown that this retrofit plan is also applicable.
- The aim of both retrofitting plans is to reduce the forces in the existing system. In the conventional method, as the mass of the structure increases with additional piles, its period becomes longer, and in the event of an earthquake, the structure receives less acceleration and therefore less force. At the same time, it alleviates the burden on existing piles by redistributing loads onto additional piles. This relaxation of the existing structure enhances

its seismic performance. In the second method, the structure's period is extended by the isolators' working principle. As a result, a substantial reduction in forces acting on the structure is observed.

- In this study, analysis and calculations were carried out for single structure selected as a case study. However, the results advised that for similar structures using lead rubber bearings is applicable and advantageous.
- For both methods, construction methodologies and work items were determined, and costs were calculated. As shown in Table 4-16, the cost of the retrofitting method with lead rubber bearings is significantly lower than the conventional method. Another important advantage is that in addition to the construction cost, the dolphin system will not be completely closed, as there will be no additional construction on the platform.

5.2 Recommendations

- Future studies can focus on enhancing design and performance while aiming for economic advantages. For instance, the incorporation of high-damping rubber bearings and lead rubber bearings customized to the structure's requirements may result in improved performance.
- Further analyses can be conducted on larger marine structures, such as piers. Additionally, investigating structures designed to withstand breasting and mooring loads would provide a comprehensive evaluation of isolator performance under static condition.

REFERENCES

American Petroleum Institute. (2014). Recommended practice for planning, designing & constructing fixed offshore platforms (API RP 2A). Working Stress Design, 22nd Edition.

American Petroleum Institute & American National Standards Institute. (2014). Geotechnical and foundation design considerations ansi (1. ed. April 2011 [with] Addendum 1 October 2014). API Publ. Services.

Applied Technology Council. (1996). ATC 40: Seismic Evaluation and Retrofit of Concrete Buildings. Seismic Safety Commission.

ASCE. (2022). Minimum Design Loads for Buildings and Other Structures (7th–22nd ed.). ASCE.

ASCE 61-14. (2014). Seismic design of piers and wharves. American Society of Civil Engineering (ASCE) Standard.

California State Lands Commission, Marine Facilities Division. (2002). Marine Oil Terminal Engineering and Maintenance Standards (MOTEMS).

Makris, N. (2019). Seismic isolation: Early history, Earthquake Engineering &

Structural Dynamics, 48(2), 269–283.

Naeim, F. ve Kelly, J.M. (1999). Design of seismic isolated structures: from theory to practice, John Wiley & Sons.

Naval Facilities Engineering Command. (2005). Unified Facilities Criteria, UFC 4-152-01: Design: Piers and Wharves.

Polat, Ş.Ş. (2008). Deformation Based Seismic Design of Pile Supported Marine Facilities (Doktora Tezi). Boğaziçi Üniversitesi, Kandilli Rasathanesi ve Deprem Araştırmaları Enstitüsü.

Port of Long Beach. (2021). Port of Long Beach Wharf Design Criteria Version 5.0.

Su, L., Wan, H., Lu, J., Ling, X., Elgamal, A., & Arulmoli, A. (2021). Seismic Performance Evaluation of a Pile-Supported Wharf System at Two Seismic Hazard Levels. Ocean Engineering, 219, 108333.

TBEC (2018). Turkish Building Earthquake Code. Disaster and Emergency Management Authority, Ankara.

Venkatalakshmi, P., Sree, J., & Rao, P. V. (2017). Performance Based Design of Jetties. International Journal of Innovative Research in Science, Engineering and Technology, 6(8).

APPENDICES

A. Nonlinear P-Y Curves and Pile Toe Link

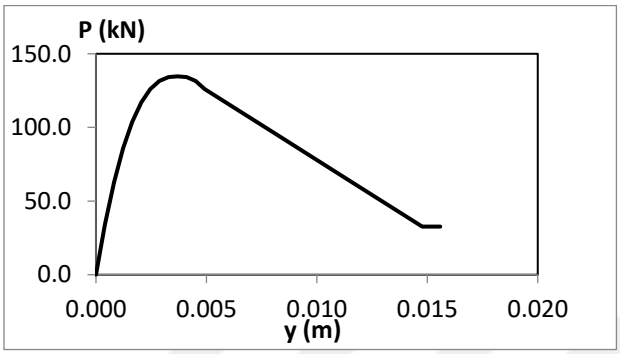

Figure A. 1 p-y curves for 32" S275 steel piles (z=1,00 m)

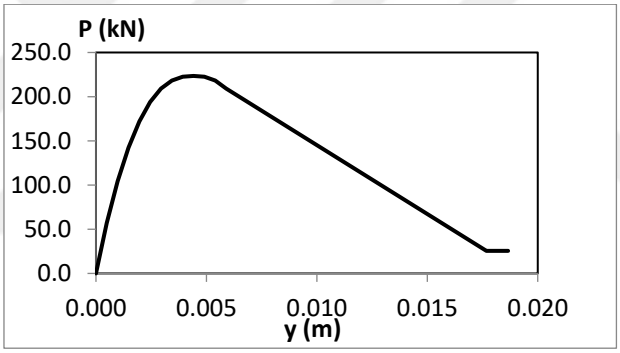

Figure A. 2 p-y curves for 32" S275 steel piles (z=2,00 m)

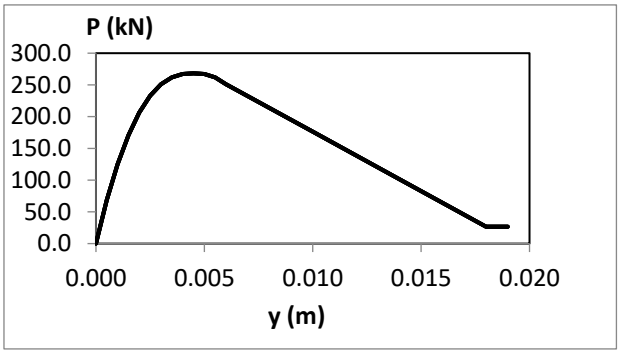

Figure A. 3 p-y curves for 32" S275 steel piles (z=3,00 m)

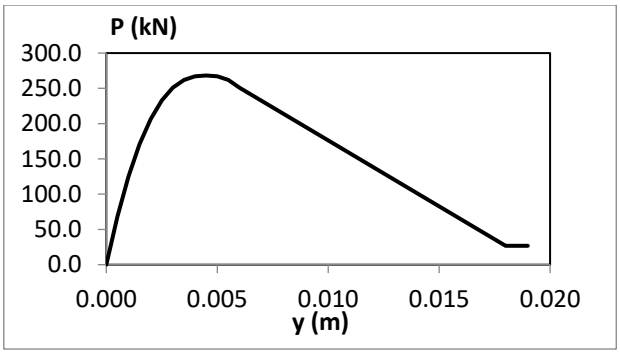

Figure A. 4 p-y curves for 32" S275 steel piles (z=4,00 m)

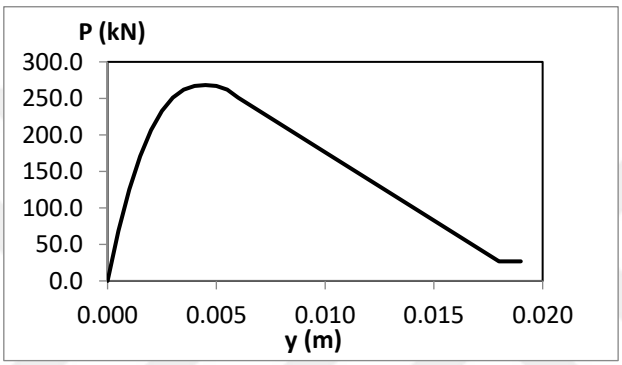

Figure A. 5 p-y curves for 32" S275 steel piles (z=5,00 m)

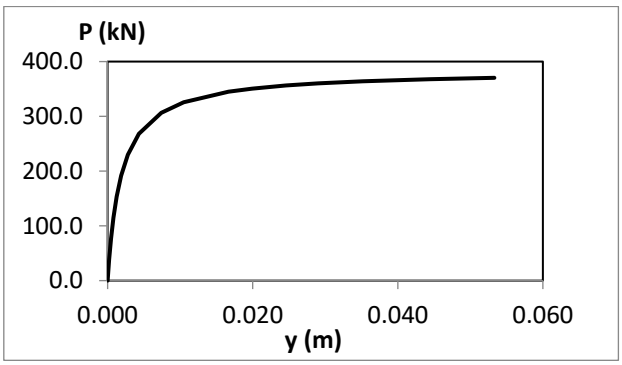

Figure A. 6 p-y curves for 32" S275 steel piles (z=6,00 m)

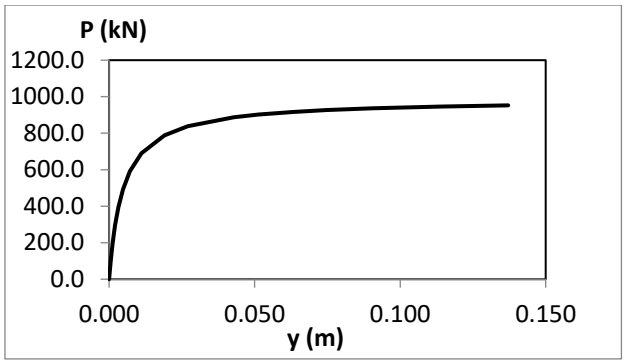

Figure A. 7 p-y curves for 32" S275 steel piles (z=7,00 m)

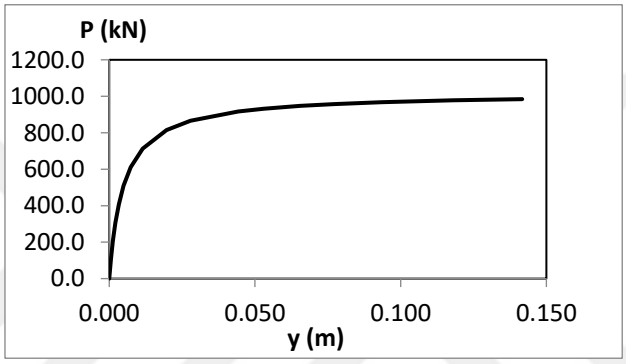

Figure A. 8 p-y curves for 32" S275 steel piles (z=8,00 m)

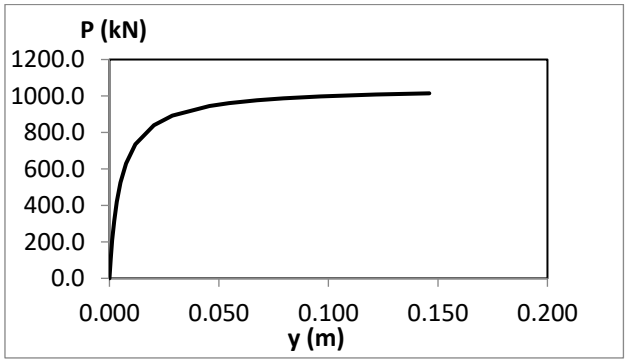

Figure A. 9 p-y curves for 32" S275 steel piles (z=9,00 m)

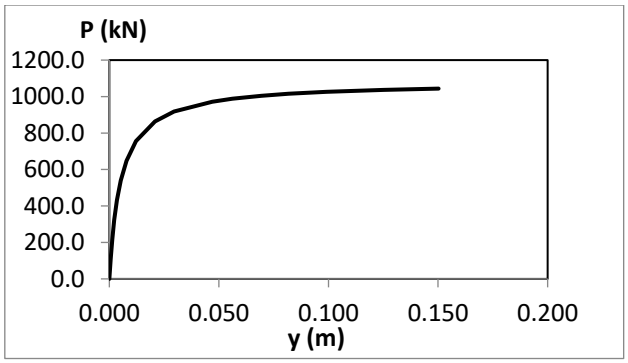

Figure A. 10 p-y curves for 32" S275 steel piles (z=10,00 m)

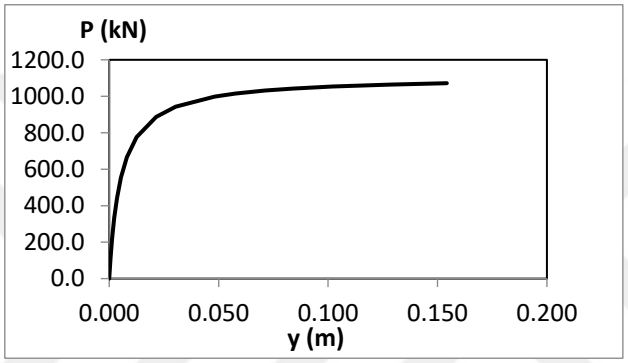

Figure A. 11 p-y curves for 32" S275 steel piles (z=11,00 m)

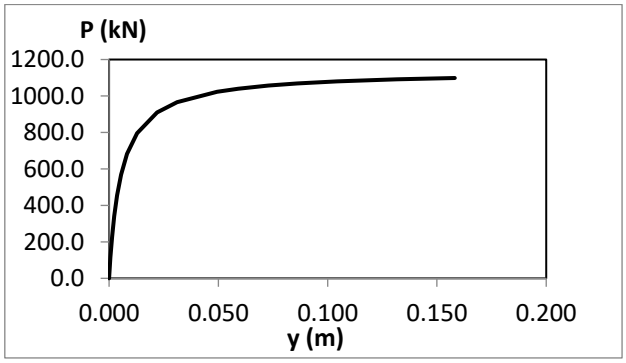

Figure A. 12 p-y curves for 32" S275 steel piles (z=12,00 m)

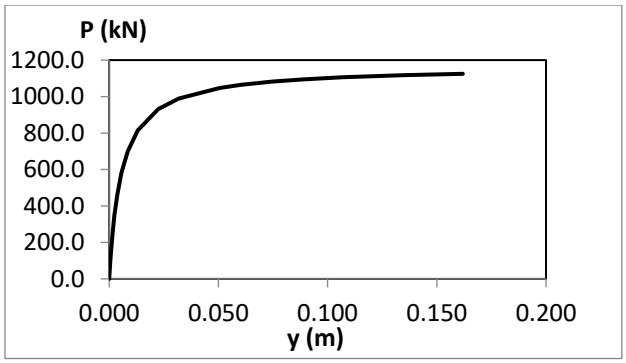

Figure A. 13 p-y curves for 32" S275 steel piles (z=13,00 m)

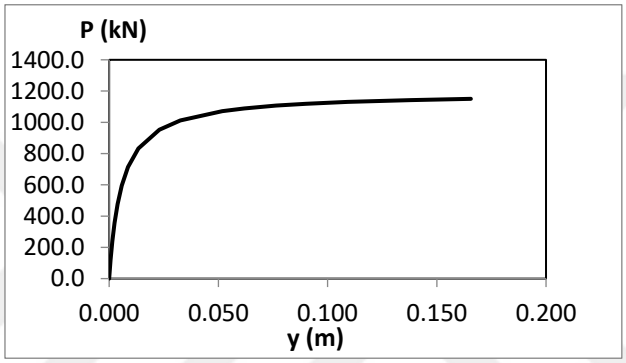

Figure A. 14 p-y curves for 32" S275 steel piles (z=14,00 m)

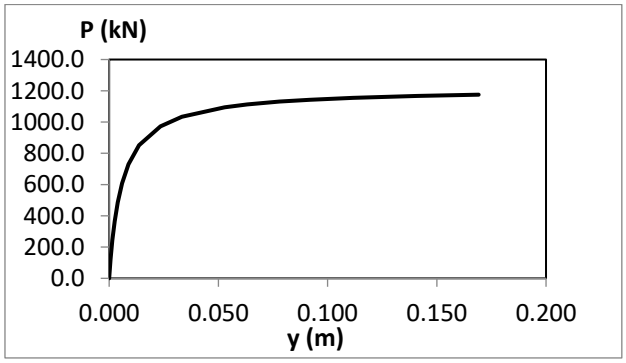

Figure A. 15 p-y curves for 32" S275 steel piles (z=15,00 m)

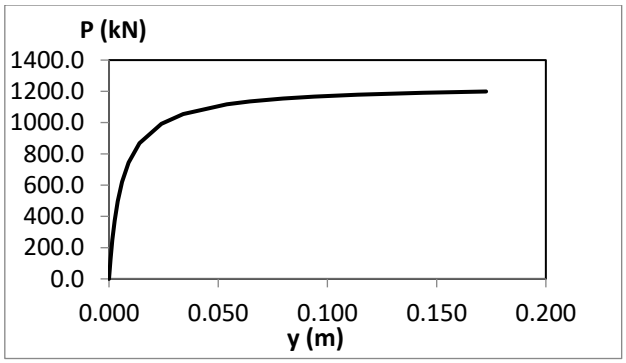

Figure A. 16 p-y curves for 32" S275 steel piles (z=16,00 m)

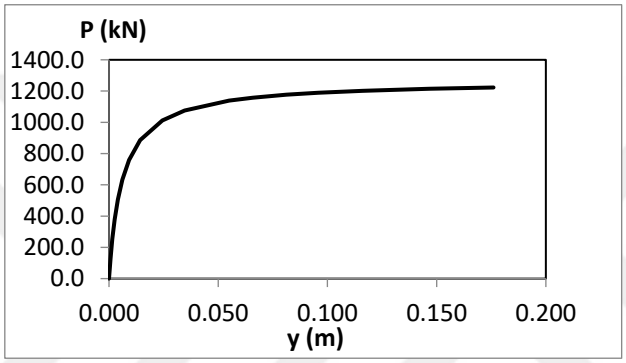

Figure A. 17 p-y curves for 32" S275 steel piles (z=17,00 m)

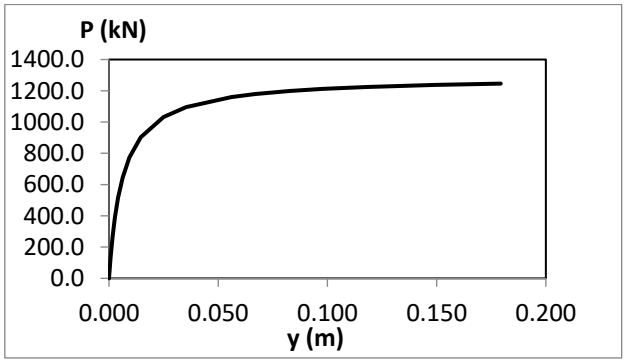

Figure A. 18 p-y curves for 32" S275 steel piles (z=18,00 m)

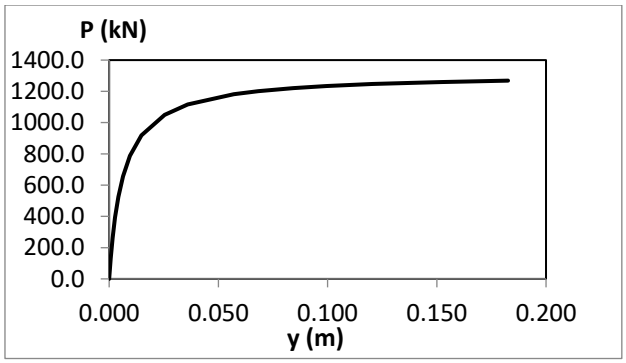

Figure A. 19 p-y curves for 32" S275 steel piles (z=19,00 m)

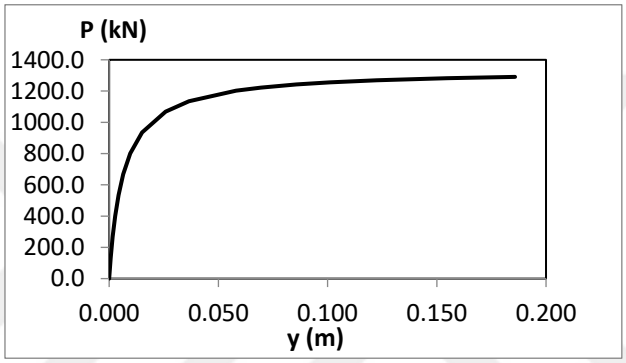

Figure A. 20 p-y curves for 32" S275 steel piles (z=20,00 m)

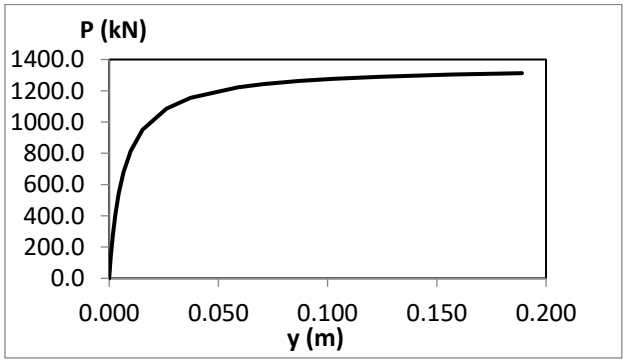

Figure A. 21 p-y curves for 32" S275 steel piles (z=21,00 m)

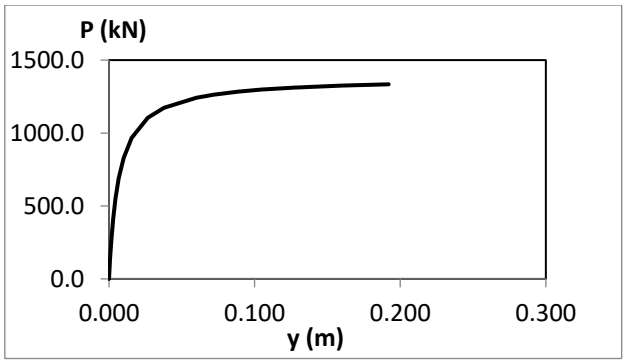

Figure A. 22 p-y curves for 32" S275 steel piles (z=22,00 m)

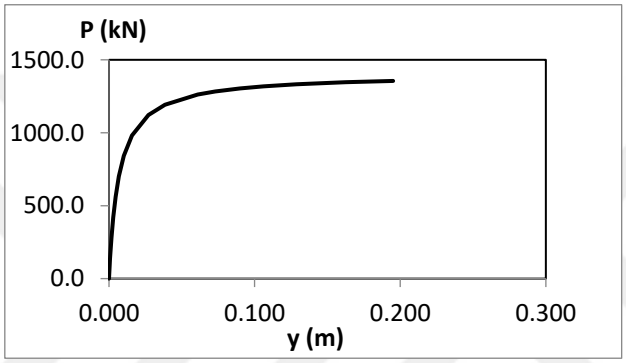

Figure A. 23 p-y curves for 32" S275 steel piles (z=23,00 m)

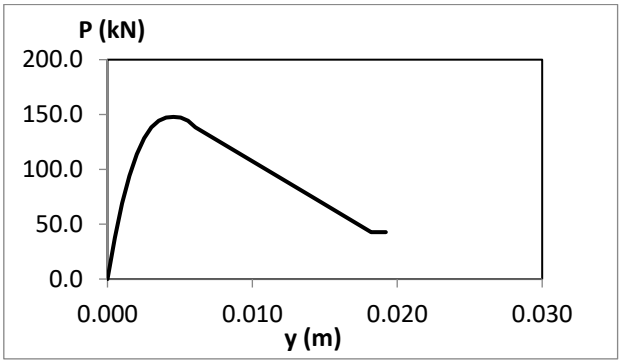

Figure A. 24 p-y curves for 52" S355 steel piles (z=1,00 m)

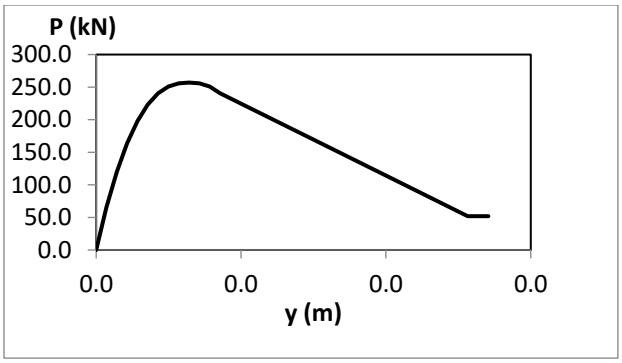

Figure A. 25 p-y curves for 52" S355 steel piles (z=2,00 m)

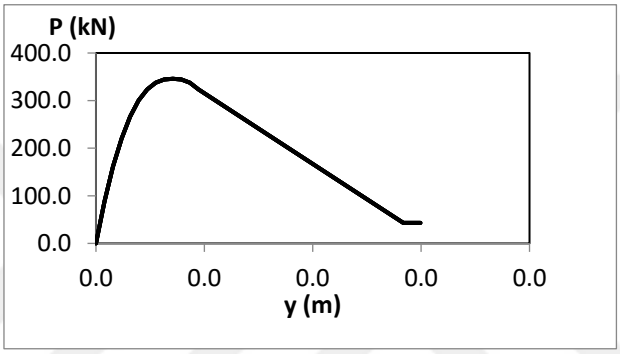

Figure A. 26 p-y curves for 52" S355 steel piles (z=3,00 m)

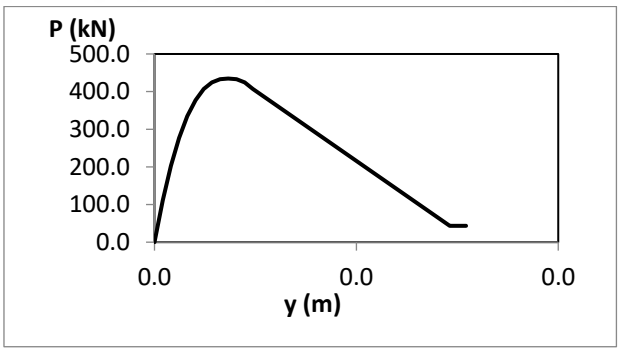

Figure A. 27 p-y curves for 52" S355 steel piles (z=4,00 m)

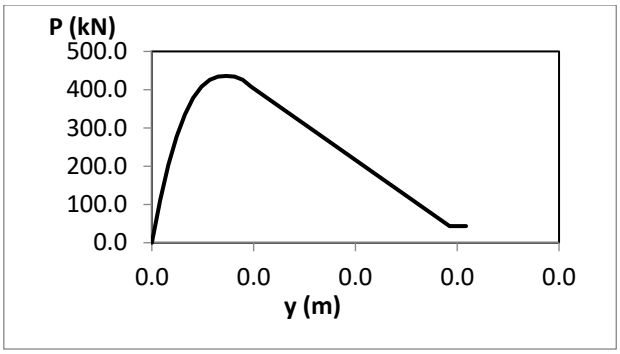

Figure A. 28 p-y curves for 52" S355 steel piles (z=5,00 m)

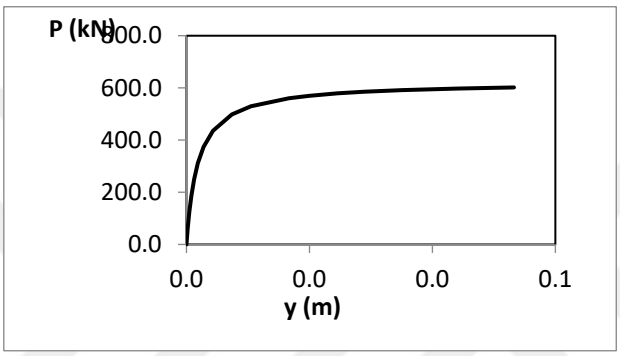

Figure A. 29 p-y curves for 52" S355 steel piles (z=6,00 m)

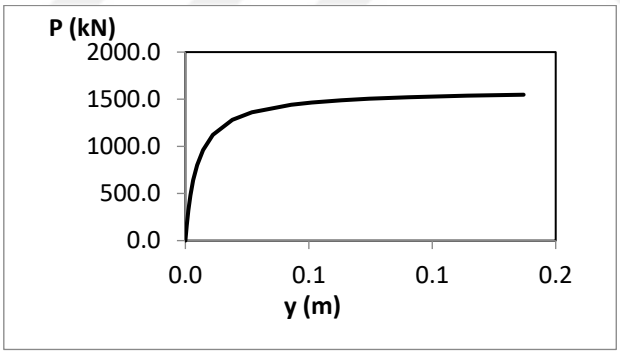

Figure A. 30 p-y curves for 52" S355 steel piles (z=7,00 m)

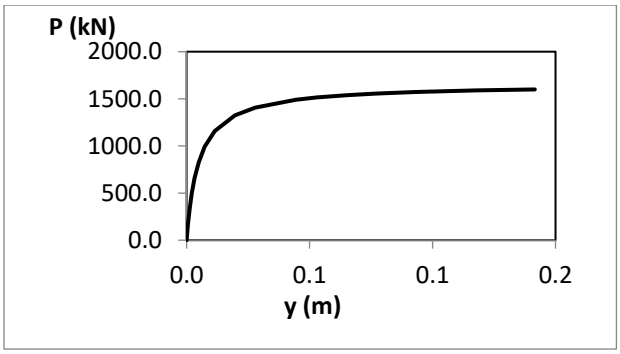

Figure A. 31 p-y curves for 52" S355 steel piles (z=8,00 m)

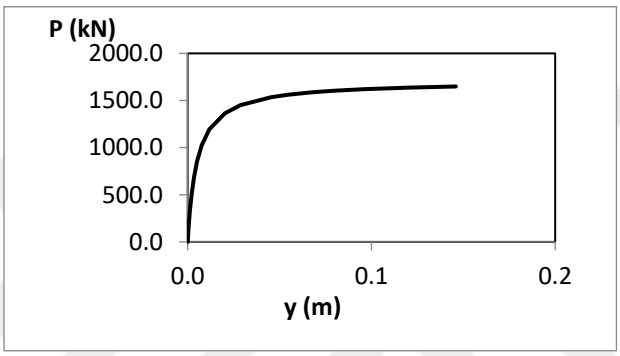

Figure A. 32 p-y curves for 52" S355 steel piles (z=9,00 m)

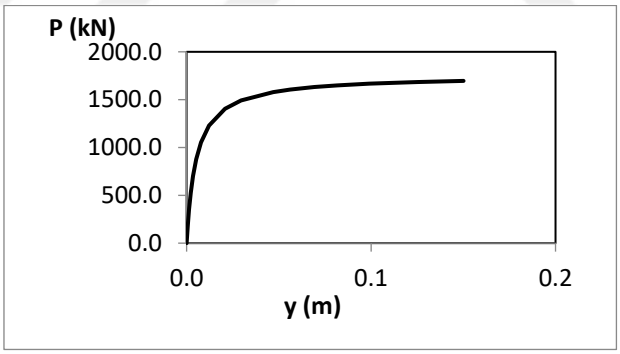

Figure A. 33 p-y curves for 52" S355 steel piles (z=10,00 m)

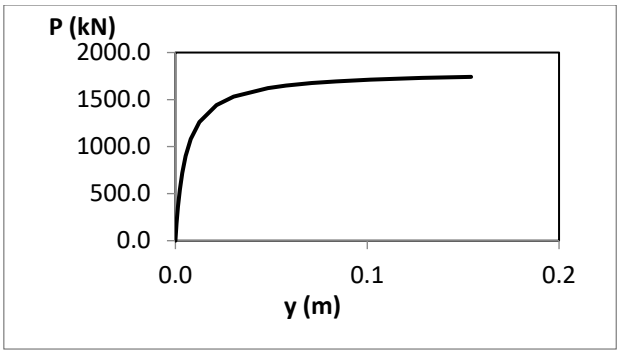

Figure A. 34 p-y curves for 52" S355 steel piles (z=11,00 m)

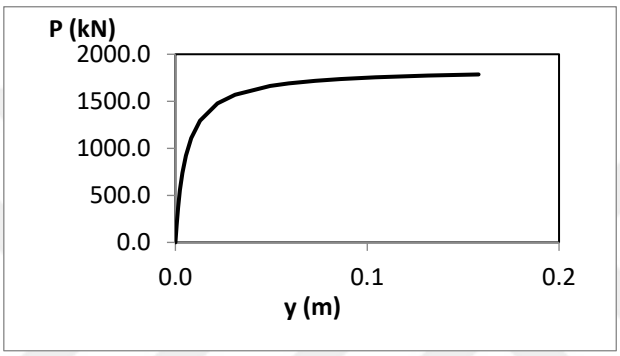

Figure A. 35 p-y curves for 52" S355 steel piles (z=12,00 m)

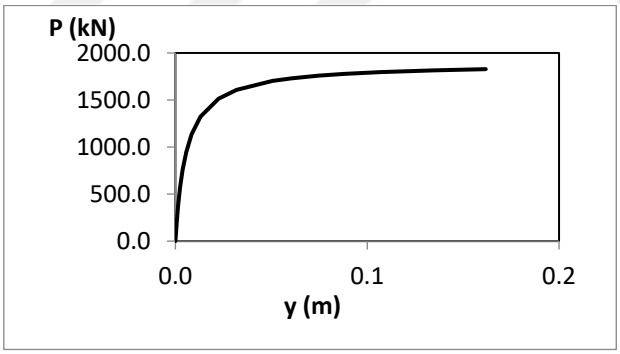

Figure A. 36 p-y curves for 52" S355 steel piles (z=13,00 m)

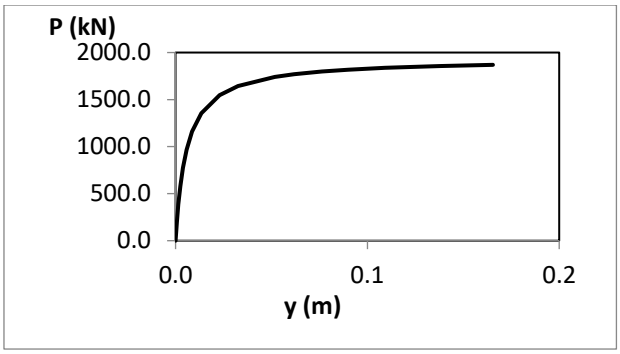

Figure A. 37 p-y curves for 52" S355 steel piles (z=14,00 m)

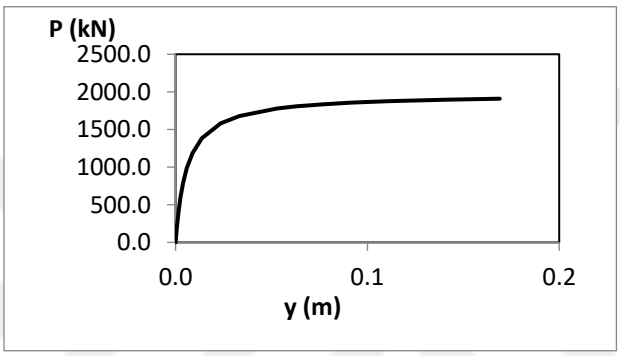

Figure A. 38 p-y curves for 52" S355 steel piles (z=15,00 m)

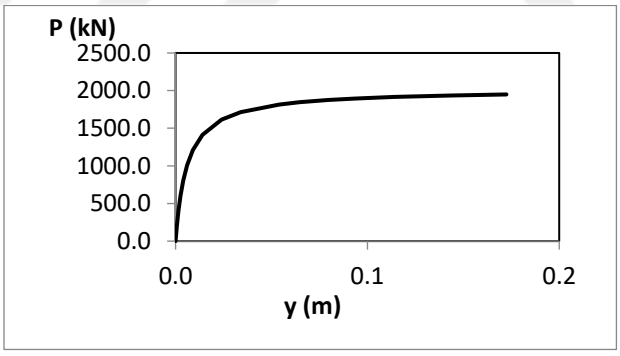

Figure A. 39 p-y curves for 52" S355 steel piles (z=16,00 m)

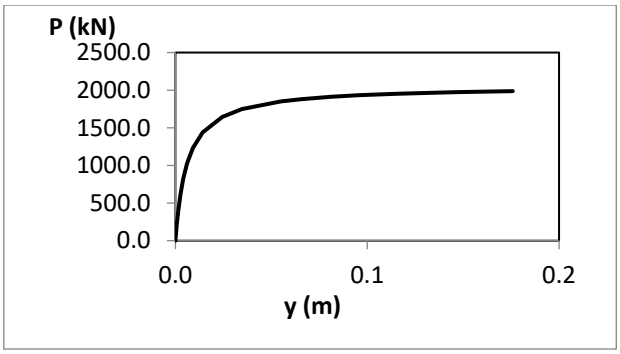

Figure A. 40 p-y curves for 52" S355 steel piles (z=17,00 m)

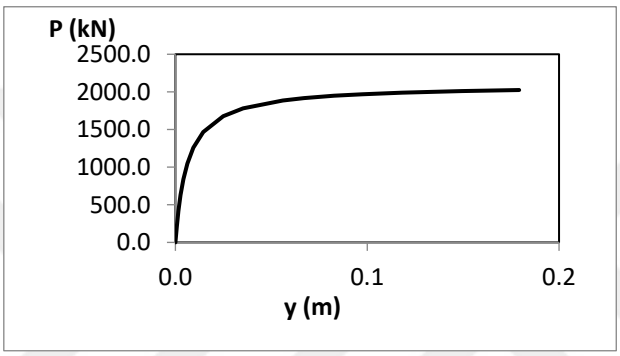

Figure A. 41 p-y curves for 52" S355 steel piles (z=18,00 m)

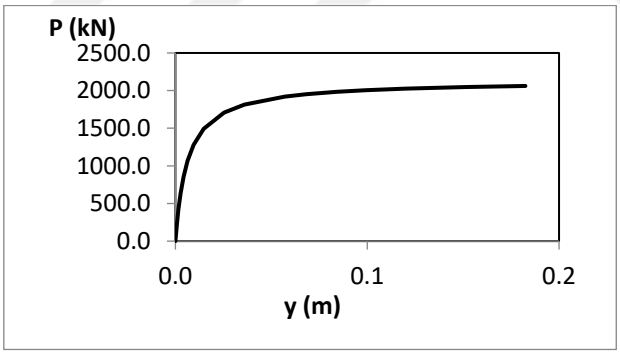

Figure A. 42 p-y curves for 52" S355 steel piles (z=19,00 m)

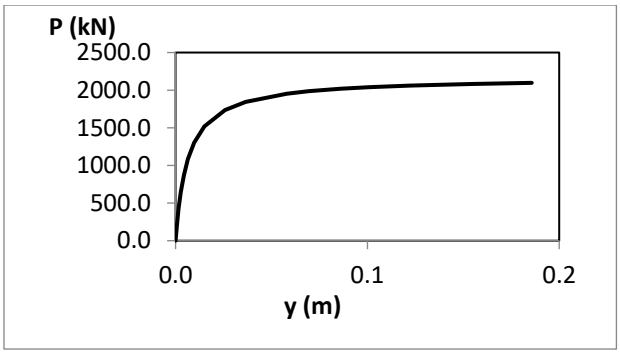

Figure A. 43 p-y curves for 52" S355 steel piles (z=20,00 m)

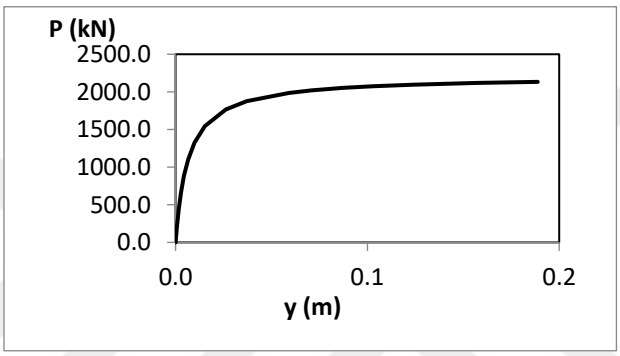

Figure A. 44 p-y curves for 52" S355 steel piles (z=21,00 m)

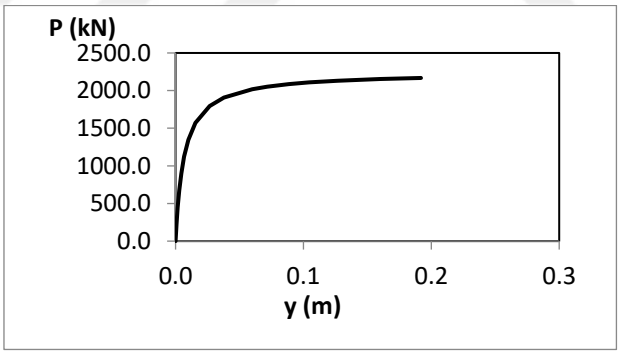

Figure A. 45 p-y curves for 52" S355 steel piles (z=22,00 m)

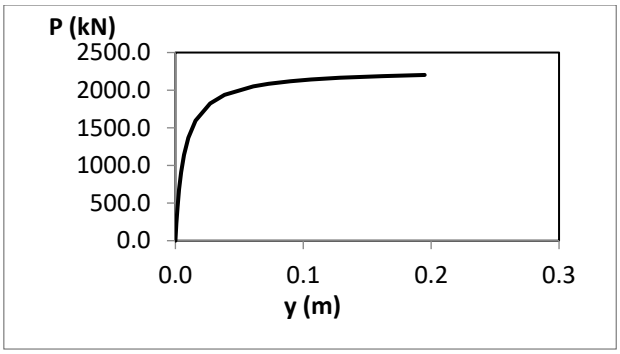

Figure A. 46 p-y curves for 52" S355 steel piles (z=23,00 m)

B. Selected Ground Motions

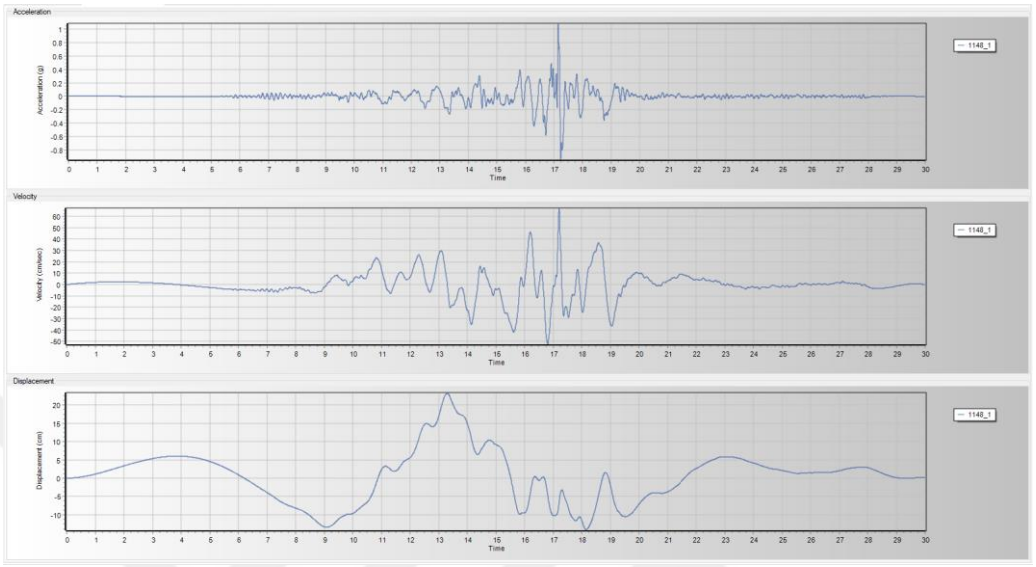

Figure B. 1 Kocaeli Earthquake RSN1148 Station Records

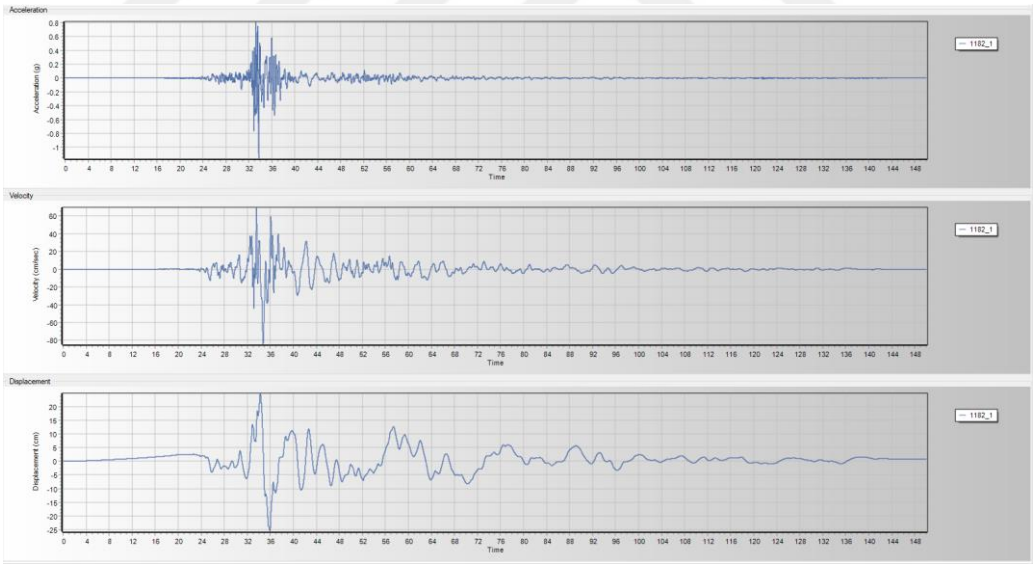

Figure B. 2 Thaiwan Chi-Chi Earthquake RSN1148 Station Records

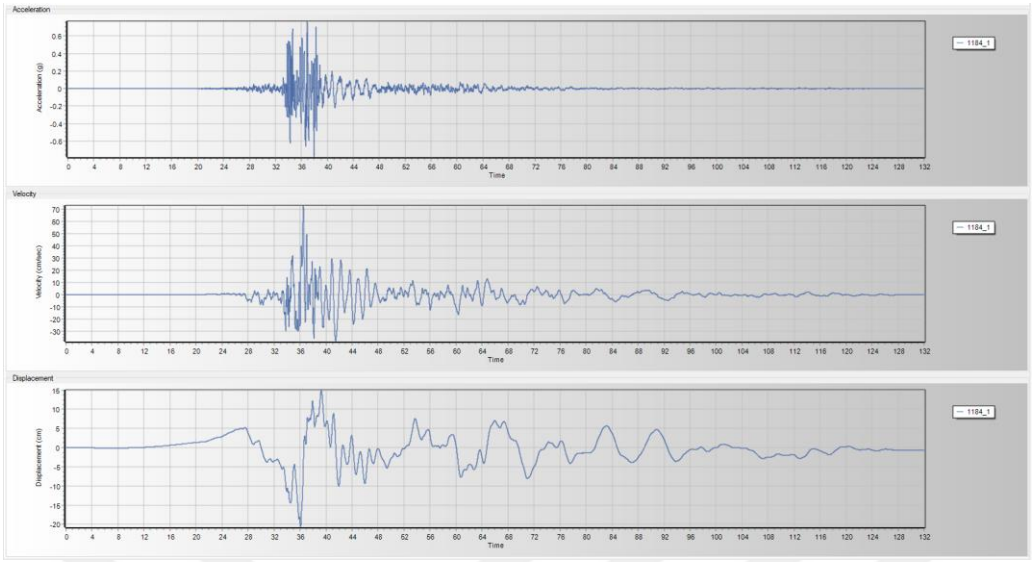

Figure B. 3 Thaiwan Chi-Chi Earthquake RSN1184 Station Records

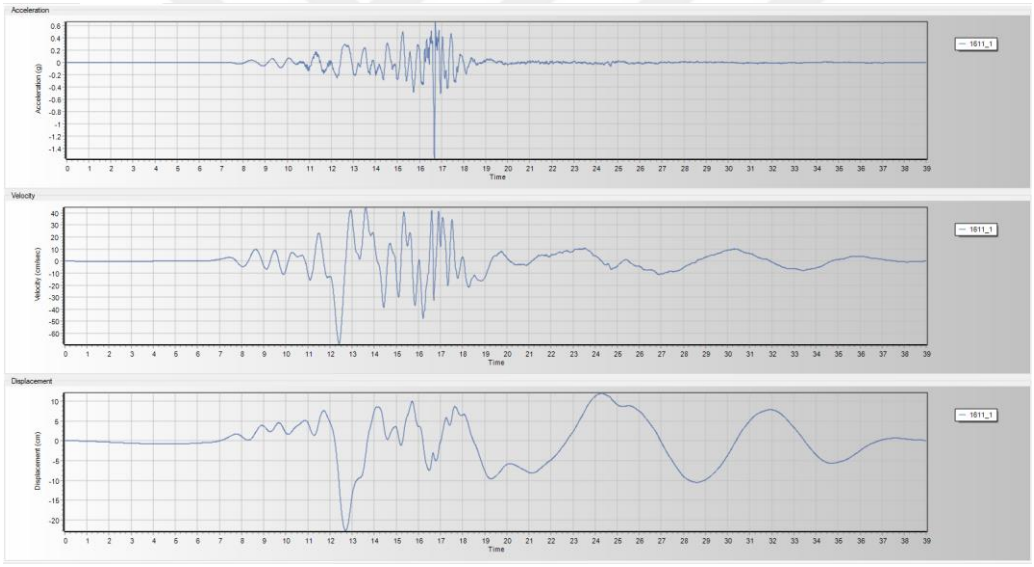

Figure B. 4 Düzce Earthquake RSN1611 Station Records

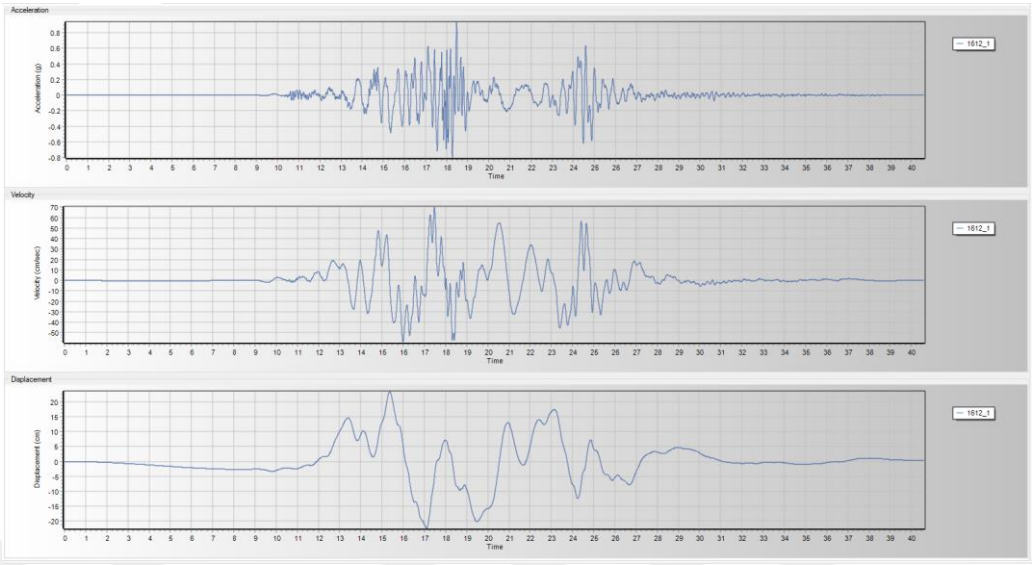

Figure B. 5 Düzce Earthquake RSN1612 Station Records

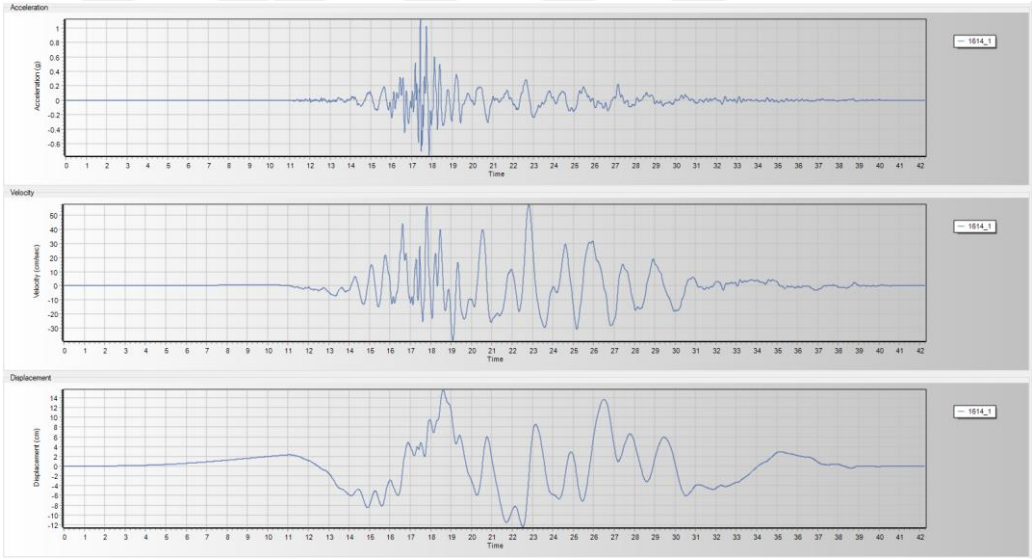

Figure B. 6 Düzce Earthquake RSN1614 Station Records

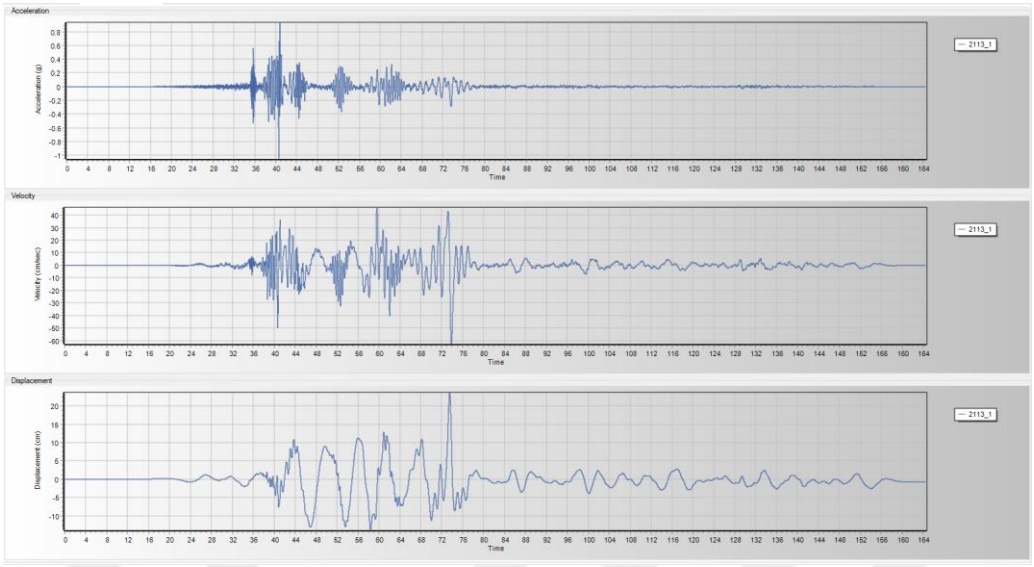

Figure B. 7 Denali Earthquake RSN2113 Station Records

C. Minimum Pile Thickness Computations

According to KYLDY-2020 10.4.1.

$$\frac{D}{t} \le c\frac{E_S}{\sigma_Y} \qquad \frac{D}{t} \le 80$$

Elastic modulus of steel:		200000000	kN/m²
Yield stress of steel:		355000	kN/m²
Pile diameter:		1320.8	mm
Minimum wall thickness:	tmin =	20.00	mm
	tmin =	16.51	mm
Selected steel pipe pile wall thickness:	**t =**	**22.00**	**mm** **OK**

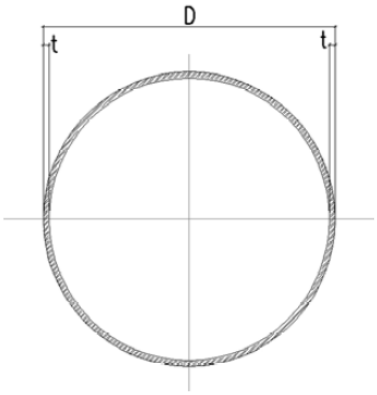

Figure C. 1 Minimum wall thickness of 52” steel piles

D. SAP2000 Model Views

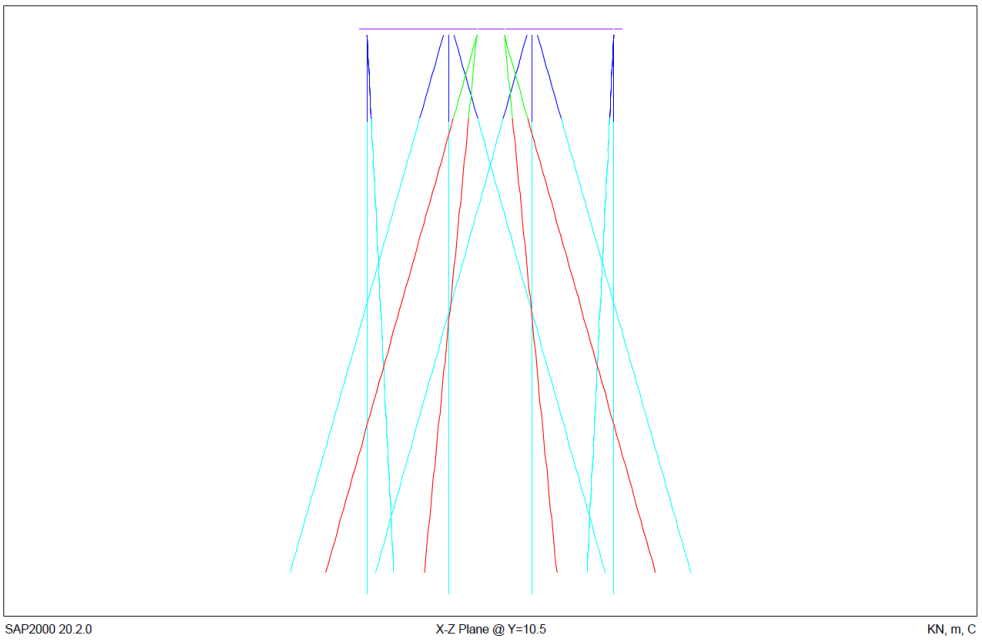

Figure D. 1 Conventional retrofit model X-Z View

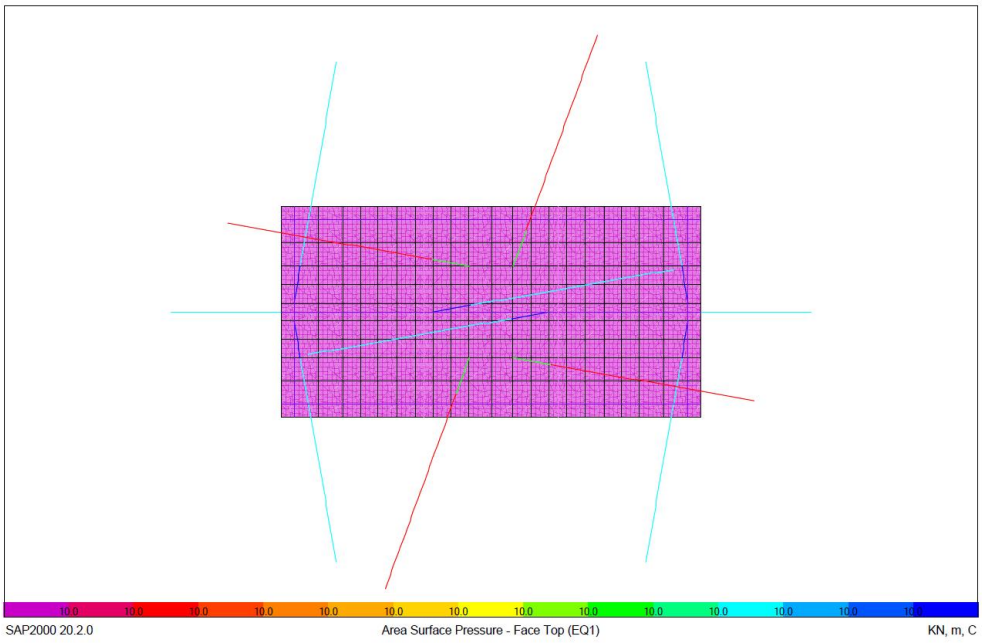

Figure D. 2 Live load (EQ)

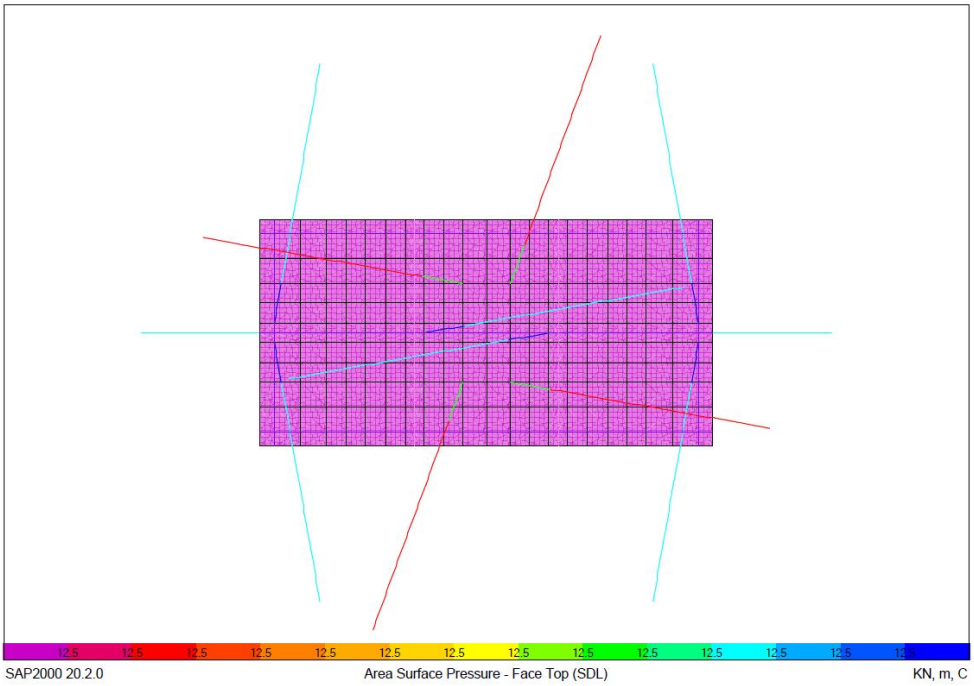

Figure D. 3 Super imposed dead load (SDL)

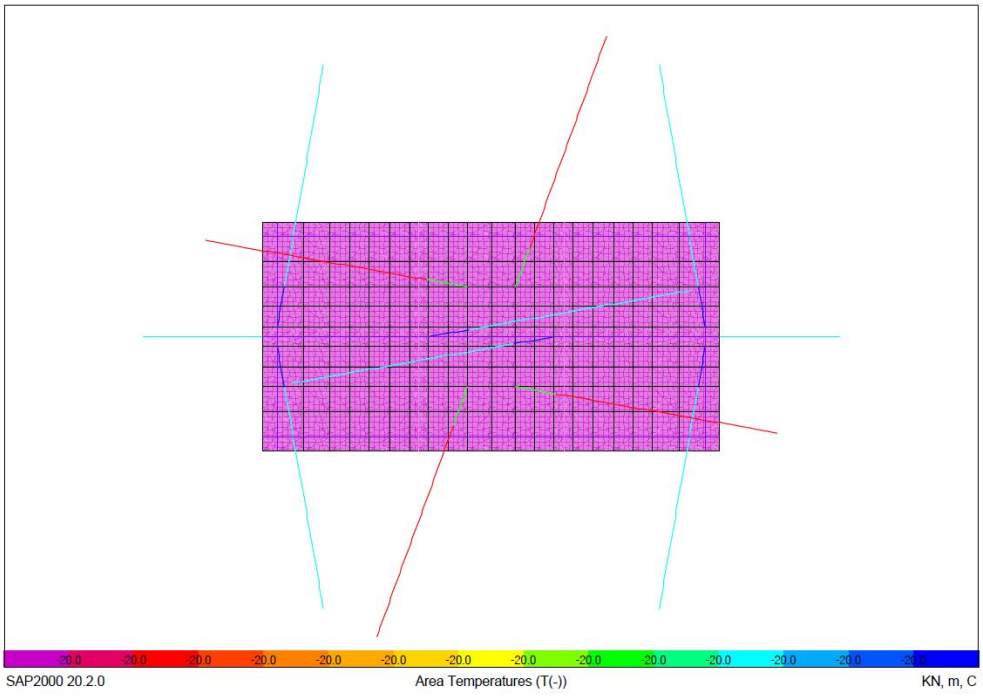

Figure D. 4 Temperature load (T-)

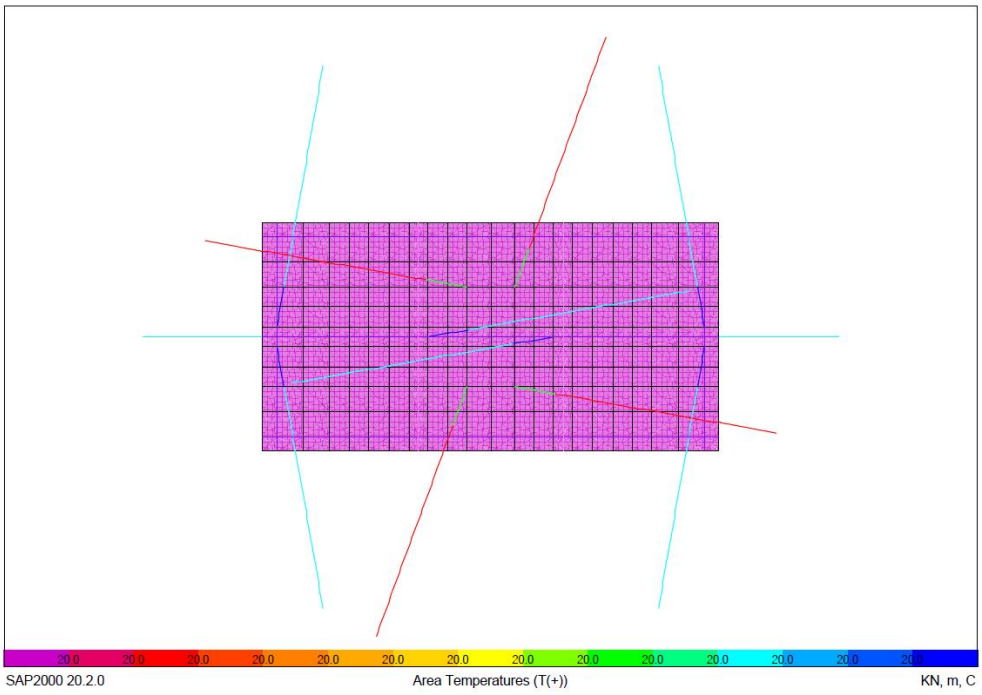

Figure D. 5 Temperature load (T+)

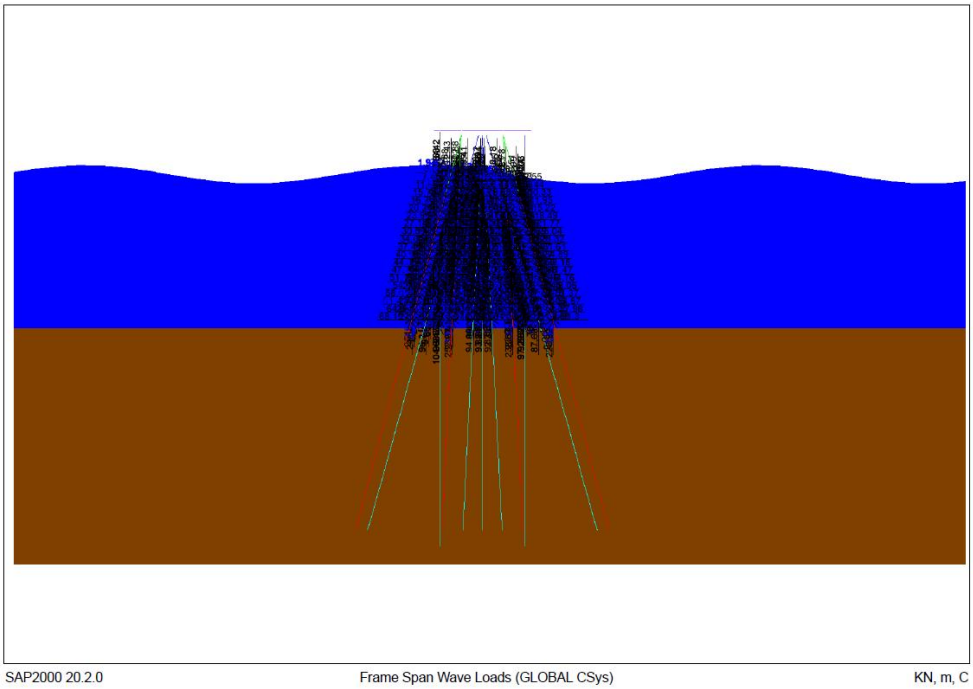

Figure D. 6 Wave load (Sw)

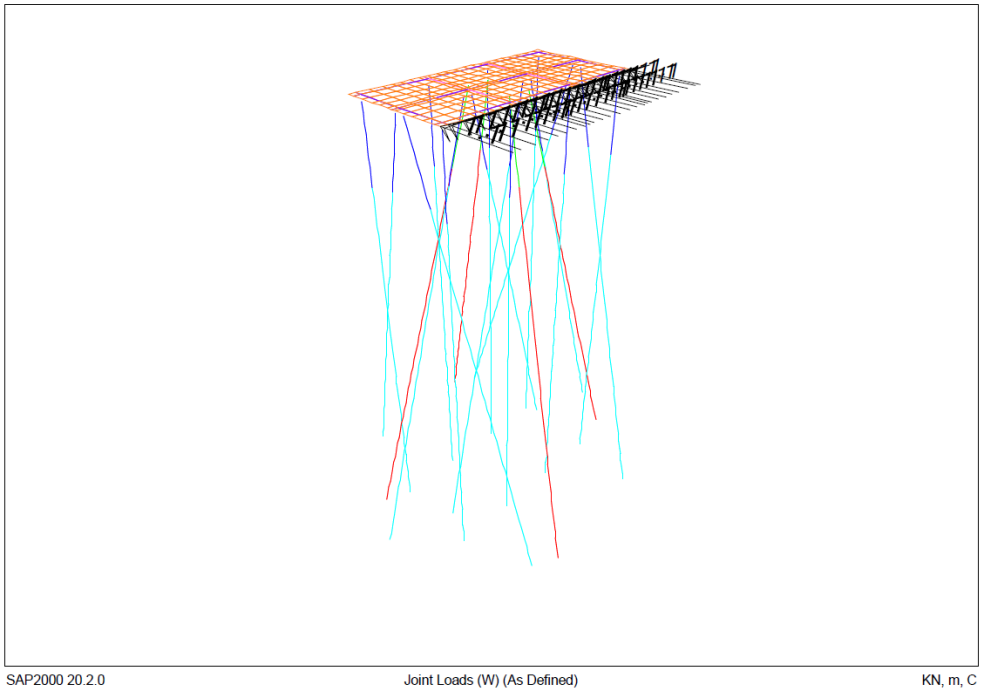

Figure D. 7 Wind load

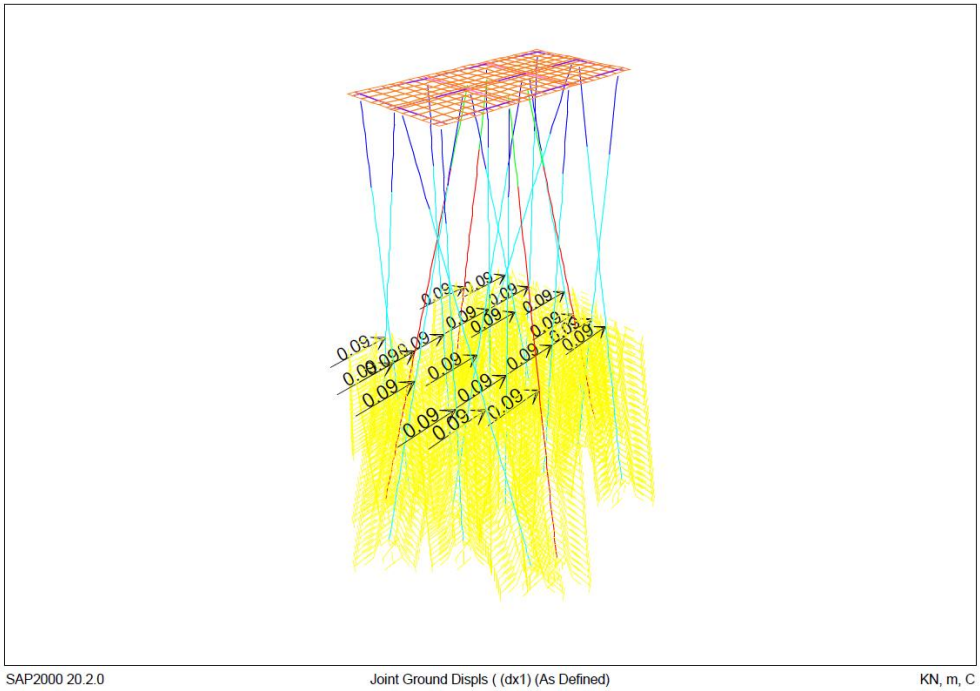

Figure D. 8 Ground displacement in the first layer

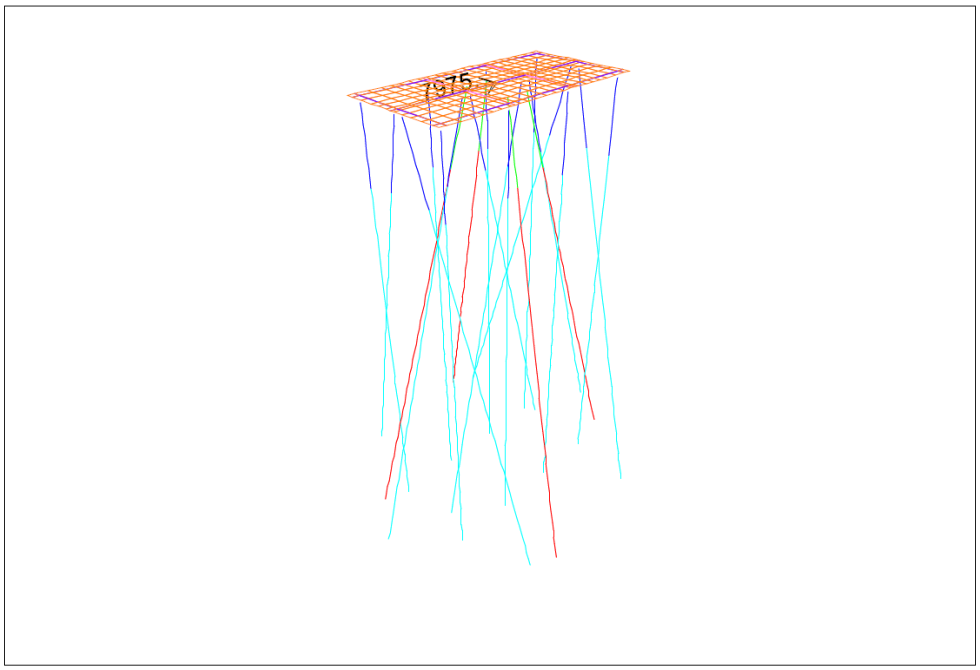

Figure D. 9 Conventional retrofit shear force (+x direction)

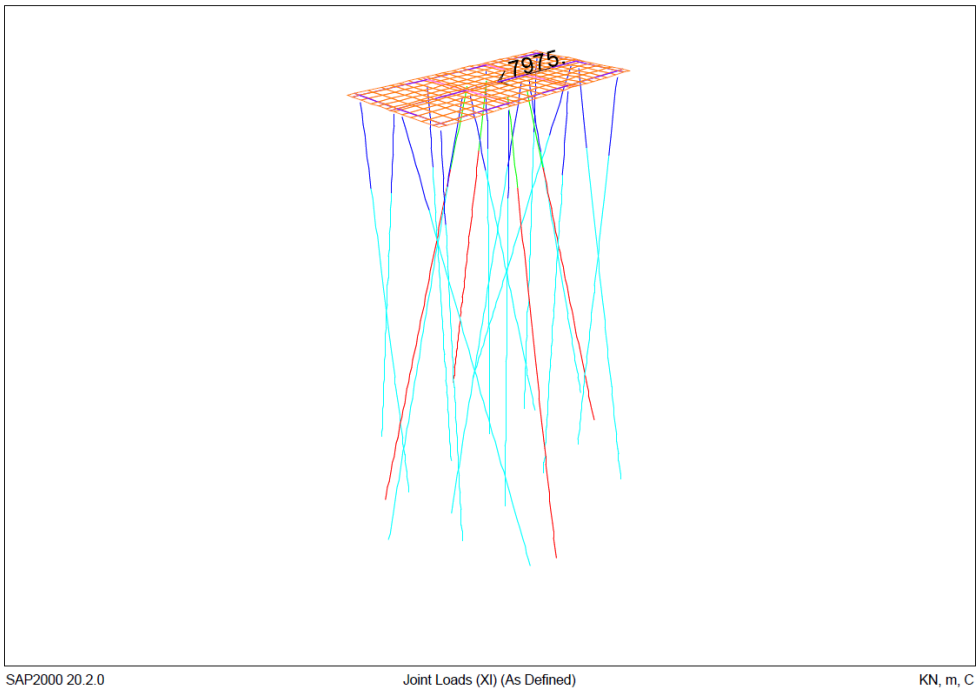

Figure D. 10 Conventional retrofit shear force (-x direction)

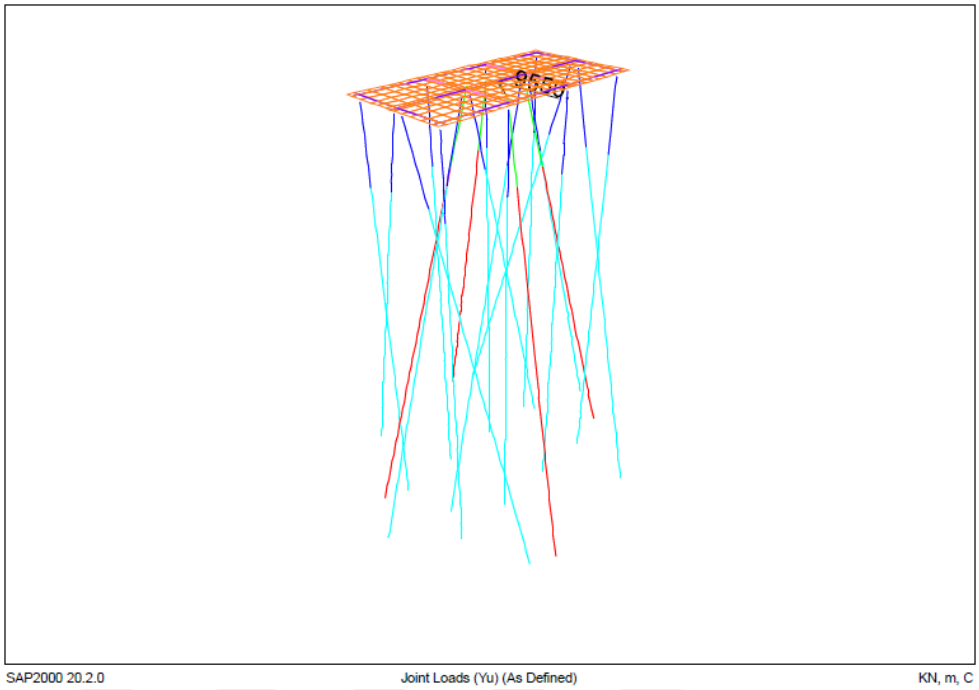

Figure D. 11 Conventional retrofit shear force (+y direction)

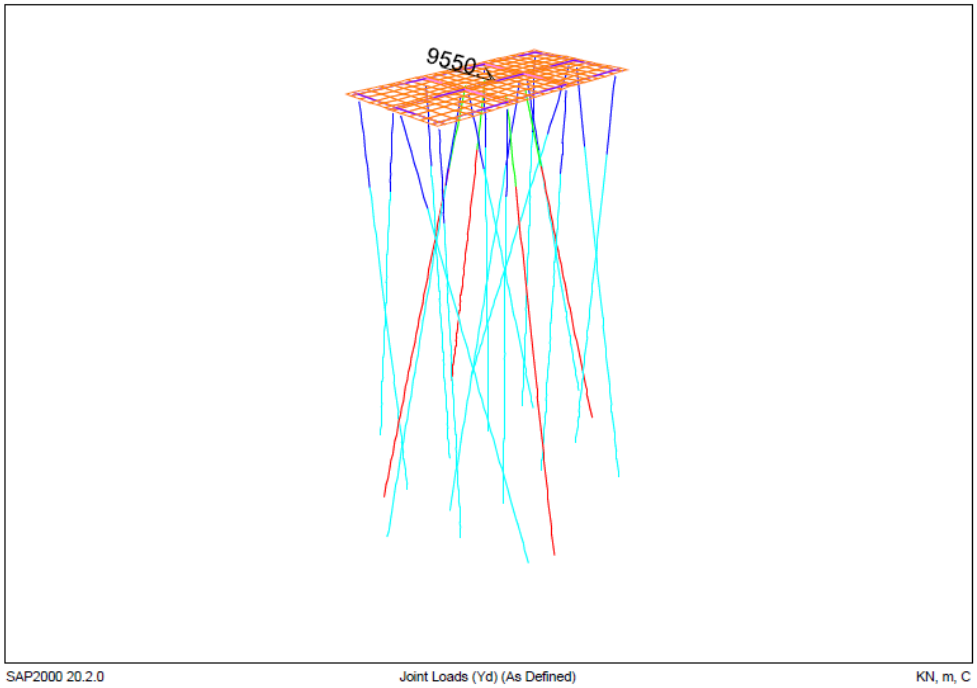

Figure D. 12 Conventional retrofit shear force (-y direction)

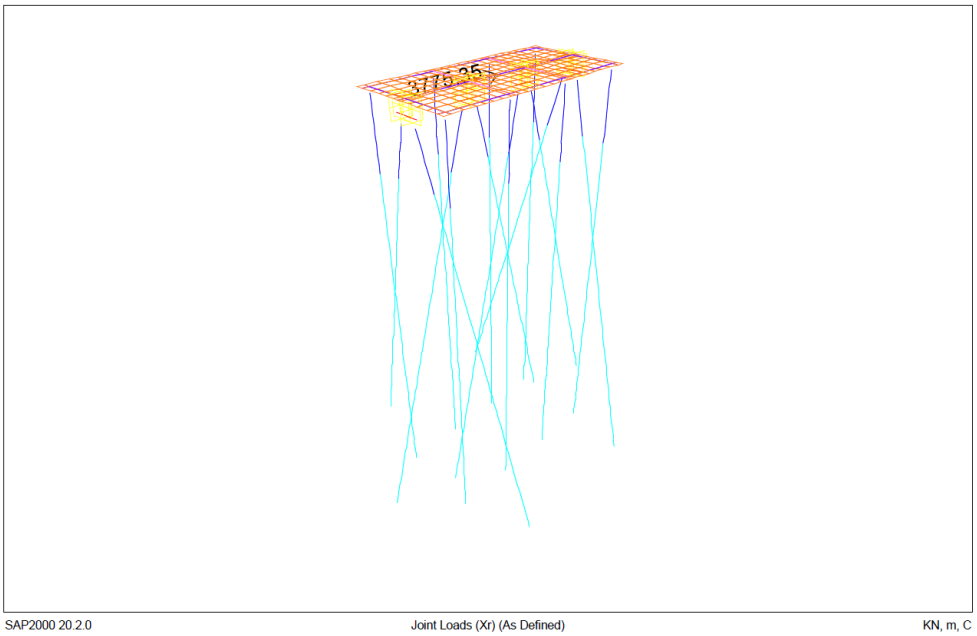

Figure D. 13 Lead rubber bearing retrofit shear force (+x direction)

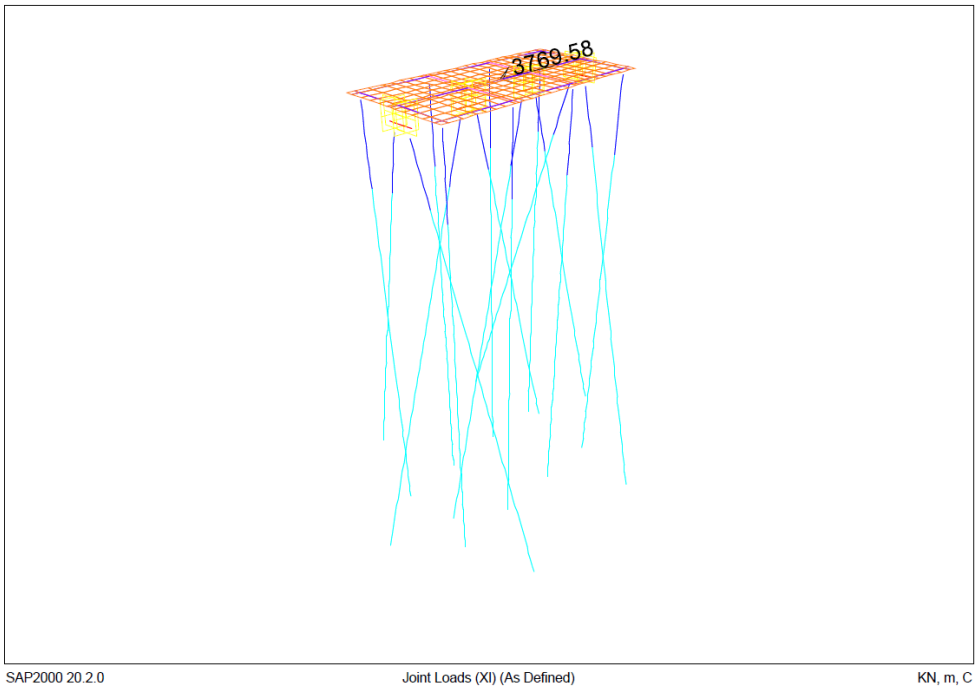

Figure D. 14 Lead rubber bearing retrofit shear force (-x direction)

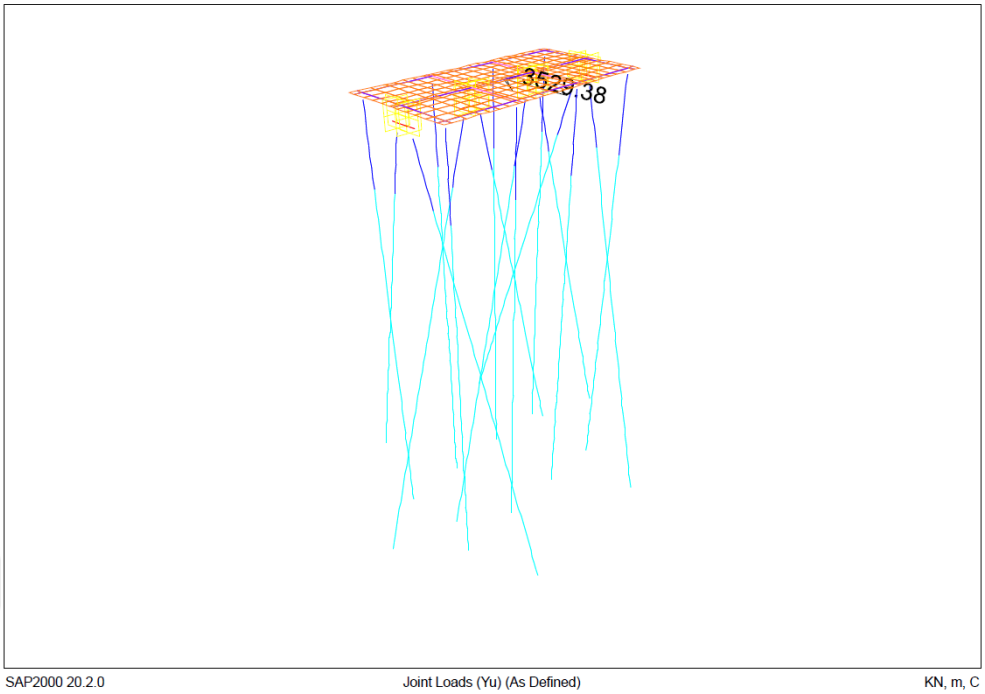

Figure D. 15 Lead rubber bearing retrofit shear force (+y direction)

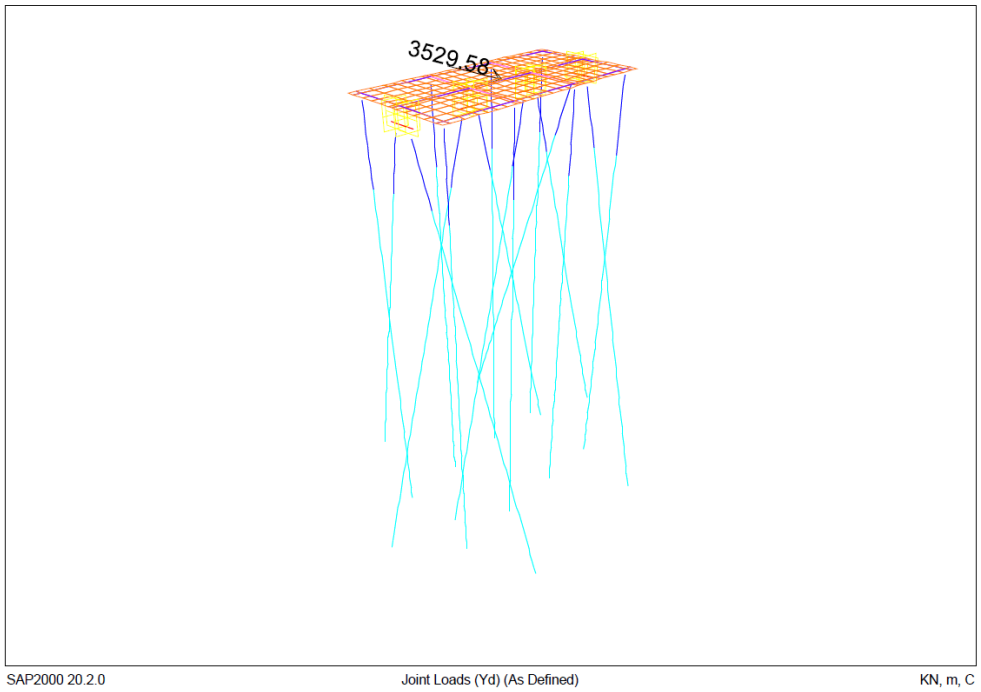

Figure D. 16 Lead rubber bearing retrofit shear force (-y direction)